

TRACE VAPOR DETECTION OF HYDROGEN PEROXIDE:
AN EFFECTIVE APPROACH TO IDENTIFICATION OF
IMPROVISED EXPLOSIVE DEVICES

by

Miao Xu

A dissertation submitted to the faculty of
The University of Utah
in partial fulfillment of the requirements for the degree of

Doctor of Philosophy

Department of Materials Science and Engineering

The University of Utah

August 2014

Copyright © Miao Xu 2014

All Rights Reserved

ABSTRACT

Vapor detection has been proven as one of the practical, noninvasive methods suitable for explosives detection among current explosive detection technologies. Optical methods (especially colorimetric and fluorescence spectral methods) are low in cost, provide simple instrumentation alignment, while still maintaining high sensitivity and selectivity, these factors combined facilitate broad field applications. Trace vapor detection of hydrogen peroxide (H_2O_2) represents an effective approach to noninvasive detection of peroxide-based explosives, though development of such a sensor system with high reliability and sufficient sensitivity (reactivity) still remains challenging. Three vapor sensor systems for H_2O_2 were proposed and developed in this study, which exploited specific chemical reaction towards H_2O_2 to ensure the selectivity, and materials surface engineering to afford efficient air sampling. The combination of these features enables expedient, cost effective, reliable detection of peroxide explosives.

First, an expedient colorimetric sensor for H_2O_2 vapor was developed, which utilized the specific interaction between $\text{Ti}(\text{oxo})$ and H_2O_2 to offer a yellow color development. The $\text{Ti}(\text{oxo})$ salt can be blended into a cellulose microfibril network to produce tunable interface that can react with H_2O_2 . The vapor detection limit can reach 400 ppb. To further improve the detection sensitivity, a naphthalimide based fluorescence turn-on sensor was designed and developed. The sensor mechanism was based on H_2O_2 -mediated oxidation of a boronate fluorophore, which is nonfluorescent in ICT band, but becomes strongly

fluorescent upon conversion into the phenol state. The detection limit of this sensory material was improved to be below 10 ppb. However, some technical factors such as sensor concentration, local environment, and excitation intensity were found difficult to control to make the sensor system sufficiently reproducible. To solve the problem, we developed a ratiometric fluorescence sensor, which allows for dual-band emission monitoring and thus enhances the detection reliability. Moreover, the significant spectral overlap between the fluorescence of the pristine sensor and the absorption of the reacted state enables effective Förster Resonance Energy Transfer (FRET). This FRET process can significantly enhance the fluorescence sensing efficiency in comparison to the normal single-band sensor system, for which the sensing efficiency is solely determined by the stoichiometric conversion of sensor molecules.

To my beloved wife, Xiaoyun

TABLE OF CONTENTS

ABSTRACT.....	iii
LIST OF ABBREVIATIONS.....	viii
ACKNOWLEDGEMENTS.....	xii
1. INTRODUCTION	1
1.1 Current Sensing Methods for Peroxide-based Explosives.....	3
1.1.1 Ion Mobility Spectroscopy	4
1.1.2 Mass Spectroscopy	6
1.1.3 Raman Spectroscopy	7
1.1.4 Chemiresistive Sensors.....	8
1.1.5 Colorimetric Sensors	12
1.1.6 Fluorescence Sensors.....	16
1.1.7 Chemiluminescence Sensors	22
1.2 Motivations and Objectives	24
1.3 Reference	25
2. PAPER-BASED VAPOR DETECTION OF HYDROGEN PEROXIDE: COLORIMETRIC SENSING WITH TUNABLE INTERFACE	35
2.1 Abstract.....	35
2.2 Introduction.....	36
2.3 Results and Discussion	38
2.4 Conclusion	44
2.5 Experimental Methods and Materials	44
2.5.1 Materials and General Instrumentations.....	44
2.5.2 UV-vis Absorption Titration of Colorimetric Reaction between Titanyl Salt and H ₂ O ₂	46
2.5.3 Homogeneous Distribution of Titanyl Salt via Drop-Casting	46
2.5.4 Time Course of Color Formation as Monitored by UV-vis Absorption	46
2.5.5 Selectivity Test Against Potential Interferences.....	47
2.6 References.....	47

3. A SELECTIVE FLUORESCENCE TURN-ON SENSOR FOR TRACE VAPOR DETECTION OF HYDROGEN PEROXIDE	59
3.1 Abstract	59
3.2 Introduction.....	59
3.3 Results and Discussion	61
3.4 Conclusion	65
3.5 Experimental Methods and Materials	66
3.5.1 Materials and General Instrumentations.....	66
3.5.2 Synthesis.....	67
3.5.3 Other Experimental Details	69
3.6 References	77
4. FLUORESCENCE RATIOMETRIC SENSOR FOR TRACE VAPOR DETECTION OF HYDROGEN PEROXIDE	99
4.1 Abstract	99
4.2 Introduction.....	100
4.3 Results and Discussion	102
4.4 Conclusion	108
4.5 Experimental Methods and Materials	109
4.5.1 Materials and General Instrumentations.....	109
4.5.2 Synthesis.....	109
4.5.3 Other Experimental Details	111
4.6 References.....	117
5. DISSERTATION CONCLUSIONS AND PROPOSED FUTURE WORK.....	138
5.1 Dissertation Conclusions	139
5.2 Suggestions for Future Work	141

LIST OF ABBREVIATIONS

Δ	delta, heat, or change
$^{\circ}$	degree
$^{\circ}\text{C}$	degree Celsius
μL	microliter
μm	micrometer
3D	three-dimensional
9,10-DPA	9,10-diphenylanthracene
a.u.	arbitrary units
C6NIB	2-hexyl-6-(4,4,5,5-tetramethyl-1,3,2-dioxaborolan-2-yl)-1H-benzo[de]isoquinoline-1,3(2H)-dione
C6NIO	2-hexyl-6-hydroxy-1H-benzo[de]isoquinoline-1,3(2H)-dione
CID	collision-induced dissociation
cm	centimeter
CTAB	cetrimonium bromide
DADP	diacetone diperoxide
DAT-B	diethyl 2,5-bis((((4-(4,4,5,5-tetramethyl-1,3,2-dioxaborolan-2-yl)benzyl)oxy)carbonyl)amino)terephthalate
DAT-N	diethyl 2,5-diaminoterephthalate
DESI	desorption electrospray ionization
DNT	dinitrotoluene
d-PET	donor-excited photoinduced electron transfer
dppf	1,1'-Bis(diphenylphosphino)ferrocene
eq	equivalents
ESIPT	excited-state intramolecular proton transfer
et al.	and others

etc.	and the rest
EtOH	ethanol
FRET	Föster Resonance Energy Transfer
GC	gas chromatography
GC-MS	gas chromatography–mass spectrometry
h	hour
H ₂ O ₂	hydrogen peroxide
HEPES	4-(2-hydroxyethyl)-1-piperazineethanesulfonic acid
HMTD	hexamethylene triperoxide diamine
HOMO	highest occupied molecular orbital
HRP	horseradish peroxidase
I	fluorescence intensity
I ₀	initial fluorescence intensity
ICT	intramolecular charge transfer
IMS	ion mobility spectroscopy
IR	infrared (spectroscopy or radiation)
k	reaction rate constant; s ⁻¹
k _{nr}	nonradiative decay rate
L	liter
LDA	linear discriminant analysis
LOD	limit of detection
LUMO	lowest unoccupied molecular orbital
M	mol·L ⁻¹
mg	milligram
min	minutes
MS	mass spectroscopy
MS	mass spectrometry
ms	millisecond
MTO	methyltrioxorhenium

ng	nanogram
nm	nanometer
nmol	nanomolar
NMR	nuclear magnetic resonance
NP	nanoparticle
PA	picric acid
PB	Prussian-blue
Pc	phthalocyanine
PET	photoinduced electron transfer
PETN	pentaerythritol tetranitrate
pH	$\text{pH} = -\log[\text{H}^+]$
PL1	Peroxy Lucifer 1
pmol	picomolar
ppb	parts per billion
ppm	parts per million
P_{vap}	vapor pressure
R^2	coefficient of determination
RDX	cyclotrimethylene trinitramine
ROS	reactive oxygen species
s	second
SCE	saturated calomel electrode
SERS	surface-enhanced Raman spectroscopy
SOMO	singly occupied molecular orbital
SPME	solid-phase microextraction
t	time
TATP	triacetone triperoxide
TBAH	tetrabutylammonium hydroxide
TBHP	tert-butyl hydroperoxide
tBu	tertiary butyl

TLC	thin-line chromatography
TMB	3,3',5,5'-tetramethylbenzidine
TMS	trimethylsilyl or trimethylsilane
TNT	trinitrotoluene
UV	ultra-violet
UV-vis	ultra-violet-visible radiation
ν	wave number, cm^{-1}
vs	versus, against
δ	chemical shift; ppm
ϵ	molar extinction coefficient; $\text{M}^{-1} \text{cm}^{-1}$
λ	wavelength, lambda
λ_{abs}	wavelength of absorption, lambda
λ_{em}	wavelength of emission, lambda
λ_{ex}	wavelength of excitation, lambda
λ_{max}	wavelength of maximum absorption/emission, lambda
π	pi; bond or orbital
π^*	pi-star; antibonding π orbital
τ_{F}	fluorescence lifetime
Φ	fluorescence quantum yield

ACKNOWLEDGEMENTS

I would like to thank my advisor, Professor Ling Zang, for bringing me into his lab and mentoring me for the last four years. He has a deep insight of both chemistry and life. Whenever I have problems, I know he is there and willing to help me out. He gives me tons of advice not only on chemistry but also about my life and career. I really enjoyed our discussion on chemistry, life and so on. I also want to thank my committee for their helpful discussion and advice.

I would like to thank all the past and current Zang lab members, Dr. Xiaomei Yang, Dr. Yanke Che, Dr. Chengyi Zhang, Dr. Zengxing Zhang, Dr. Ligui Li, Dr. Jimin Han, Dr. Helin Huang, Benjamin R. Bunes, Daniel L. Jacobs, Chen Wang, Yaqiong Zhang and Na Wu. It has really been my pleasure to work with all of you. Besides, I want to thank Dr. Dustin E. Gross and Professor Jian Pei for their help on material preparation. I also want to thank Professor Tao Yi for her advice and tutoring, making me realize that chemistry can be so beautiful and is my passion.

I would like to give my special appreciation to my wife Xiaoyun, who gave me two lovely children and keeps reminding how lucky I am. I would like to thank my parents for all these years of encouragement and support. I also want to thank my little Zhanghe and Carol, who make me laugh and proud every day. I am also grateful for the funding support from DHS, NSF and USTAR.

Chapter 2, in parts, is a reprint of the material as it appears in the following paper: Xu,

M.; Bunes, B. R.; Zang, L., Paper-Based Vapor Detection of Hydrogen Peroxide: Colorimetric Sensing with Tunable Interface. *ACS Appl. Mater. Interfaces* **2011**, *3*, 642-647.

Chapter 3, in parts, is a reprint of the material as it appears in the following paper: Xu, M.; Han, J.-M.; Zhang, Y.; Yang, X.; Zang, L., A Selective Fluorescence Turn-on Sensor for Trace Vapor Detection of Hydrogen Peroxide. *Chem. Commun.* **2013**, *49*, 11779-11781.

Chapter 4, in parts, is a reprint of the material as it appears in the following paper: Xu, M.; Han, J.-M.; Wang, C.; Yang, X.; Pei, J.; Zang, L., Fluorescence Ratiometric Sensor for Trace Vapor Detection of Hydrogen Peroxide. *ACS Appl. Mater. Interfaces* **2014**, *6*, 8708-8714.

CHAPTER 1

INTRODUCTION

In the past decade, the detection of peroxide-base explosives has drawn much research interest in the scientific community due to the increasing concerns about homeland security, military operational safety, as well as environmental and industrial safety. (1-9) This concern has resulted in the development of novel analytical methods and sensor techniques for fast and sensitive detection of the homemade explosives such as triacetone triperoxide (TATP, acetone) and hexamethylenetriperoxidediamine (HMTD). In this chapter, the recent advances of analytical methods and sensor techniques will be reviewed.

The synthesis of TATP (10) and HMTD (11) was accomplished in the late 18th century (for structure see Table 1.1), which includes three major precursors: hydrogen peroxide (H_2O_2), an acid (as catalyst), and acetone (for TATP) or hexamine (for HMTD). However, due to the extreme sensitivity to mechanical press, high volatility, weak stability, and lower explosive power (compared to trinitrotoluene (TNT)), these peroxide-based explosives were much less utilized in military or civilian applications than nitro explosives (e.g., TNT, dinitrotoluene (DNT), cyclotrimethylenetrinitramine (RDX), pentaerythritol tetranitrate (PETN) and picric acid (PA)). No requirement of blasting caps, ease of synthesis, along with readily commercially available sourcing materials make peroxide-based explosives highly favorable in improvised explosive devices (IEDs) for criminal and terrorist activities.

The use of peroxidized-base explosives in terrorist attacks was first found in Israel in 1980. (12) The development of detection methods for peroxidized-based explosives has drawn increasing attention during the last decade due to specific high profile terrorist attacks. For example, American Airlines Flight 63 in 2001, the Casablanca explosions in 2003, the London underground subway attacks in 2005 and a UK transatlantic flight bombing plot in 2006. (13-15) However, the detection of these explosives through direct sensing of the peroxide compounds remains difficult mainly due to the weak oxidizing power (weak electron affinity), lack of nitro-groups, weak UV-vis absorption, and lack of fluorescence emission, which prevent the detection through fluorescence sensing (usually based on electron transfer quenching), the conventional electronic detection systems and optical spectroscopy, respectively. Although chromatography has been explored for TATP detection, it can only work with liquid samples. Therefore, it must be combined with an effective sampling system for introducing the peroxide compounds into a solution, which is normally composed of an organic solvent like acetonitrile. (16) The operation of such multistep systems is typically time-consuming, often taking minutes to tens of minutes. Moreover, the use of organic (poisonous) solvents causes secondary pollution and safety threats. Additionally, chromatography based detection often suffers due to the poor selectivity and low sensitivity; although, these can be enhanced by combination with the spectrometry analysis (17-21). Indeed, the only reliable way that is currently available for identifying TATP and other peroxide compounds is to use these integrated chemical analysis systems in a laboratory, which otherwise are not suited for expedient onsite monitoring and screening.

To this end, H_2O_2 – which is a synthetic precursor (often leaked from the organic peroxides as synthetic impurities) and degradation product of TATP and HMTD – is

generally regarded as a signature compound for detecting peroxide explosives (12,22-24). TATP is one of the few explosives that can explode when wet or even kept under water, thereby removing the need of sophisticated purification after production. This is indeed an important practical reason why TATP and the analogous peroxides are highly favored by terrorists, as they can make the explosives simply in one-step mixing, and the raw products act just as powerful as the highly purified ones. As a consequence, water and H₂O₂ (which coexists with water) are common impurities present in homemade peroxide explosives. Moreover, H₂O₂ molecules can also be produced from the chemical decomposition of peroxide explosives (25-26), particularly under UV irradiation (17,27-28).

1.1 Current Sensing Methods for Peroxide-based Explosives

Scientists and engineers have developed various methods for peroxide-based explosive detection either based on their intrinsic properties (spectroscopic approaches, e.g., ion mobility spectroscopy, mass spectroscopy, Raman spectroscopy) or on the interaction with other species (sensor techniques, e.g., electrical, colorimetric and fluorescence sensors). In general, these detection techniques either suffer from sophisticated sample preparation, inaccuracy (a false positive signal due to environmental contaminants or a false negative due to interfering compounds), slow response (longer response time), low sensitivity (high warning threshold), or a lack of portability. Every method provides its own advantages and disadvantages. The method used is typically selected on the basis of an assessment of the field needs and the operations time/cost budget. Of the methods developed so far, explosives detection via optical spectral methods (colorimetry, fluorescence, and chemiluminescence) is growing most rapidly due to the promising results published recently. (6-8) Compared to chromatography techniques, these optical methods are lower

in cost (materials and instrumentation), require simpler instrumentation alignment (high portability), and possess higher sensitivity and selectivity, which combined facilitate broad field application. However, most of the optical methods developed so far are solution based, designed for biological, clinic, and environmental analysis; they are not suited for rapid, onsite vapor detection, since they will have to be combined with a vapor sampling unit to afford vapor detection of H_2O_2 . (29-30) In such cases, the preconcentration of H_2O_2 in a solution up to the level that is detected by the solution-based sensor could be time consuming and bring challenges to the device design and operation. Vapor detection, primarily relying on the gas-solid interfacial reaction, normally provides a much enhanced sensitivity compared to the solution-based sensory systems, where the analyte molecules are diluted in a relatively large volume of solvent (for which concentrating the analyte up to a certain detection threshold often takes time). In the following section, the methods currently used for peroxide-based explosive detection will be discussed in more detail.

1.1.1 Ion Mobility Spectroscopy

Ion mobility spectroscopy (IMS) is broadly used for field explosive detection mainly due to its portability, ease of use, rapid response, and high sensitivity (low detection limit). (31) The working principle of IMS is to characterize the drift time of ionized sample vapor under a certain electrical field (Figure 1.1). By determining the mass/charge ratio, the detection results are obtained by a comparison of the sample molecular mass with a standard targeting molecules library. In this system, a positive signal reflects a match of molecular mass between the sample and a target molecule. IMS is quite sensitive and selective, but its lack of portability for most cases, occasional detector saturation problems, and the need for careful system calibrations make it impractical for many cases and needs.

Another drawback is the ionization source, the most common sources are ^{63}Ni and ^{241}Am (32), which raises concerns about safety and environmental impact due to the intrinsic radioactivity of these sources.

The exploitation for IMS detection of TATP was first proposed by McGann et al. (33) In this report, the test conditions were optimized for targeting TATP. The positive mode was found more reasonable for TATP, which suggested that TATP tended to form a positive ion in the gas phase. Buttigieg et al. demonstrated another early example of IMS detection for TATP. (34) They also used the positive ion mode of IMS to detect TATP, before which the negative mode was dominant in explosive detection (targeting nitro-explosives). In 2008, Oxley et al. developed a method to use IMS to identify the explosive residue in human hair. (35) The high vapor pressure of TATP led to a quick desorption from a hair sample and became an experiment barrier. This barrier resulted in the need for a longer sample exposure time and larger sample amount for detecting TATP than nitro explosives. The limit of detection (LOD) was reported as $3.9\ \mu\text{g}$ in positive mode. A lot of research effort has been put on the miniaturisation and portability of IMS devices for field application. An aspiration-type IMS with semiconductor detectors was demonstrated to be efficient for vapor detection of TATP by Räsänen et al. (36) The semiconductor detectors were placed in individual channels to improve selectivity through the difference of landing species in different channels. A LOD of low milligrams per cubic meter in ambient condition was reported for this paper. However, the test of this device in more complicated conditions (with environmental interference) was not addressed in this report.

1.1.2 Mass Spectroscopy

Mass spectrometry (MS) has been explored as an effective explosive detection method for its specificity in identifying substances and fast detection speed. The working principle of MS is to separate and analyze the chemical composition of a sample based on their mass-to-charge (m/e) ratio. The separation methods can be concluded in two major categories, time separation and geometric separation. MS is superior in both detection time and extreme specificity; however, the high cost and large size of instrumentation, occasional detector saturation problems, and complicated sample preparation for high sensitivity hindered its wide application in explosive detection.

Kende et al. used gas chromatography-mass spectrometry (GC-MS) with solid-phase microextraction (SPME) for trace identification of TATP on various pre- and post-explosion models. (37) The polydimethylsiloxane fibers were used to trap TATP vapor and then were transferred to the injector of a gas chromatography (GC) system. The analysis process was finished within 20 min and the LOD was reported at 5 ng for TATP. Desorption electrospray ionization (DESI) mass spectrometry is used to detect and characterize the fragmentation of TATP. (19) Recently, Cooks et al. reported the use of DESI MS method for the rapid and trace detection of TATP directly from ambient surfaces without sample preparation. (20) The unique collision-induced dissociation (CID) of TATP complexes with Na^+ , K^+ , and Li^+ led to an elimination of a fragment of 30 mass units. The LODs of this method for peroxide-based explosives were reported in the low nanogram (ng) range. The ease for field application was demonstrated by the short analysis time (< 5 s to obtain spectra), no requirement of sample preparation combined with the high selectivity.

1.1.3 Raman Spectroscopy

Raman spectroscopy and surface-enhanced Raman spectroscopy (SERS) are based on optical scattering spectroscopy, which offer precise detection and identification for various targets, cost-effective instrumentation, and portability. (38) The working principle of Raman spectroscopy is that the specific vibrational transitions in a sample, through the collection and analysis of scattered photons under laser excitation, are determined based on its chemical structure. However, less flexible testing protocols and consistency issues (particularly for SERS) inhibit the more widespread use of this detection technique.

The near infrared radiation (IR) excitation laser in Raman spectrometry makes it possible to be used for standoff screening of explosives. Stoke et al. reported the use of Raman microscopy for direct and noninvasive detection of H₂O₂. (39) By monitoring the most distinct difference band (ν O-O, compared to water molecule) located at 871cm⁻¹, the LOD reached to < 1 % v/v (using 514.5nm and 632.8 nm lasers). The authors also applied this system on screening closed plastic bottles, and found that this setup reliably identified 30 % (w/w) H₂O₂ in 100 ms. Tsukruk and his co-workers reported the exploration of label free SERS to improve the LOD towards explosives down to the molecule-level. (40) The Raman signal can be enhanced greatly by the large electromagnetic fields which exists in the small gaps between metal nanoparticles (NPs). In their experiments, three-dimensional (3D) alumina membranes with cylindrical nanopores modified with polyelectrolytes coating were loaded with gold NPs clusters and served as the SERS substrate. The novelty of this substrate lies in both the utilization of additional waveguide ability of cylindrical nanopores and the high light transmission, in which the interaction between the incident light and the gold nanoparticle clusters was greatly increased. Compared to previous reports on using nanopores to enhance Raman signal, their work was not only exploring

the enlargement of the surface area but also the waveguiding or antenna properties of the substrate. This method gave a greatly enhanced LOD of around 1 pg for HMTD precipitated on this unique substrate. However, the need for appropriate SERS substrate and related sample preparation obstructed the field application of SERS on explosive detection. Pacheco-Londoño et al. demonstrated the successful improvement on Raman spectroscopy based explosive detection, which increased the signal to noise ratio and thus improved stand-off distance by using a continuous wave laser technique. (41) For Raman spectroscopy, 10 mg of TATP was detected at a distance of 7 m using 488 and 514.5 nm laser as excitation light. However, the experiments were conducted in the dark to minimize interferences from environmental light and thus were obstructed for application in the field.

1.1.4 Chemiresistive Sensors

The working principle of the chemiresistive sensor is based on the specific interaction between the sensor molecule and the analyte, which leads to a change in the resistance of the sensor material as a signal output. Recently, the development of chemiresistive sensors has drawn increasing interest due to the devices simplicity, high sensitivity, and reliability. (14) The main limitation of chemiresistive sensors is the lack of sufficient selectivity. There are two major approaches to address this issue: one is the surface modification to increase a specific interaction between the sensor, and the other is to use a sensor array combined with appropriate data analysis and a classification algorithm to enable differential sensing.

Wang and his co-workers have explored the application of Prussian-blue (PB)-modified electrode as a H_2O_2 sensor in both a solution and vapor phase. (42-44) The authors demonstrated the employment of PB electrodes as a rapid, expedient, reliable and sensitive electrochemical detection method for H_2O_2 in solution. The mechanism was based on the

high electrocatalytic activity of PB-modified electrodes towards H_2O_2 , which was generated from TATP by strong acid treatment. Due to the high operational stability of PB sensors, this sensing system was able to function under strong acidic medium (as low as pH 0.3). This method was superior to the peroxides-based assays because of the elimination of an extra neutralization step, which often suffered from the acid-induced enzyme deactivation processes. The optimized sensor system can detect 55 nM TATP (250 pg) in the electrochemical cell, considering the various dilutions. Later, Wang et al. expanded this PB-modified electrodes sensing system to trace vapor detection of H_2O_2 . (44) The authors used an agarose-casted PB modified thick-film carbon transducer for sensitive and selective amperometric vapor detection of H_2O_2 . The sensing system demonstrated an LOD of 0.1 % (w/w) H_2O_2 solution generated vapor (~286 ppb) in chronoamperometric mode and a much lower LOD of 0.008 % (w/w) H_2O_2 solution generated vapor (~23 ppb) in amperometric mode. These PB modified electrodes showed a well-defined selectivity over common interferences (i.e., common beverages). Recently, Karyakin et al. reported on novel PB modified electrodes on a membrane, which detected the H_2O_2 vapor generated from very diluted H_2O_2 solution (down to submicromolar). (45) The electrodes were made by screen printing on the polyethylene terephthalate membrane. The deposition of PB and nickel hexacyanoferrate double layer was performed *in situ* on the polyethylene terephthalate membrane. The interelectrode distance was chosen as 0.5 mm for response and noise concerns. This Ni-Fe transducer showed more stable response (no noticeable performance drop after 50 detection cycles) than regular PB modified electrodes.

Trogler and his co-worker exploited phthalocyanine (Pc) as the active layer for a chemiresistive H_2O_2 vapor sensor. (46) The sensing mechanism relies on the different charge carriers (holes) of metal-free ($\text{H}_2\text{-Pc}$) or metalated Pc (MPc) changes caused by the

Pc catalyzed chemical reaction (H_2O_2 decomposition for CoPc and radical reaction for NiPc, CuPc, H₂Pc). This study opened a new way to selectively target detection via catalytic redox difference. However, the organic-semiconductor based device apparently suffered from poor selectivity against humidity, oxygen and other oxidants present in the atmosphere. More importantly, the response time was found in the range of tens of minutes, which is insufficient for real case application, particularly for security monitoring in a moving traffic area.

There are several attempts at using metal oxides as chemiresistors for peroxide-based explosives. Metal oxides are superior in their ease of synthesis, have highly organized structure, and have high thermal stability for sensing applications. Misra et al. have explored Zn^{2+} doped titania nanotube array as a TATP sensor. (47) The large number of hydroxyl (Ti-OH) groups made it possible for doping zinc ion onto the nanotubular surface via ion exchange. As the TATP passed through the doped titania nanotube, the current on the nanotube increased. This increase in current was caused by the coordination interaction between the TATP and the zinc ion, which resulted in the lone pair of electron of oxygen in TATP released to the vacant d-orbitals of the zinc ion. It should be noted that all the measurements were carried out in glove box instead of ambient condition to eliminate the interference of other oxygen bonded compounds, i.e., water, carbon dioxide etc. Zhang et al. have employed In_2O_3 NPs (diameter ~16 nm) as vapor sensor for TATP. (48) The working principle of their device was that the charge carriers (electrons, generated owing to surface oxygen species) were captured when exposed to TATP vapor, and thus resulted in an increase in resistance. The optimal operational temperature was chosen as 270 °C for both response and recovery consideration. At a higher temperature, the surface oxygen species reacted with the TATP vapor, decreased the surface oxygen ion concentration,

increased the charge carrier concentration, and thus reduced the response. The response of the as-prepared device toward 10 mg TATP at 270 °C varied less than 10 % after 180 days, which proved the long-term stability and high reproducibility of this sensor device. This device was also exposed to various vapors of common decomposition compounds of TATP, (i.e., CH₄, acetone, CO₂, H₂O₂) and showed much lower response towards these vapors at 270 °C. This lower response indicated that few TATP vapors decomposed at 270 °C. The authors also examined the influence of common environmental interferences and found that the effect of water, CO₂ or other species in the air was minimal. The high power consumption of this sensor device (operational temperature 270 °C), the repeatability of the nanostructure and charge carrier density limit its field application. Recently, Dobrokhotov and his co-workers have used a nanospring-based silica structure coated with ZnO via atomic layer deposition, followed by metal NPs decoration as chemresistors, for TATP vapor. (49) This novel nanostructure combined the benefits of high surface area, gas-sensing ability from the metal oxides layer and catalytic properties from metal NPs, which led to high sensitivity (in ppb level) towards several high explosive vapors (e.g., TNT, TATP). The sensing mechanism mainly lies in the oxidization reaction between the analyte and surface oxygen ion, which at high temperature released electrons and thus increased the charge carrier density. The maximum sensor response was achieved at 400 °C; lower temperatures gave low surface oxygen vacancies and higher temperatures gave an increase in the oxygen desorption rate. The authors developed a linear discriminant analysis (LDA) algorithm and an integrated sensor-array for simultaneous real-time resistance monitoring. This setup was then examined for several flammable vapors, for which LODs were found at ppm levels. It should be noted that the repeatability of these nanospring structures was not fully discussed in this paper, nor was the power consumption issue of

the sensor array.

1.1.5 Colorimetric Sensors

Colorimetry methods are based on chemical binding or reaction of sensor molecules with a target analyte that can change the absorption in the visible light range and thus mutate the color of the sensing material. This method gives promising selectivity over other interferences due to the nature of the binding or reaction. This method offers high sensitivity to trace residue of explosive samples, which can be applied in vapor detection of explosive and small-scale liquid kits. It should be pointed out that deep color interferences can contaminate the test sample and result in a false positive signal.

Ti (IV) oxo complexes have been used as colorimetric indicators for H₂O₂ since the 1940s. (50) The sensing mechanism of these Ti (IV) oxo complexes towards peroxide is mainly based on coordination interaction between the H₂O₂ and the titanium metal center, which results in development of a deep color. The reaction kinetics of oxotitanium (IV) complexes towards H₂O₂ at various conditions were carefully examined by Tanaka et al. (51) The authors used a stopped-flow spectrophotometer to follow the faster reactions and a normal sample meter for slower reactions. The rate constant was found to be proportional to the H₂O₂ concentration when large excess H₂O₂ was presented. By considering the rate constant, enthalpy, entropy and activation volume of these reactions, the authors concluded that all the reactions of these titanium (IV) complexes with H₂O₂ were associatively activated. Takamura and Matsubara further explored the sensory application of oxo (5,10,15,20-tetra-4-pyridylporphinato) titanium (IV), TiO(tpyp) toward H₂O₂. (52) The high apparent molar absorptivity of the reacted TiO₂(tpypH₄)⁴⁺ complex ($1.1 \times 10^5 \text{ M}^{-1}\text{cm}^{-1}$) made it a promising candidates for colorimetric determination of H₂O₂. By monitoring

the absorption band of the reacted $\text{TiO}_2(\text{tpypH}_4)^{4+}$ complex at 450 nm, the LOD can be achieved as low as 25 pmol (batch method) and 0.5 pmol (flow injection analysis) in solution. Recently, Yu et al. reported on a facile synthesis of $\text{TiO}_2:\text{Ti}^{3+}$ NPs, which exhibited good detection ability on H_2O_2 and required no peroxidase substrate. (53) In solution the response time was much shorter than current colorimetric methods (less than 1 s) and the detection limit reached 5×10^{-7} M. The color change reaction was attributed to the Ti^{3+} (blue) in coordination with H_2O_2 and produced the yellow H_2TiO_4 . (54-55) The reducibility and high reaction rate were explained by the presence of Ti^{3+} on the surface of NPs and the high surface-to-volume area, respectively. These synthesized NPs demonstrated no obvious color change upon exposure to a large excess of HCl, NaClO, ethanol and acetone. However, little effort has been put into the stability of this material and employment of Ti complex as a vapor sensor for H_2O_2 .

There have been several attempts on H_2O_2 detection to take advantage of the redox reaction between H_2O_2 and other species. Mills et al. described a colorimetric method to detect H_2O_2 , in which a polymer film doped with triarlmethane dye, lissamine green was used as an indicator. (56) Upon exposure to H_2O_2 vapor, the original blue color of lissamine green gradually faded with increased time. This bleaching process was fitted in the first order kinetics with respect to the concentration of lissamine green and H_2O_2 . The film thickness seemed to influence the reaction kinetics, indicating the possible dependence upon the diffusion of the H_2O_2 vapor through the polymer film. Although this lissamine green showed a response to other strong oxidizing agents such as ozone and chlorine, the authors believed the faster response (less than 5 min), facile operation process (no wetting needed) and high stability made it a promising indicator candidate for strong oxidizing agents, especially TATP. Apak et al. reported on a copper(II)neocuproine assay, which

selectively detected TATP or HMTD (after acidic treatment) in solution at a submicro molar level ($\sim 9 \times 10^{-7}$ M). (57) The Cu(I)-neocuproine chromophore (reaction product) had a strong absorption band at 454 nm with a molar absorptivity around $4 \times 10^4 \text{ M}^{-1}\text{cm}^{-1}$. The recovery of TATP from a synthetic soil sample was higher than 90 %. This copper(II)neocuproine assay showed no response toward 100-fold excess of common ions (Ca^{2+} , K^+ , Cl^- , SO_4^{2-} , Mg^{2+} and NO_3^-) and 10-fold excess of nitro-explosives (e.g., TNT, RDX, PETN). The authors also validated this method with standard reference methods of TiOSO_4 colorimetry and GC-MS. It should be noted that the acidic treatment sample needed to be neutralized before exposure to assay. Zhan, X.Q. and Yan, J.H. described a colorimetric detection of H_2O_2 , which employed the H_2O_2 -mediated transformation of boronate to phenolate. (58) The sensor molecule gave a color change from colorless ($\lambda_{\text{max}} = 391 \text{ nm}$) to red ($\lambda_{\text{max}} = 522 \text{ nm}$). This strong red absorption ($\epsilon = 8.7 \times 10^4 \text{ M}^{-1}\text{cm}^{-1}$) was attributed to the intramolecular charge transfer (ICT) band. The linear range of this sensor response was in 1×10^{-7} to 2.5×10^{-5} M with the detection limit of 6.8×10^{-8} M under optimum conditions. Due to the specificity of the deprotection by H_2O_2 , the sensor showed almost no response to other common interferences (e.g., Ca^{2+} , K^+ , Cl^- , SO_4^{2-} , NO , Cl_2 , Mg^{2+} and NO_3^-). The authors applied this sensor to analyze the H_2O_2 concentration in rain water.

There are also many other efforts that have been focused on the employment of peroxidase-like activity of nanostructures to catalyze a reaction between a specific dye (e.g. 3,3',5,5'-tetramethylbenzidine (TMB)) and H_2O_2 to afford a deep color product. Perrett et al. reported on the discovery of such peroxidase-like activity on Fe_3O_4 NPs in 2007. (59) The authors found that the magnetic NPs catalyzed the reaction between TMB and H_2O_2 as peroxidase. The activity of the NPs was dependent on the concentration of H_2O_2 , pH and temperature. In general, the enzyme will lose its activity under harsh conditions such

as high temperature and extreme conditions. This loss in activity was much less in NPs than common peroxidase. By attaching the TMB on the surface of the NPs, the authors demonstrated that this Fe_3O_4 NPs could be used as a peroxidase mimetic. Li et al. demonstrated that positively-charged gold NPs (diameter ~ 34 nm) had an intrinsic peroxidase-like activity. (60) The catalyzed reaction between peroxidase substrate TMB and H_2O_2 resulted in a development of a deep blue color and thus enabled it to be a promising colorimetric detection method for H_2O_2 . The fabricated colorimetric assay showed good response toward H_2O_2 , which gave a LOD at 5×10^{-7} M under optimum conditions. These positively-charged Au NPs gave better activity under an acidic condition than neutral or basic condition, which was attributed to the maintenance of a surface positive charge under acidic conditions. There is little attempt on transferring this kind of peroxidase-like nanostructures to vapor detection of H_2O_2 .

Colorimetric sensor array has been explored as an effective detection method for volatile organic compounds. (61-63) Suslick K. S. and his co-workers have used a colorimetric sensor array for detection of TATP vapor. (26) The authors applied a sulfonic acid-functionalized ion-exchange resin (Amberlyst-15) as a catalyst to decompose TATP into acetone and H_2O_2 . The reason for choosing this catalyst was two-fold: 1) the researchers proposed a possible acid-catalyzed TATP decomposition mechanism, (64) and 2) this specific resin would not absorb as much TATP vapor (compared to silica gel). After passing through the solid acid catalyst (Amberlyst-15), the TATP molecule decomposed into acetone and H_2O_2 , and thus reacted with the redox sensitive dyes in the colorimetric array to afford a color change as a signal output. This colorimetric array was proven to be very sensitive toward the TATP decomposition products and gave a LOD as low as 2 ppb. The authors also investigated the potential interferences (e.g., humidity, personal hygiene

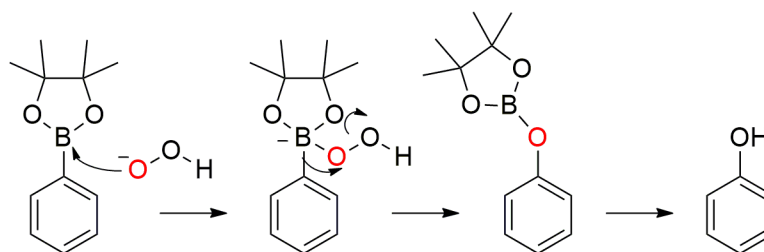
products, perfume, laundry supplies, volatile organic compound, etc.) and found that the sensor array showed minimal response toward these interferences. More important, the array could differentiate TATP from other oxidants, e.g., H₂O₂, bleach, tert-butylhydroperoxide, peracetic acid. This selectivity came from the ability of this array to respond to both acetone and H₂O₂. It should be noted that the data processing and algorithm of the discrimination process were complicated and hard to integrate into a real-time monitoring program.

1.1.6 Fluorescence Sensors

The fluorescence method (especially fluorescence turn-on and ratiometric sensor) is generally superior to colorimetry for its high sensitivity and low background (observing the emission change of the indicator molecule). (8) The sensing mechanism of fluorescence sensors is typically based on the quantum yield difference or emission wavelength shift of the sensor molecule after reacting with target analyte. The reasons for the quantum yield change are due to the formation of the intramolecular electron donor-acceptor structure (65), the inhibition of nonradiative deactivation (α -cleavage/radical recombination pathway) (66), or inhibition of photoinduced electron transfer (PET) process (67). The emission wavelength shift of the ratiometric sensor is typically due to the openness of the ICT band of the reacted state of the sensor molecule. In general, the reasons for high sensitivity of fluorescence turn-on sensors are: 1) detecting the appearance of a bright signal in a completely dark environment is easier than detecting the decrease of the bright signal, and 2) the stoichiometric binding event between turn-on sensors and analytes is more efficient than the collisional encounter event of the quenching sensors. The limitations of these fluorescent turn-on sensors come from the reproducibility issues caused by the influence

of sensor concentration, local environment, and excitation intensity. Ratiometric method, in which the change in two wavelengths can be monitored simultaneously, can greatly enhance the reliability and is also ideal for detection. The challenge lies in overcoming the high fluorescence background for ratiometric sensors.

Boronate oxidation reaction has been successfully employed to detect H_2O_2 in solution (Scheme 1.1). (68) The advantages of this chemical reaction are: 1) the high selectivity of H_2O_2 over other reactive oxygen species (ROS), and 2) this reaction is irreversible, and thus allows for the opportunity to accumulate a signal. The early example of a fluorescence turn-on sensor for H_2O_2 comes from Lo and colleagues. (69) Borylbenzyl alcohol was attached to the fluorophore coumarin to afford a low fluorescent compound. After exposure to H_2O_2 , the deboronation process resulted in a high fluorescent reporter coumarin and an emission enhancement. Chang and co-workers applied this boronate oxidation reaction in the detection of H_2O_2 in living cells. (70) The turn-on efficiency (defined as the emission intensity of the reacted state over the emission intensity of the pristine state) can reach to almost 1000. When exposed to other common ROS (e.g., tert-butyl hydroperoxide (TBHP), O_2^- , NO, $\cdot\text{OH}$, $\cdot\text{O}'\text{Bu}$, $\cdot\text{OCl}$), the sensor demonstrated almost no response to TBHP, O_2^- , NO and $\cdot\text{OCl}$ and much less response to $\cdot\text{OH}$ and $\cdot\text{O}'\text{Bu}$ with respect to H_2O_2 . Due to the two boronate function groups design, the sensitivity of the probe was not ideal. Later, Chang et al. reported on a molecule probe with a single boronate function group, which was first able to image peroxide produced for brain cell signaling. (71) These monoboronate caged fluorophores benefited from an improved sensitivity and so could be



Scheme 1.1 The reaction between boronate group and H_2O_2 .

applied on endogenous H_2O_2 detection. Knapp and his coworkers combined this boronate oxidization reaction with the metal complex to afford a turn-on fluorescent sensor for simple peroxides. (72) The sensing mechanism is that after the designed prochelator was exposed to H_2O_2 , the deboronation product H_2Salen binded free Zn^{2+} in the solution and became fluorescent $\text{Zn}(\text{Salen})$ as the reporter. The LODs for H_2O_2 , TATP and benzoyl peroxide were below 10 nM. It should be noted that the detection of TATP required an acidic treatment of the TATP sample before exposure to the sensory kit. Trogler et al. reported the application of a boronate-functionalized polymer as fluorescent sensor for H_2O_2 vapor. (73) They synthesized the energetically favored six-membered di-ester ring polymer from a monomer to improve the thermodynamic stability and prevent oxidization under ambient and UV light irradiation. The fluorescent response comes from the strong green emission from the oxidization state after being exposed to H_2O_2 . The LOD toward the H_2O_2 vapor was projected as low as 3 ppb over an 8 h period. For the liquid sample, the detection limit reached 1 ppm after 5 min of exposure. It should be noted that the hydrophobic surface of the polymer possibly inhibited the sampling of the H_2O_2 vapor, which is more hydrophilic. Besides, the polymer film used here gave a neutral environment for this reaction, but this boronate oxidization reaction is favored in basic condition.

Although the fluorescence enhancement method provides high sensitivity, the

influence of sensor concentration, local environment, and excitation intensity on the reliability limits the development of these molecular sensors. (74) In general, these challenges can be overcome by the exploitation of ratiometric fluorescence sensors. The early example of ratiometric fluorescent sensors for H_2O_2 comes from Chang and colleagues. (75) Their detection strategy relied on the control over the ICT states of a fluorophore to generate an emission wavelength shift upon reaction with H_2O_2 . The probe Peroxy Lucifer 1 (PL1) featured a specific chemical transformation upon exposure to H_2O_2 and an obvious emission color change (blue-to-green). Further experiments showed that PL1 was cell-permeable and able to visualize H_2O_2 produced in living cells by ratiometric imaging. Shabat and Sella synthesized a self-immolative dendritic probe through multiple cleavage reaction triggered by H_2O_2 or TATP. (76) The novelty of this study relied on the innovative molecular design which enabled the multirelease of fluorophore and amplified sensor response toward peroxide. The signal intensity generated from the dendritic polymer sensor was approximately three times higher than the control monomer, with similar background noise level. This dendritic polymer sensor was able to detect TATP at a microgram level. It should be noted that due to the nature of multistep release reaction, the response time of this sensor was relatively long (90-120 min incubation time). Recently, Jiang et al. reported a ratiometric fluorescent probe for H_2O_2 , which utilized excited-state intramolecular proton transfer (ESIPT) to further separate the emission of the pristine and reacted state and enhanced the turn-on efficiency. (77) The maximum emission wavelength of the pristine state was 405 nm (20 mM 4-(2-hydroxyethyl)-1-piperazineethanesulfonic acid (HEPES) buffer, 0.3 mM cetrimonium bromide (CTAB)), the emission wavelength red shifted to 510 nm after reacting with H_2O_2 . This probe was well encapsulated by CTAB molecules through the hydrophobic interaction of the long alkyl chains, and resulted in the

formation of the cationic aggregates. This formation of aggregates dramatically accelerated the reaction rate of the sensor with H_2O_2 . The authors concluded that they established a new route for the detection of H_2O_2 as well as a new strategy to design aggregation induced ratiometric based fluorescence sensors.

A few studies are focused on the manipulation of the oxidization state of sulfur to control the quantum yield between the pristine and reacted compounds to generate a signal output for H_2O_2 exposure. Finney et al. have done a systematic study on a series of pyrene derivatives, which contain either sulfur, sulfoxide or a highly oxidized state sulfone. (27) The authors found that for these pyrene derivatives, the sulfone substitute exhibited the strongest fluorescence (highest quantum yield); in contrast, the sulfoxide substitute gave the lowest quantum yield. They reasoned that the oxidized sulfone structure could suppress the dominant nonradiative deactivation pathway (α -cleavage/radical recombination) (66) for the excited state and led to an increase in the quantum yield. The authors found that with the presence of methyltrioxorhenium (MTO), the sulfoxide derivatives reacted with UV irradiated TATP and afforded a visual detection. The LOD of this visual method was 100 nmol of TATP. This method also demonstrated superior selectivity over $t\text{BuOOH}$, NaOCl , LiClO_4 , $\text{K}_2\text{Cr}_2\text{O}_7$, or air. The only interference they tested was KMnO_4 , which caused an increase in fluorescence intensity spontaneously. Swager and his coworkers applied this control of the sulfur oxidization state into fluorescent conjugated polymer to afford an oxidant agent sensor. (78) The synthesized model compounds and polymers containing thioethers showed an increase in fluorescence quantum yield after oxidized. The authors speculated that the increase in quantum yield caused by sulfur atoms oxidation was due to the increase of the rate of fluorescence (k_F), the decrease in the rate of nonradiative decay (k_{nr}) and thus an increase in the fluorescence lifetime (τ_F). Upon further investigation on

the photophysical studies and computation, they proposed that a larger overlap of the frontier molecular orbitals in the oxidized compounds compared to the unoxidized compounds was the reason for the increase in k_F . The model compounds and the polymer also showed fluorescence intensity enhancement upon H_2O_2 exposure with the presence of MTO, which demonstrated the potential to fabricate a sensor device for peroxide-based explosives.

The inhibition of the PET process is also applied to the design turn-on fluorescent sensor for H_2O_2 . The PET process is usually used to design fluorescence quenching sensors for nitro explosives, e.g., TNT, DNT, PA. (7,79) In the PET process an electron in the singly occupied molecular orbital (SOMO) of an excited fluorophore donates to the lowest unoccupied molecular orbital (LUMO) of the analyte (lower than the SOMO level) and cannot return to the highest occupied molecular orbital (HOMO) of the fluorophore, thus causing fluorescence quenching. Due to the similarity in the redox potential of nitro explosives, the selectivity of this fluorescence quenching method (making a distinction between different nitro compounds) is usually poor, hindering its broader application. Nagano et al. designed a fluorescein based fluorophore, for which the existence of the PET process dimmed the fluorescence, and the oxidization of the fluorophore inhibited the PET process and recovered the fluorescence. (67) The employment of the unique reaction between benzyl and H_2O_2 ensured the selectivity of this reaction. (80) According to their previous study, the fluorescein derivatives whose benzene moiety has a reduction potential higher than -1.8 V (vs saturated calomel electrode (SCE)) showed almost no fluorescence due to the donor-excited photoinduced electron transfer(d-PET) process. (81-82) The high reduction potential of benzil (-1.1 V) suggested that benzil should work as a fluorescence quenching moiety in the d-PET process, if it was close enough to the fluorophore. As a result, the benzil modified fluorescein had quantum yield (Φ_{FL}) of 0.004, which increased

to almost 0.8 after it reacted with H₂O₂. The complicated synthesized route and the typically low quantum yield of fluorescein in the solid state hinder its further exploration in vapor detection.

1.1.7 Chemiluminescence Sensors

Chemiluminescence refers to the luminescence (emission) which is a result of a chemical reaction. Chemiluminescence methods typically require reaction agents (to generate the high energy intermediate) and the reporter (highly fluorescent dye) to generate luminescence. The application of chemiluminescence in H₂O₂ detection has been known for decades (83); typical sensor systems include luminol chemiluminescence (84-85), peroxyoxalate chemiluminescence (86-87). Benefits from chemiluminescence detection can be concluded as: 1) no need for excitation light, and 2) simpler instrumentation required (only need a single light intensity detector, no requirement for monochromator or even filter). However, the high energy intermediate can be quenched during the diffusion process and the low quantum efficiency for nonenzymatic reactions (resulting in very weak light intensity) obstructs the further exploration of chemiluminescence detection.

Murthy and his co-workers described a peroxyoxalate chemiluminescence method for *in vivo* imaging of H₂O₂ with high specificity and sensitivity. (88) The novelty of their work lies in the encapsulation of the reporter and peroxyoxalate polymer into NP, which reduced the diffusion length of the high energy intermediate as well as increased local concentration of the reporter. Girotti et al. reported a quantitative chemiluminescent assay for peroxide-base explosives, the LOD of which can reach to 1.9×10^{-4} M (40 ng mL⁻¹) under optimal conditions. (89) The authors first treated the sample with an acidic solution to produce peroxides, which was transformed to radical derivatives by horseradish peroxidase (HRP),

and then quantified with luminescence from reaction with the luminol agent. When equipped with a portable luminometer, the authors demonstrated the application of this method in field application. The detection time of this method was short, only 5-10 min. Although the highly concentrated neutral detergent solution gave a signal comparable to the target samples, this assay showed good selectivity over numbers of interference, e.g., chlorates, perborates, percarbonates. The authors suggested using a parallel experiment to further distinguish between the target and the interferences (i.e., the emission from the acid-treated sample higher than the nonacidic one can be ascribed to the presence of the target analyte). Yao and Zhao et al. reported on the employment of organic nanowire with core/sheath structure as H_2O_2 vapor sensor for H_2O_2 , which can detect H_2O_2 vapor as low as 40 ppb. (90) The authors first described a general way to grow a one-dimensional core/sheath nanostructure, which had a H_2O_2 sensitive shell and a highly fluorescent core. Then this nanostructure was demonstrated to be selective and sensitive to H_2O_2 vapor via chemiluminescence method, due to the reactivity of the shell molecule towards H_2O_2 . The response time of this chemiluminescence method was relatively long (a few hundred seconds) as a result of the multistep energy transfer process. Finally, they proposed the utilization of evanescent wave coupling of the core and shell as an organic single-wire optical sensor with fast response (35 ms) toward H_2O_2 vapor. It should be noted that the light intensity of chemiluminescence was relatively low and thus the operational condition of the detector (photomultiplier) was relatively harsh (e.g., liquid nitrogen cooled and 1300 V operational voltage).

1.2 Motivations and Objectives

Trace vapor detection of H_2O_2 represents a practical approach to noninvasive detection of peroxide-based explosives, including liquid mixtures of H_2O_2 and fuels, and energetic peroxide derivatives, such as TATP, DADP and HMTD. Development of a simple chemical sensor system that responds to peroxide-based explosives with high reliability and sufficient sensitivity (reactivity) still remains a challenge. The challenge mainly comes from the weak oxidizing power (weak electron affinity), lack of nitro-groups, weak UV-vis absorption, and lack of fluorescence emission in the peroxide-based explosives. To this end, H_2O_2 – which is a synthetic precursor (often leaked from the organic peroxides as synthetic impurities) and degradation product of TATP and HMTD – is generally considered as a signature compound for detecting the peroxide explosives.

Compared to IMS, MS, Raman spectroscopy, chemiresistive sensors, optical sensor methods (e.g., those based on colorimetric and fluorescence modulation) have proven to be expedient, cost effective, reliable and sensitive approaches for trace detection of H_2O_2 . Vapor detection, primarily depending on the gas-solid interfacial reaction, normally provides enhanced sensitivity compared to the solution-based sensory systems and is more suitable for field application. The successful development of an optical sensor system suitable for trace vapor detection of H_2O_2 would rely on systematic optimization of several parameters of the sensor system, including: design of sensor molecule structure for specific surface reaction with H_2O_2 (to assure selectivity), interface engineering of material for efficient air sampling, and selection of reaction medium for fast sensor response.

To develop an ideal sensor system for trace vapor detection of H_2O_2 , my dissertation work was implemented around the following objectives:

- (1) Investigation of the molecule structure and chemical reaction employed in the

sensory system with the aim to approach high sensitivity and selectivity.

- (2) Interface engineering of the proposed sensor material to maximize the capture of the gas analyte and enhance the sensitivity.
- (3) Selection and examination of varying reaction media with the goal of reaching an optimal system that gives the fastest sensor response.
- (4) Systematic optimization of the sensory system to further enhance the detection sensitivity and reliability.

1.3 Reference

- (1) Yang, J.-S.; Swager, T. M. Fluorescent Porous Polymer Films as TNT Chemosensors: Electronic and Structural Effects. *J. Am. Chem. Soc.* **1998**, *120*, 11864-11873.
- (2) Naddo, T.; Che, Y.; Zhang, W.; Balakrishnan, K.; Yang, X.; Yen, M.; Zhao, J.; Moore, J. S.; Zang, L. Detection of Explosives with a Fluorescent Nanofibril Film. *J. Am. Chem. Soc.* **2007**, *129*, 6978-6979.
- (3) Zyryanov, G. V.; Palacios, M. A.; Anzenbacher, P. Simple Molecule-Based Fluorescent Sensors for Vapor Detection of TNT. *Org. Lett.* **2008**, *10*, 3681-3684.
- (4) Kartha, K. K.; Babu, S. S.; Srinivasan, S.; Ajayaghosh, A. Attogram Sensing of Trinitrotoluene with a Self-Assembled Molecular Gelator. *J. Am. Chem. Soc.* **2012**, *134*, 4834-4841.
- (5) Che, Y.; Gross, D. E.; Huang, H.; Yang, D.; Yang, X.; Discekici, E.; Xue, Z.; Zhao, H.; Moore, J. S.; Zang, L. Diffusion-Controlled Detection of Trinitrotoluene: Interior Nanoporous Structure and Low Highest Occupied Molecular Orbital Level of Building Blocks Enhance Selectivity and Sensitivity. *J. Am. Chem. Soc.* **2012**, *134*, 4978-4982.
- (6) Toal, S. J.; Trogler, W. C. Polymer Sensors for Nitroaromatic Explosives Detection. *J. Mater. Chem.* **2006**, *16*, 2871-2883.
- (7) Thomas, S. W.; Joly, G. D.; Swager, T. M. Chemical Sensors Based on Amplifying Fluorescent Conjugated Polymers. *Chem. Rev.* **2007**, *107*, 1339-1386.
- (8) Germain, M. E.; Knapp, M. J. Optical Explosives Detection: From Color Changes to Fluorescence Turn-On. *Chem. Soc. Rev.* **2009**, *38*, 2543-2555.
- (9) Caygill, J. S.; Davis, F.; Higson, S. P. J. Current Trends in Explosive Detection

Techniques. *Talanta* **2012**, 88, 14-29.

(10) Wolffenstein, R. Ueber Die Einwirkung Von Wasserstoffsuperoxyd Auf Aceton Und Mesityloxyd. *Ber. Dtsch. Chem. Ges.* **1895**, 28, 2265-2269.

(11) Legler, L. Ueber Die Sogenannte Aether- Oder Lampensäure. *Ber. Dtsch. Chem. Ges.* **1881**, 14, 602-604.

(12) Oxley, J. C. In *Detection of Liquid Explosives and Flammable Agents in Connection with Terrorism*; Schubert, H., Kuznetsov, A., Eds.; Springer Netherlands: 2008, p 27-38.

(13) Schulte-Ladbeck, R.; Vogel, M.; Karst, U. Recent Methods for the Determination of Peroxide-Based Explosives. *Anal. Bioanal. Chem.* **2006**, 386, 559-565.

(14) Wang, J. Electrochemical Sensing of Explosives. *Electroanalysis* **2007**, 19, 415-423.

(15) Burks, R.; Hage, D. Current Trends in the Detection of Peroxide-Based Explosives. *Anal. Bioanal. Chem.* **2009**, 395, 301-313.

(16) Chromatography Based Technologies Have Been Developed at Nanotherapeutics, Inc. For Detection of Peroxide Explosives: www.virtualacquisitionshowcase.com/docs/2007/nanothera-brief.pdf. *SBIR report of ONR* **2007**.

(17) Schulte-Ladbeck, R.; Edelmann, A.; Quintás, G.; Lendl, B.; Karst, U. Determination of Peroxide-Based Explosives Using Liquid Chromatography with on-Line Infrared Detection. *Anal. Chem.* **2006**, 78, 8150-8155.

(18) Widmer, L.; Watson, S.; Schlatter, K.; Crowson, A. Development of an Lc/Ms Method for the Trace Analysis of Triacetone Triperoxide (TATP). *Analyst* **2002**, 127, 1627-1632.

(19) Cotte-Rodriguez, I.; Chen, H.; Cooks, R. G. Rapid Trace Detection of Triacetone Triperoxide (TATP) by Complexation Reactions During Desorption Electrospray Ionization. *Chem. Commun.* **2006**, 953-955.

(20) Cotte-Rodriguez, I.; Hernandez-Soto, H.; Chen, H.; Cooks, R. G. In Situ Trace Detection of Peroxide Explosives by Desorption Electrospray Ionization and Desorption Atmospheric Pressure Chemical Ionization. *Anal. Chem.* **2008**, 80, 1512-1519.

(21) Wilson, P. F.; Prince, B. J.; McEwan, M. J. Application of Selected-Ion Flow Tube Mass Spectrometry to the Real-Time Detection of Triacetone Triperoxide. *Anal. Chem.* **2006**, 78, 575-579.

(22) Pacheco-Londono, L.; Primera, O. M.; Ramirez, M.; Ruiz, O.; Hernandez-Rivera, S. In *Proc. SPIE 5778* 2005; Vol. 5778, p 317-326.

(23) Oxley, J. C.; Smith, J. L.; Huang, J.; Luo, W. Destruction of Peroxide Explosives.

J. Forensic Sci. **2009**, *54*, 1029-1033.

(24) Oxley, J. C.; Smith, J. L.; Brady Iv, J. E.; Steinkamp, L. Factors Influencing Destruction of Triacetone Triperoxide (TATP). *Propellants, Explos., Pyrotech.* **2013**, *39*, 289-298.

(25) Dubnikova, F.; Kosloff, R.; Almog, J.; Zeiri, Y.; Boese, R.; Itzhaky, H.; Alt, A.; Keinan, E. Decomposition of Triacetone Triperoxide Is an Entropic Explosion. *J. Am. Chem. Soc.* **2005**, *127*, 1146-1159.

(26) Lin, H.; Suslick, K. S. A Colorimetric Sensor Array for Detection of Triacetone Triperoxide Vapor. *J. Am. Chem. Soc.* **2010**, *132*, 15519-15521.

(27) Malashikhin, S.; Finney, N. S. Fluorescent Signaling Based on Sulfoxide Profluorophores: Application to the Visual Detection of the Explosive TATP. *J. Am. Chem. Soc.* **2008**, *130*, 12846-12847.

(28) Schulte-Ladbeck, R.; Kolla, P.; Karst, U. A Field Test for the Detection of Peroxide-Based Explosives. *Analyst* **2002**, *127*, 1152-1154.

(29) Li, J. Z.; Dasgupta, P. K. Selective Measurement of Gaseous Hydrogen Peroxide with Light Emitting Diode-Based Liquid-Core Waveguide Absorbance Detector. *Anal. Sci.* **2003**, *19*, 517-523.

(30) Li, J.; Dasgupta, P. K. Measurement of Atmospheric Hydrogen Peroxide and Hydroxymethyl Hydroperoxide with a Diffusion Scrubber and Light Emitting Diode-Liquid Core Waveguide-Based Fluorometry. *Anal. Chem.* **2000**, *72*, 5338-5347.

(31) Ewing, R. G.; Atkinson, D. A.; Eiceman, G. A.; Ewing, G. J. A Critical Review of Ion Mobility Spectrometry for the Detection of Explosives and Explosive Related Compounds. *Talanta* **2001**, *54*, 515-529.

(32) Ewing, R.; Waltman, M. Mechanisms for Negative Reactant Ion Formation in an Atmospheric Pressure Corona Discharge. *Int. J. Ion Mobility Spectrom.* **2009**, *12*, 65-72.

(33) McGann, W.; Haigh, P.; Neves, J. L. Expanding the Capability of Ims Explosive Trace Detection. *Int. J. Ion Mobility Spectrom.* **2002**, *5*, 119-122.

(34) Buttigieg, G. A.; Knight, A. K.; Denson, S.; Pommier, C.; Bonner Denton, M. Characterization of the Explosive Triacetone Triperoxide and Detection by Ion Mobility Spectrometry. *Forensic Sci. Int.* **2003**, *135*, 53-59.

(35) Oxley, J. C.; Smith, J. L.; Kirschenbaum, L. J.; Marimganti, S.; Vadlamannati, S. Detection of Explosives in Hair Using Ion Mobility Spectrometry. *J. Forensic Sci.* **2008**, *53*, 690-693.

(36) Räsänen, R.-M.; Nousiainen, M.; Peräkorpi, K.; Sillanpää, M.; Polari, L.; Anttalainen, O.; Utriainen, M. Determination of Gas Phase Triacetone Triperoxide with Aspiration Ion Mobility Spectrometry and Gas Chromatography-Mass Spectrometry. *Anal.*

Chim. Acta **2008**, 623, 59-65.

(37) Kende, A.; Lebics, F.; Eke, Z.; Torkos, K. Trace Level Triacetone-Triperoxide Identification with Spme–Gc–Ms in Model Systems. *Microchim. Acta* **2008**, 163, 335-338.

(38) Moore, D. S.; Scharff, R. J. Portable Raman Explosives Detection. *Anal. Bioanal. Chem.* **2009**, 393, 1571-1578.

(39) Lindley, R.; Normand, E.; McCulloch, M.; Black, P.; Howieson, I.; Lewis, C.; Foulger, B. In *Proc. SPIE 7119* 2008; Vol. 7119, p 71190K-71190K-71111.

(40) Chang, S.; Ko, H.; Singamaneni, S.; Gunawidjaja, R.; Tsukruk, V. V. Nanoporous Membranes with Mixed Nanoclusters for Raman-Based Label-Free Monitoring of Peroxide Compounds. *Anal. Chem.* **2009**, 81, 5740-5748.

(41) Pacheco-Londoño, L. C.; Ortiz-Rivera, W.; Primera-Pedrozo, O. M.; Hernández-Rivera, S. P. Vibrational Spectroscopy Standoff Detection of Explosives. *Anal. Bioanal. Chem.* **2009**, 395, 323-335.

(42) Lu, D.; Cagan, A.; Munoz, R. A. A.; Tangkuaram, T.; Wang, J. Highly Sensitive Electrochemical Detection of Trace Liquid Peroxide Explosives at a Prussian-Blue 'Artificial-Peroxidase' Modified Electrode. *Analyst* **2006**, 131, 1279-1281.

(43) Munoz, R. A. A.; Lu, D.; Cagan, A.; Wang, J. 'One-Step' Simplified Electrochemical Sensing of TATP Based on Its Acid Treatment. *Analyst* **2007**, 132, 560-565.

(44) Benedet, J.; Lu, D. L.; Cizek, K.; La Belle, J.; Wang, J. Amperometric Sensing of Hydrogen Peroxide Vapor for Security Screening. *Anal. Bioanal. Chem.* **2009**, 395, 371-376.

(45) Komkova, M. A.; Karyakina, E. E.; Marken, F.; Karyakin, A. A. Hydrogen Peroxide Detection in Wet Air with a Prussian Blue Based Solid Salt Bridged Three Electrode System. *Anal. Chem.* **2013**, 85, 2574-2577.

(46) Bohrer, F. I.; Colesniuc, C. N.; Park, J.; Schuller, I. K.; Kummel, A. C.; Trogler, W. C. Selective Detection of Vapor Phase Hydrogen Peroxide with Phthalocyanine Chemiresistors. *J. Am. Chem. Soc.* **2008**, 130, 3712-3713.

(47) Subarna, B.; Susanta, K. M.; Mano, M.; Indu, B. M. The Detection of Improvised Nonmilitary Peroxide Based Explosives Using a Titania Nanotube Array Sensor. *Nanotechnology* **2009**, 20, 075502.

(48) Zhang, W.-H.; Zhang, W.-D.; Chen, L.-Y. Highly Sensitive Detection of Explosive Triacetone Triperoxide by an In₂O₃ Sensor. *Nanotechnology* **2010**, 21, 315502/315501-315502/315505.

(49) Dobrokhoto, V.; Oakes, L.; Sowell, D.; Larin, A.; Hall, J.; Kengne, A.; Bakharev, P.; Corti, G.; Cantrell, T.; Prakash, T.; Williams, J.; McIlroy, D. N. Toward the

Nanospring-Based Artificial Olfactory System for Trace-Detection of Flammable and Explosive Vapors. *Sens. Actuators, B* **2012**, *168*, 138-148.

(50) Eisenberg, G. Colorimetric Determination of Hydrogen Peroxide. *Ind. Eng. Chem. Anal. Ed.* **1943**, *15*, 327-328.

(51) Inamo, M.; Funahashi, S.; Tanaka, M. Kinetics of the Reaction of Hydrogen Peroxide with Some Oxotitanium (Iv) Complexes as Studied by a High-Pressure Stopped-Flow Technique. *Inorg. Chem.* **1983**, *22*, 3734-3737.

(52) Takamura, K.; Matsubara, C. Versatility of the Titanium(Iv) - Porphyrin Reagent for Determining Hydrogen Peroxide. *Bull. Chem. Soc. Jpn.* **2003**, *76*, 1873-1888.

(53) Pan, S. S.; Lu, W.; Zhao, Y. H.; Tong, W.; Li, M.; Jin, L. M.; Choi, J. Y.; Qi, F.; Chen, S. G.; Fei, L. F.; Yu, S. F. Self-Doped Rutile Titania with High Performance for Direct and Ultrafast Assay of H₂O₂. *ACS Appl. Mater. Interfaces* **2013**, *5*, 12784-12788.

(54) Jin, X.; Wang, X.; Wang, Y.; Ren, H. Oxidative Degradation of Amoxicillin in Aqueous Solution with Contact Glow Discharge Electrolysis. *Ind. Eng. Chem. Res.* **2013**, *52*, 9726-9730.

(55) Rehman, F.; Abdul Majeed, W. S.; Zimmerman, W. B. Hydrogen Production from Water Vapor Plasmolysis Using Dbd-Corona Hybrid Reactor. *Energy Fuels* **2013**, *27*, 2748-2761.

(56) Mills, A.; Grosshans, P.; Snadden, E. Hydrogen Peroxide Vapour Indicator. *Sens. Actuators, B* **2009**, *136*, 458-463.

(57) Eren, S.; Uezer, A.; Can, Z.; Kapudan, T.; Ercag, E.; Apak, R. Determination of Peroxide-Based Explosives with Copper(II)-Neocuproine Assay Combined with a Molecular Spectroscopic Sensor. *Analyst* **2010**, *135*, 2085-2091.

(58) Zhan, X.-Q.; Su, B.-Y.; Zheng, H.; Yan, J.-H. Sensing Hydrogen Peroxide Involving Intramolecular Charge Transfer Pathway: A Boronate-Functioned Styryl Dye as a Highly Selective and Sensitive Naked-Eye Sensor. *Anal. Chim. Acta* **2010**, *658*, 175-179.

(59) Gao, L.; Zhuang, J.; Nie, L.; Zhang, J.; Zhang, Y.; Gu, N.; Wang, T.; Feng, J.; Yang, D.; Perrett, S.; Yan, X. Intrinsic Peroxidase-Like Activity of Ferromagnetic Nanoparticles. *Nat. Nanotechnol.* **2007**, *2*, 577-583.

(60) Jv, Y.; Li, B.; Cao, R. Positively-Charged Gold Nanoparticles as Peroxidase Mimic and Their Application in Hydrogen Peroxide and Glucose Detection. *Chem. Commun.* **2010**, *46*, 8017-8019.

(61) Janzen, M. C.; Ponder, J. B.; Bailey, D. P.; Ingison, C. K.; Suslick, K. S. Colorimetric Sensor Arrays for Volatile Organic Compounds. *Anal. Chem.* **2006**, *78*, 3591-3600.

(62) Lim, S. H.; Feng, L.; Kemling, J. W.; Musto, C. J.; Suslick, K. S. An Optoelectronic

Nose for the Detection of Toxic Gases. *Nat. Chem.* **2009**, *1*, 562-567.

(63) Askim, J. R.; Mahmoudi, M.; Suslick, K. S. Optical Sensor Arrays for Chemical Sensing: The Optoelectronic Nose. *Chem. Soc. Rev.* **2013**, *42*, 8649-8682.

(64) Armitt, D.; Zimmermann, P.; Ellis-Steinborner, S. Gas Chromatography/Mass Spectrometry Analysis of Triacetone Triperoxide (TATP) Degradation Products. *Rapid Commun. Mass Spectrom.* **2008**, *22*, 950-958.

(65) Gruen, H.; Goerner, H. Trans-Fwdarw. Cis Photoisomerization, Fluorescence, and Relaxation Phenomena of Trans-4-Nitro-4'-(Dialkylamino)Stilbenes and Analogues with a Nonrotatable Amino Group. *J. Phys. Chem.* **1989**, *93*, 7144-7152.

(66) Guo, Y.; Jenks, W. S. Photolysis of Alkyl Aryl Sulfoxides: A-Cleavage, Hydrogen Abstraction, and Racemization I. *J. Org. Chem.* **1997**, *62*, 857-864.

(67) Abo, M.; Urano, Y.; Hanaoka, K.; Terai, T.; Komatsu, T.; Nagano, T. Development of a Highly Sensitive Fluorescence Probe for Hydrogen Peroxide. *J. Am. Chem. Soc.* **2011**, *133*, 10629-10637.

(68) Lippert, A. R.; Van de Bittner, G. C.; Chang, C. J. Boronate Oxidation as a Bioorthogonal Reaction Approach for Studying the Chemistry of Hydrogen Peroxide in Living Systems. *Acc. Chem. Res.* **2011**, *44*, 793-804.

(69) Lo, L. C.; Chu, C. Y. Development of Highly Selective and Sensitive Probes for Hydrogen Peroxide. *Chem. Commun.* **2003**, 2728-2729.

(70) Chang, M. C. Y.; Pralle, A.; Isacoff, E. Y.; Chang, C. J. A Selective, Cell-Permeable Optical Probe for Hydrogen Peroxide in Living Cells. *J. Am. Chem. Soc.* **2004**, *126*, 15392-15393.

(71) Miller, E. W.; Tulyanthan, O.; Isacoff, E. Y.; Chang, C. J. Molecular Imaging of Hydrogen Peroxide Produced for Cell Signaling. *Nat. Chem. Biol.* **2007**, *3*, 263-267.

(72) Germain, M. E.; Knapp, M. J. Turn-on Fluorescence Detection of H₂O₂ and TATP. *Inorg. Chem.* **2008**, *47*, 9748-9750.

(73) Sanchez, J. C.; Trogler, W. C. Polymerization of a Boronate-Functionalized Fluorophore by Double Transesterification: Applications to Fluorescence Detection of Hydrogen Peroxide Vapor. *J. Mater. Chem.* **2008**, *18*, 5134-5141.

(74) Yuan, L.; Lin, W.; Zheng, K.; Zhu, S. FRET-Based Small-Molecule Fluorescent Probes: Rational Design and Bioimaging Applications. *Acc. Chem. Res.* **2013**, *46*, 1462-1473.

(75) Srikun, D.; Miller, E. W.; Domaille, D. W.; Chang, C. J. An Ict-Based Approach to Ratiometric Fluorescence Imaging of Hydrogen Peroxide Produced in Living Cells. *J. Am. Chem. Soc.* **2008**, *130*, 4596-4597.

- (76) Sella, E.; Shabat, D. Self-Immolative Dendritic Probe for Direct Detection of Triacetone Triperoxide. *Chem. Commun.* **2008**, 5701-5703.
- (77) Li, G.; Zhu, D.; Liu, Q.; Xue, L.; Jiang, H. Rapid Detection of Hydrogen Peroxide Based on Aggregation Induced Ratiometric Fluorescence Change. *Org. Lett.* **2013**, *15*, 924-927.
- (78) Dane, E. L.; King, S. B.; Swager, T. M. Conjugated Polymers That Respond to Oxidation with Increased Emission. *J. Am. Chem. Soc.* **2010**, *132*, 7758-7768.
- (79) Zang, L.; Che, Y.; Moore, J. S. One-Dimensional Self-Assembly of Planar Π -Conjugated Molecules: Adaptable Building Blocks for Organic Nanodevices. *Acc. Chem. Res.* **2008**, *41*, 1596-1608.
- (80) Sawaki, Y.; Foote, C. S. Acyclic Mechanism in the Cleavage of Benzils with Alkaline Hydrogen Peroxide. *J. Am. Chem. Soc.* **1979**, *101*, 6292-6296.
- (81) Ueno, T.; Urano, Y.; Setsukinai, K.-i.; Takakusa, H.; Kojima, H.; Kikuchi, K.; Ohkubo, K.; Fukuzumi, S.; Nagano, T. Rational Principles for Modulating Fluorescence Properties of Fluorescein. *J. Am. Chem. Soc.* **2004**, *126*, 14079-14085.
- (82) Urano, Y.; Kamiya, M.; Kanda, K.; Ueno, T.; Hirose, K.; Nagano, T. Evolution of Fluorescein as a Platform for Finely Tunable Fluorescence Probes. *J. Am. Chem. Soc.* **2005**, *127*, 4888-4894.
- (83) Schuster, G. B. Chemiluminescence of Organic Peroxides. Conversion of Ground-State Reactants to Excited-State Products by the Chemically Initiated Electron-Exchange Luminescence Mechanism. *Acc. Chem. Res.* **1979**, *12*, 366-373.
- (84) Huntress, E. H.; Stanley, L. N.; Parker, A. S. The Oxidation of 3-Aminophthalhydrazide ("Luminol") as a Lecture Demonstration of Chemiluminescence. *J. Chem. Educ.* **1934**, *11*, 142.
- (85) Nieman, T. In *Chemiluminescence and Photochemical Reaction Detection in Chromatography*; Wiley: New York, 1989, p 99-123.
- (86) Givens, R. S. S., R. L. In *Chemiluminescence and Photochemical Reaction Detection in Chromatography*; Wiley: New York, 1989, p 125-147.
- (87) Orosz, G.; Givens, R. S.; Schowen, R. L. A Model for Mechanism of Peroxyoxalate Chemiluminescence as Applied to Detection in Liquid Chromatography. *Crit. Rev. Anal. Chem.* **1996**, *26*, 1-27.
- (88) Lee, D.; Khaja, S.; Velasquez-Castano, J. C.; Dasari, M.; Sun, C.; Petros, J.; Taylor, W. R.; Murthy, N. In Vivo Imaging of Hydrogen Peroxide with Chemiluminescent Nanoparticles. *Nat. Mater.* **2007**, *6*, 765-769.
- (89) Girotti, S.; Ferri, E.; Maiolini, E.; Bolelli, L.; D'Elia, M.; Coppe, D.; Romolo, F. S. A Quantitative Chemiluminescent Assay for Analysis of Peroxide-Based Explosives. *Anal.*

Bioanal. Chem. **2011**, *400*, 313-320.

(90) Zheng, J. Y.; Yan, Y.; Wang, X.; Shi, W.; Ma, H.; Zhao, Y. S.; Yao, J. Hydrogen Peroxide Vapor Sensing with Organic Core/Sheath Nanowire Optical Waveguides. *Adv. Mater.* **2012**, *24*, OP194-OP199.

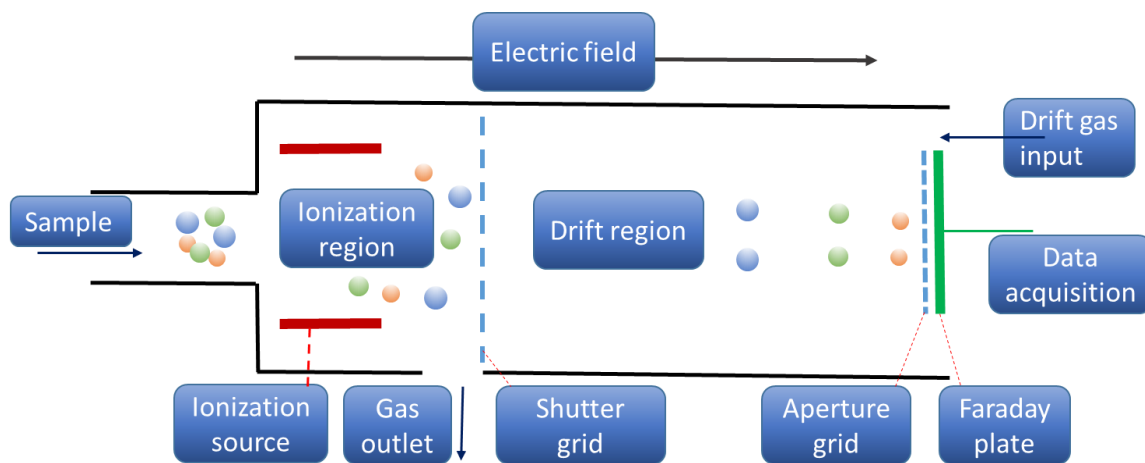
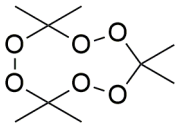
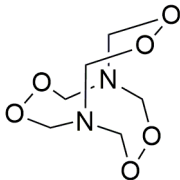


Figure 1.1 A schematic of a simplified ion mobility spectrometer.

Table 1.1 Properties of targeted explosives. Adapted with permission from Burks, R.; Hage, D. Current Trends in the Detection of Peroxide-Based Explosives. *Anal. Bioanal. Chem.* **2009**, 395, 301-313. Copyright (2009) Springer-Verlag

Explosive	Explosive Category	Structure	MP(°C)	P _{vap} (Pa)	Detonation velocity (m s ⁻¹)
TATP	primary		96	7.87	5300
HMTD	primary		148	n/a	5100

CHAPTER 2

PAPER-BASED VAPOR DETECTION OF HYDROGEN PEROXIDE: COLORIMETRIC SENSING WITH TUNABLE INTERFACE¹

2.1 Abstract

Vapor detection of hydrogen peroxide still remains challenging for conventional sensing techniques, though such vapor detection implies important applications in various practical areas, including locating-IEDs. We report herein a new colorimetric sensor system that can detect hydrogen peroxide vapor down to lower ppb levels. The sensory materials are based on the cellulose microfibril network of paper towels, which provide a tunable interface for modification with Ti(IV) oxo complexes for binding and reacting with H₂O₂. The Ti(IV)-peroxide bond thus formed turns the complex from colorless to bright yellow with an absorption maximum around 400 nm. Such complexation-induced color change is exclusively selective for hydrogen peroxide, with no color change observed in the presence of water, oxygen, common organic reagents or other chelating reagents. This paper-based sensor material is disposable and one-time use, representing a cheap, simple approach to detect peroxide vapors. The reported sensor system also proves the technical

¹ Reprinted with permission from Xu, M.; Bunes, B. R.; Zang, L., Paper-Based Vapor Detection of Hydrogen Peroxide: Colorimetric Sensing with Tunable Interface. *ACS Appl. Mater. Interfaces* **2011**, 3, 642-647. Copyright (2011) American Chemical Society.

feasibility of developing enhanced colorimetric sensing using nanofibril materials that will provide plenty of room to enlarge the surface area (by shrinking the fiber size), so as to enhance the surface interaction with gas phase.

2.2 Introduction

Nanofibril-based materials have widely been employed in various electrical, optical and optoelectronic sensor systems for vapor detection of chemical reagents, mainly due to their large surface area and the interface tunability for strong, highly selective surface binding. (1-15) Compared to conventional solid films, nanofibers, upon deposition onto a substrate, form a layer of materials through cross-piling of the fibers. (13) This film-like material possesses continuous three-dimensional porosity, which allows free diffusion of gas molecules throughout the materials matrix, resulting in expedient gas collection and accumulation, and thus fast response for vapor detection of gas analytes. Indeed, fast sensing response in the time range of seconds or even milliseconds, were previously reported from the nanofibril based fluorescent materials. (13,16-19) Fast response is crucial for fast, onsite detection of threatening chemicals, particularly explosives and hazardous gases.

In the past few years, various fluorescent nanofibers were developed for chemical vapor detection through fluorescent emission quenching. These sensor systems have proven to be one of the most sensitive and convenient methods used for expedient detection of nitro-based explosives and organic amines. (13) However, few studies have been performed to extend the nanofibril sensor systems beyond fluorescence quenching, to other chemical sensing mechanisms, particularly colorimetric sensing, while still maintaining the superior features of nanofibril materials that are suited for vapor detection, including the large

porosity, large surface area and interface tunability. Colorimetric sensing, relying on chemical binding/complexation induced color change, represents a simple, but sensitive, detection technique widely used in chemical detection in solution, (20-25) though there are few cases reported for vapor detection, especially with nanofibril materials. We report here, for the first time, a proof-of-concept study of colorimetric vapor detection of hydrogen peroxide using fibril based sensory materials.

The driving force behind this work is twofold; one reason is to expand the fundamental science of colorimetric sensing to fibril mesostructured materials for vapor detection and the other is more practically driven, to develop a methodology for vapor detection of hydrogen peroxide, which still remains challenging for current sensing techniques. (26) Particularly, the fibril sensory materials employed in this study were fabricated from common paper towels, which compose cellulose fibril network (Figure 2.1) suited for interface engineering to enable efficient vapor sensing. Although the fiber size is in the range of microns (not as essentially as small as nanometers), this fibril network structure is ideal as a test to prove the feasibility of using colorimetric sensing for vapor detection, for which the bleach paper possesses a bright, high-contrast background for color change reading. Moreover, toward practical application, development of sensor systems based on papers represents a simple, cheap approach that may lead to manufacturing of portable, disposable devices as evidenced by the works of Whitesides and others. (27-30)

Vapor detection of hydrogen peroxide not only implies practical applications in industrial and biorelated monitoring, but will provide a new way to detect the peroxide explosives such as triacetone triperoxide (TATP), from which hydrogen peroxide can be identified as a signature compound. (31-33) Peroxide explosives are essentially as deadly as conventional high explosives, but can be manufactured cheaply and easily at home from

off-the-shelf ingredients, and therefore are often used for making improvised explosives devices (IEDs). Moreover, detection of these explosives through direct sensing of the peroxide compounds remains difficult for fluorescence sensing and conventional electronic detection systems. (34-37) To this end, H_2O_2 , which often leaks from organic peroxides as synthetic impurities or can be generated from the chemical decomposition of peroxide explosives, (37-38) particularly under UV irradiation (31-33), is generally considered as a signature compound for detecting peroxide explosives. However, the development of vapor sensing of hydrogen peroxide is not as advanced as the solution-based approach, for which various molecular probes have been developed. (22,26,39-48) This is mainly because of the lack of appropriate sensory materials that can not only demonstrate sensitive, selective response to the adsorption of hydrogen peroxide, but also provide fast collection and accumulation of hydrogen peroxide in the vapor phase, particularly in an open atmosphere.

2.3 Results and Discussion

We report herein a new colorimetric sensor system that can be used for efficient vapor detection of hydrogen peroxide. As shown in Figure 2.1, the colorimetric sensing employed in this study relies on the peroxide complexation to the Ti(IV) oxo complex ($>\text{Ti}=\text{O}$), which is intrinsically colorless (i.e., with no absorption in the visible region), but turns to bright yellow upon complexation with hydrogen peroxide through formation of the Ti(IV)-peroxide bond (with absorption maximum around 400 nm). (22,39,49-50) Such complexation-induced color change is exclusively selective for hydrogen peroxide, with no color change observed in the presence of water, oxygen, or common organic reagents such as alcohols, hexane, acetone, etc. The Ti(IV)-peroxide colorimetric complexation was previously employed for the spectrophotometry detection of hydrogen peroxide in

solutions. (22,39,41-42,44,49-52) To adapt the colorimetric sensing from solution phase to a solid state suitable for vapor detection, the Ti(IV) species must be well dispersed throughout the supporting matrix to maximize exposure to gases, while maintaining its chemical activity (for complexation with hydrogen peroxide) and stability (against hydrolysis into the inactive oxides, e.g., TiO₂).

In this study, we used paper towel as the template material, wherein the cellulose microfibril networks provide a large interface to be modified with the Ti(IV) oxo species to facilitate efficient colorimetric sensing of hydrogen peroxide. These paper-based sensory materials thus prepared possess the unique features that are desirable for vapor sampling and detection, including 1) continuous pore channels, allowing for efficient diffusion of gaseous molecules throughout the film matrix, making it possible to fabricate a thick film to increase the optical density and thus enhance the sensing accuracy; 2) a three-dimensional microscopic structure that allows for maximal distribution of the Ti(IV) oxo moiety on the surface, thus enabling maximal exposure to the gaseous analytes; 3) a colorless background in the pristine state (i.e., before exposure to hydrogen peroxide) allowing for high contrast measurement of the color formation.

Ammonium titanyl oxalate (structure shown in Figure 2.1) was chosen for this study because of its colorless background and robust stability against hydrolysis, as well as its high solubility in water (significantly higher than its potassium salt). Another colorless Ti(IV) oxo complex, titanium(IV) oxysulfate was also tested initially, though it was not chosen for the following sensor investigations due to its limited aqueous solubility. To confirm the stoichiometric colorimetric reaction between the titanyl salt and hydrogen peroxide, we performed a titration experiment over a solution of ammonium titanyl oxalate solution (1.2×10^{-4} M) with the addition of hydrogen peroxide at various molar ratios,

shown in Figure 2.2; the color formation (due to production of titanium-peroxide, Figure 2.1) was monitored by measuring the UV-vis absorption spectra of the solution. A plot of the absorbance at the maximum (378 nm) as a function of the molar ratio of $\text{H}_2\text{O}_2/\text{Ti(IV)}$ indicates that the color formation saturates at a molar ratio of 1:1, proving the 1:1 stoichiometric reaction between H_2O_2 and Ti(IV) salt as illustrated in Figure 2.1.

As detailed in the Experimental Methods section, titanyl oxalate was coated onto the cellulose fibrils by drop-casting a fixed volume of water solution of the salt onto a small piece of paper towel. By changing the concentration of titanyl oxalate, the loading amount within the paper matrix can be adjusted as needed. This drop-casting method proved effective for producing a homogeneous distribution of titanyl salt among the cellulose fibril networks of the paper towel (see Figure 2.3). These paper-based sensor materials demonstrated bright yellow color formation upon exposure to the vapor of hydrogen peroxide (Figure 2.1), whereas no response was observed to other common liquids or solid chemicals, proving extreme selectivity towards hydrogen peroxide. To prove the selectivity of titanyl oxalate salt towards hydrogen peroxide, we performed UV-vis absorption spectral measurements for the colorimetric reaction between H_2O_2 and Ti(IV) salt (deposited on a quartz slide as a thin film), and compared to various other common solvents by exposing the same Ti(IV) salt film to these vapors. As shown in Figure 2.4, despite the much higher vapor pressure of the solvents, the titanyl oxalate film demonstrated negligible colorimetric response to these solvents, i.e., minimal absorbance was detected at the same maximum wavelength after 600 seconds of vapor exposure. In contrast, upon exposure to the saturated vapor of 35 wt % H_2O_2 solution, the same film demonstrated intense color formation as measured at 386 nm.

Generally, the higher the load of the titanyl oxalate species, the more hydrogen

peroxide can be captured and complexed within a certain time, thus leading to increased sensing efficiency. However, a further increase in the salt loading would restrain the porosity, causing a decrease in vapor accessibility. Such a tradeoff is clearly shown by the data in Figure 2.5a, where initially the color change (defined as Δb , the color change between yellow and blue in the CIELAB color space system) increases with the loading amount of titanyl salt. After passing the loading level of 20 μmol (for a $2.5 \times 2.5 \text{ cm}^2$ paper towel), a continuous increase of titanyl salt led to a decrease in the color change, indicative of a shrinking of surface area. Figure 2.5b shows the values of Δb recorded at three time intervals (20, 100, 240 s) plotted as a function of the molar amount of titanyl salt loaded. All the three plots show the same trend of change, yielding an optimal loading level of titanyl salt, 20 μmol .

The data presented in Figure 2.5a can be fitted following the reaction kinetics equation,

$$\Delta b = K'(1 - e^{-Kt}) \quad (2.1)$$

where K and K' are constants with K related to the given vapor pressure of H_2O_2 and the total load of titanyl salt and K' referred to as the ratio of the color density to the molar amount of surface complexed hydrogen peroxide. Derivation of this equation is based on the surface adsorption kinetics, i.e., rate of absorption is proportional to the surface density of the unreacted Ti(IV) sites. From equation (2.1), we can get the color change rate,

$$\partial(\Delta b) / \partial t = K'Ke^{-Kt} \quad (2.2)$$

At time zero ($t = 0$), we have the initial color change rate $\partial(\Delta b)/\partial t = K'K$. Since both K and K' can be deduced from the fitting shown in Figure 2.5a, the initial color change rates were thus obtained for the different loading levels of titanyl salt. Plotting these initial rates as a function of the molar load of titanyl salt (right axis of Figure 2.5b) gives the same trend of change as plotted for the absolute color change at different time intervals (left axis of Figure 2.5b), indicating the same optimal loading of 20 μmol . The color change rate represents a parameter that directly relates to the response speed of a sensor material, while the absolute value of color change recorded at a given time is usually used for evaluating the sensitivity or detection limit. Interestingly, plots regarding both parameters (as shown in Figure 2.5b) produce the same optimal value for the load of titanyl salt. In the following experiments, all paper towels were kept at the same size of $2.5 \times 2.5 \text{ cm}^2$ and loaded with titanyl salt at a fixed amount of 20 μmol , with the aim to detect hydrogen peroxide at various diluted vapor pressures.

We expected that the wide interface and large porosity of the cellulose fibril networks would make the paper towel ideal for fast vapor response. To compare, we investigated the time course of the colorimetric reaction between the H_2O_2 vapor and the solid thin film of Ti(IV) salt, shown in Figure 2.6. The thin film was made by drop-casting 130 μL of 0.1 M aqueous solution of ammonium titanyl oxalate onto a quartz slide to make a film of an area of ca. 4 cm^2 , so that the molar amount of Ti(IV) salt per unit area is approximately the same as the amount of 20 μmol loaded onto a $2.5 \times 2.5 \text{ cm}^2$ size of paper towel as shown in Figure 2.5. The UV-vis absorption spectrum of the film (with bare quartz slide as reference) was measured at various time intervals after exposure to the saturated vapor of 35 wt % H_2O_2 solution (225.4 ppm), shown in Figure 2.6a. The color formation saturates after about 600 s of vapor exposure (Figure 2.6b), about four times slower than the paper towel sample,

for which the same amount of titanyl salt saturates around 150 s (Figure 2.5).

Shown in Figure 2.7a are the values of Δb as a function of exposure time, measured under a series of equilibrium vapor pressures of H_2O_2 , which were obtained by diluting the 35 wt % aqueous solution with water. All data fit very well to equation (2.1). It can be clearly seen from Figure 2.7a that the higher the vapor pressure of hydrogen peroxide, the faster the color forms. This is consistent with the surface adsorption kinetics as discussed above. When the vapor pressure of H_2O_2 was low, i.e., around or below 1.0 ppm, it took much longer to reach the equilibrium plateau, and more interestingly, within the early time regime (e.g., 900 s as investigated in our study here) Δb changes almost linearly with time. This is not surprising, if considering the small value of Kt , which allows the kinetics equation (2.1) to be simplified to a linear dependence on time,

$$\Delta b = K'K t \quad (2.3)$$

Therefore, for low vapor pressures of H_2O_2 , we have the slope $\Delta b/\Delta t = K' K$. Since K is proportional to the vapor pressure, it is expected that $\Delta b/\Delta t$ will be linearly dependent on the vapor pressure of H_2O_2 . This linear relationship is indeed shown in Figure 2.7b, where for the low vapor pressures (0.1, 0.2, 0.3, 0.5 and 1.0 ppm) the slopes ($\Delta b/\Delta t$) as extracted from the plots in Figure 2.7a are replotted as a function of the vapor pressure of H_2O_2 . Considering the measurement sensitivity of the color reader ($\Delta b = 0.1$), and if allowing for a detection response time of 10 s, we have $\Delta b/\Delta t = 0.01$, which corresponds to a vapor pressure of 0.4 ppm as indicated in Figure 2.7b. This value (corresponding to 250 times dilution of the commercial 35 wt % H_2O_2 solution) can be roughly considered as the detection limit for the vapor of hydrogen peroxide under current measurement

conditions. Upon further improvement and optimization of the measuring system, particularly by integration into a closed detector system (for maximized vapor sampling), the detection limit is expected to be improved down to the lower ppb range.

2.4 Conclusion

In conclusion, we have developed an efficient colorimetric sensing system for the vapor detection of hydrogen peroxide. The sensory materials are based on the cellulose fibril network of paper towels, which provides a tunable interface for modification with Ti(IV) oxo complexes for binding and reaction with H₂O₂. This one time use paper-based sensor material can provide a simple and economical method for peroxides vapor detection. Prospectively, the reported vapor sensor system proves the technical feasibility of developing enhanced colorimetric sensing using nanofibril materials that will be fabricated from building-block molecules functionalized with a Ti(IV) oxo moiety. Such a “bottom-up” approach will provide plenty of opportunities to enlarge the surface area (by shrinking the fiber size), enhancing the surface interaction with gas phase. Research along this line is underway.

2.5 Experimental Methods and Materials

2.5.1 Materials and General Instrumentations

UV-vis absorption spectra were measured on a PerkinElmer Lambda 25 spectrophotometer. Optical microscopy imaging was performed with a Leica DMI4000B inverted microscope equipped with a high resolution CCD camera. The color reader model CR-10, was purchased from Konica Minolta Sensing Americas, Inc (minus value 0.1). The mini fan used for vapor exposure was purchased from Radio Shack (40mm, 12 VDC,

6500RPM). Ammonium titanyl oxalate monohydrate and other chemicals were purchased from Fisher and used as received. The paper towels were purchased from SAFECHEM (Tork Advanced perforated Towel (white), HB9201).

Paper sample preparation was as follows: 100 μL water solution of ammonium titanyl oxalate was drop-cast onto a piece of paper towel ($2.5 \times 2.5 \text{ cm}^2$ size), followed by drying in vacuum at room temperature for 1 h. To adjust the molar amount of titanyl salt loading (as marked in Figure 2.5a), various concentrations of stock solutions of titanyl oxalate were prepared and used: 0.001, 0.005, 0.01, 0.02, 0.05, 0.1, 0.2, 0.4, 0.8 and 1.0 M. Due to the bulk homogeneity of the fibril structure of the paper towel, a small droplet of water can be absorbed instantly and spread throughout the matrix of paper. For a small size of paper ($2.5 \times 2.5 \text{ cm}^2$), 100 μL of water solution was equally drop-cast at multiple points (3×3) atop the paper, thus producing homogeneous distribution of the titanyl salt within the whole area, shown by the uniform color density upon exposure to the hydrogen peroxide vapor (see Figure 2.5).

Vapor sensing test was as follows: for the measurements at a fixed vapor pressure of H_2O_2 (presented in Figure 2.5), the test was performed by hanging the loaded paper towel in the saturated vapor (225.4 ppm), above 10 mL 35 wt % H_2O_2 solution contained in a sealed 50 mL vial. The yellow color thus evolved at different time intervals was measured by the CR-10 color reader. For the measurements at a fixed load of titanyl salt (as presented in Figure 2.7), approximately 1 L of H_2O_2 solution (diluted down to various concentrations) was put in a 10 L container and sealed for 12 h to reach the equilibrium vapor pressure. The equilibrium vapor pressure corresponding to a specific diluted concentration of H_2O_2 solution was deduced from the literature.⁽⁵³⁾ The sensing test was performed by putting the loaded paper towel facing close ($\sim 0.5 \text{ cm}$) to the center of the fan, which was hung in

the vapor contained in the sealed container (about 20 cm above the solution surface). The vapor was blown onto each sample (12V, 6500RPM) for various time intervals (shown in Figure 2.7) before taken out for color reading. In this study, the various low concentrations of H_2O_2 solution were obtained by diluting the commercial 35 wt % solution with pure water by 1000, 500, 300, 200, 100, 75, 50, 25, and 10 times, producing various saturated (equilibrium) vapor pressures, correspondingly, 0.1, 0.2, 0.3, 0.5, 1.0, 1.3, 1.9, 4.0, and 10.5 ppm.(53)

2.5.2 UV-vis Absorption Titration of Colorimetric Reaction between Titanyl Salt and H_2O_2

The fluorescence spectra of titanyl salt upon addition of different molar amounts of H_2O_2 were recorded to determine the stoichiometric of the reaction between titanyl salt and H_2O_2 . (Figure 2.2)

2.5.3 Homogeneous Distribution of Titanyl Salt via Drop-Casting

Photographs were taken over a piece of paper towel (2.5×2.5 cm size) before and after exposure to 225.4 ppm H_2O_2 vapor to demonstrate the homogeneous distribution of titanyl salt via drop-casting. (Figure 2.3)

2.5.4 Time Course of Color Formation as Monitored by UV-vis Absorption

The UV-vis absorption spectra of the thin film of titanyl oxalate salt upon exposure to 225.4 ppm H_2O_2 vapor at various time intervals were measured to show the reaction kinetics on the titanyl oxalate salt film. (Figure 2.6)

2.5.5 Selectivity Test Against Potential Interferences

The increase of absorbance (ΔA) measured at 386 nm over the thin film of titanyle oxalate salt were measured to demonstrate the selectivity of the prepared sensor. (Figure 2.4)

2.6 References

- (1) Law, M.; Goldberger, J.; Yang, P. Semiconductor Nanowires and Nanotubes. *Annu. Rev. Mater. Res.* **2004**, *34*, 83-122.
- (2) Hu, J.; Odom, T. W.; Lieber, C. M. Chemistry and Physics in One Dimension: Synthesis and Properties of Nanowires and Nanotubes. *Acc. Chem. Res.* **1999**, *32*, 435-445.
- (3) Duan, X.; Huang, Y.; Agarwal, R.; Lieber, C. M. Single-Nanowire Electrically Driven Lasers. *Nature* **2003**, *421*, 241-245.
- (4) Cui, Y.; Wei, Q.; Park, H.; Lieber, C. M. Nanowire Nanosensors for Highly Sensitive and Selective Detection of Biological and Chemical Species. *Science* **2001**, *293*, 1289-1292.
- (5) Huang, M. H.; Mao, S.; Feick, H.; Yan, H.; Wu, Y.; Kind, H.; Weber, E.; Russo, R.; Yang, P. Room-Temperature Ultraviolet Nanowire Nanolasers. *Science* **2001**, *292*, 1897-1899.
- (6) Melosh, N. A.; Boukai, A.; Diana, F.; Gerardot, B.; Badolato, A.; Petroff, P. M.; Heath, J. R. Ultrahigh-Density Nanowire Lattices and Circuits. *Science* **2003**, *300*, 112-115.
- (7) Wang, J.; Gudixsen, M. S.; Duan, X.; Cui, Y.; Lieber, C. M. Highly Polarized Photoluminescence and Photodetection from Single Indium Phosphide Nanowires. *Science* **2001**, *293*, 1455-1457.
- (8) Li, C.; Zhang, D.; Lei, B.; Han, S.; Liu, X.; Zhou, C. Surface Treatment and Doping Dependence of In₂O₃ Nanowires as Ammonia Sensors. *Journal of Physical Chemistry B* **2003**, *107*, 12451-12455.
- (9) Wang, Y.; Jiang, X.; Xia, Y. A Solution-Phase, Precursor Route to Polycrystalline SnO₂ Nanowires That Can Be Used for Gas Sensing under Ambient Conditions. *J. Am. Chem. Soc.* **2003**, *125*, 16176-16177.
- (10) Huang, J. X.; Virji, S.; Weiller, B. H.; Kaner, R. B. Polyaniline Nanofibers: Facile Synthesis and Chemical Sensors. *J. Am. Chem. Soc.* **2003**, *125*, 314-315.

- (11) Zhou, Y.; Freitag, M.; Hone, J.; Staii, C.; Johnson, J. A. T. Fabrication and Electrical Characterization of Polyaniline-Based Nanofibers with Diameter Below 30 Nm. *Appl. Phys. Lett.* **2003**, *83*, 3800-3802.
- (12) Lee, H. J.; Jin, Z. X.; Aleshin, A. N.; Lee, J. Y.; Goh, M. J.; Akagi, K.; Kim, Y. S.; Kim, D. W.; Park, Y. W. Dispersion and Current-Voltage Characteristics of Helical Polyacetylene Single Fibers. *J. Am. Chem. Soc.* **2004**, *126*, 16722-16723.
- (13) Zang, L.; Che, Y.; Moore, J. S. One-Dimensional Self-Assembly of Planar - Conjugated Molecules: Adaptable Building Blocks for Organic Nanodevices. *Acc. Chem. Res. (Special Issue of Nanoscience)* **2008**, *41*, 1596-1608.
- (14) Che, Y.; Yang, X.; Liu, G.; Yu, C.; Ji, H.; Zuo, J.; Zhao, J.; Zang, L. Ultrathin N-Type Organic Nanobelts with High Photoconductivity and Application in Optoelectronic Vapor Sensing of Explosives. *J. Am. Chem. Soc.* **2010**, 5743-5750.
- (15) Che, Y.; Yang, X.; Zhang, Z.; Zuo, J.; Moore, J. S.; Zang, L. Ambient Photodoping of P-Type Organic Nanofibers: Highly Efficient Photoswitching and Electrical Vapor Sensing of Amines. *Chem. Commun.* **2010**, *46*, 4127-4129.
- (16) Zhang, C.; Che, Y.; Yang, X.; Bunes, B. R.; Zang, L. Organic Nanofibrils Based on Linear Carbazole Trimer for Explosive Sensing. *Chem. Commun.* **2010**, *46*, 5560-5562.
- (17) Che, Y.; Zang, L. Enhanced Fluorescence Sensing of Amine Vapor Based on Ultrathin Nanofibers. *Chem. Commun.* **2009**, 5106-5108.
- (18) Che, Y.; Yang, X.; Loser, S.; Zang, L. Expedient Vapor Probing of Organic Amines Using Fluorescent Nanofibers Fabricated from an N-Type Organic Semiconductor. *Nano Lett.* **2008**, 2219-2223.
- (19) Naddo, T.; Che, Y.; Zhang, W.; Balakrishnan, K.; X., Y.; Yen, M.; Zhao, J.; Moore, J. S.; Zang, L. Sensitive Detection of Explosives with a Fluorescent Nanofibril Film. *J. Am. Chem. Soc.* **2007**, *129*, 6978-6979.
- (20) Elghanian, R.; Storhoff, J. J.; Mucic, R. C.; Letsinger, R. L.; Mirkin, C. A. Selective Colorimetric Detection of Polynucleotides Based on the Distance-Dependent Optical Properties of Gold Nanoparticles. *Science* **1997**, *277*, 1078-1081.
- (21) Lee, J.-S.; Han, M. S.; Mirkin, C. A. Colorimetric Detection of Mercuric Ion (Hg²⁺) in Aqueous Media Using DNA-Functionalized Gold Nanoparticles. *Angew. Chem., Int. Ed.* **2007**, *46*, 4093-4096.
- (22) Eisenberg, G. M. Colorimetric Determination of Hydrogen Peroxide. *Ind. Eng. Chem., Anal. Ed.* **1943**, *15*, 327-328.
- (23) Mukhopadhyay, P.; Iwashita, Y.; Shirakawa, M.; Kawano, S.-i.; Fujita, N.; Shinkai, S. Spontaneous Colorimetric Sensing of the Positional Isomers of Dihydroxynaphthalene in a 1d Organogel Matrix. *Angewandte Chemie, International Edition* **2006**, *45*, 1592-1595.

- (24) Nazeeruddin, M. K.; Di Censo, D.; Humphry-Baker, R.; Gratzel, M. Highly Selective and Reversible Optical, Colorimetric, and Electrochemical Detection of Mercury(II) by Amphiphilic Ruthenium Complexes Anchored onto Mesoporous Oxide Films. *Adv. Funct. Mater.* **2006**, *16*, 189-194.
- (25) Yang, Y.-K.; Yook, K.-J.; Tae, J. A Rhodamine-Based Fluorescent and Colorimetric Chemodosimeter for the Rapid Detection of Hg²⁺ Ions in Aqueous Media. *J. Am. Chem. Soc.* **2005**, *127*, 16760-16761.
- (26) Bohrer, F. I.; Colesniuc, C. N.; Park, J.; Schuller, I. K.; Kummel, A. C.; Trogler, W. C. Selective Detection of Vapor Phase Hydrogen Peroxide with Phthalocyanine Chemiresistors. *J. Am. Chem. Soc.* **2008**, *130*, 3712-3713, and refs cited therein.
- (27) Carvalhal, R. F.; Kfoury, M. S.; de Oliveira Piazzetta, M. H.; Gobbi, A. L.; Kubota, L. T. Electrochemical Detection in a Paper-Based Separation Device. *Anal. Chem.* **2010**, *82*, 1162-1165.
- (28) Zhao, W.; Ali, M. M.; Aguirre, S. D.; Brook, M. A.; Li, Y. Paper-Based Bioassays Using Gold Nanoparticle Colorimetric Probes. *Anal. Chem.* **2008**, *80*, 8431-8437.
- (29) Martinez, A. w.; Phillips, S. T.; Butte, M. J.; Whitesides, G. M. Patterned Paper as a Platform for Inexpensive, Low-Volume, Portable Bioassays. *Angew. Chem. Int. Ed.* **2007**, *46*, 1318-1320.
- (30) Cheng, C.; Martinez, A. W.; Gong, J.; Mace, C. R.; Phillips, S. T.; Carrilho, E.; Mirica, K. A.; Whitesides, G. M. Paper-Based Elisa. *Angew. Chem. Int. Ed.* **2010**, *49*, 1-5.
- (31) Malashikhin, S.; Finney, N. S. Fluorescent Signaling Based on Sulfoxide Profluorophores: Application to the Visual Detection of the Explosive TATP. *J. Am. Chem. Soc.* **2008**, *130*, 12846-12847.
- (32) Schulte-Ladbeck, R.; Edelmann, A.; Quintas, G.; Lendl, B.; Karst, U. Determination of Peroxide-Based Explosives Using Liquid Chromatography with on-Line Infrared Detection. *Anal. Chem.* **2006**, *78*, 8150-8155.
- (33) Schulte-Ladbeck, R.; Kolla, P.; Karst, U. A Field Test for the Detection of Peroxide-Based Explosives. *Analyst* **2002**, *127*, 1152-1154.
- (34) Woodfin, R. L. E. Trace Chemical Sensing of Explosives, John Wiley & Sons: Hoboken, Nj, 2007.
- (35) Moore, D. S. Recent Advances in Trace Explosives Detection Instrumentation. *Sens. Imaging* **2007**, *8*, 9-38.
- (36) Dubnikova, F.; Kosloff, R.; Zeiri, Y.; Karpas, Z. Novel Approach to the Detection of Triacetone Triperoxide (TATP): Its Structure and Its Complexes with Ions. *J. Phys. Chem. A* **2006**, *106*, 4951-4956.

- (37) Dubnikova, F.; Kosloff, R.; Almog, J.; Zeiri, Y.; Boese, R.; Itzhaky, H.; Alt, A.; Keinan, E. Decomposition of Triacetone Triperoxide Is an Entropic Explosion. *J. Am. Chem. Soc.* **2005**, *127*, 1146-1159.
- (38) Germain, M. E.; Knapp, M. J. Turn-on Fluorescence Detection of H₂O₂ and TATP. *Inorg. Chem.* **2008**, *47*, 9748-9750.
- (39) Bailey, R.; Boltz, D. F. Differential Spectrophotometric Determination of Hydrogen Peroxide with 1,10-Phenanthroline and Bathophenanthroline. *Anal. Chem.* **1959**, *31*, 117-119.
- (40) Freeman, T. M.; Seitz, W. R. Chemiluminescence Fiber Optic Probe for Hydrogen Peroxide Based on the Luminol Reaction. *Anal. Chem.* **1978**, *50*, 1242-1246.
- (41) Sellers, R. M. Spectrophotometric Determination of Hydrogen Peroxide Using Potassium Titanium(IV) Oxalate. *Analyst* **1980**, *105*, 950-954.
- (42) Matsubara, C.; Kudo, K.; Kawashita, T.; Takamura, K. Spectrophotometric Determination of Hydrogen Peroxide with Titanium 2-((5-Bromopyridyl)Azo)-5-(N-Propyl-N-Sulfopropylamino)Phenol Reagent and Its Application to the Determination of Serum Glucose Using Glucose Oxidase. *Anal. Chem.* **1985**, *57*, 1107-1109.
- (43) Clapp, P. A.; Evans, D. F. Spectrophotometric Determination of Hydrogen Peroxide with Leuco Patent Blue Violet. *Anal. Chim. Acta* **1991**, *243*, 217-220.
- (44) Matsubara, C.; Kawamoto, N.; Takamura, K. Oxo[5,10,15,20-Tetra(4-Pyridyl)Porphyrinato]Titanium(IV): An Ultrahigh-Sensitive Spectrophotometric Reagent for Hydrogen Peroxide. *Analyst* **1992**, *117*, 1781-1784.
- (45) Wolfbeis, O. S.; Dürkop, A.; Wu, M.; Lin, Z. A Europium-Ion-Based Luminescent Sensing Probe for Hydrogen Peroxide. *Angew. Chem. Int. Ed.* **2002**, *41*, 4495-4498.
- (46) Lo, L.-C.; Chu, C.-Y. Development of Highly Selective and Sensitive Probes for Hydrogen Peroxide. *Chem. Commun.* **2003**, 2728-2729.
- (47) Chang, M. C. Y.; Pralle, A.; Isacoff, E. Y.; Chang, C. J. A Selective, Cell-Permeable Optical Probe for Hydrogen Peroxide in Living Cells. *J. Am. Chem. Soc.* **2004**, *126*, 15392-15393.
- (48) Dickinson, B. C.; Chang, C. J. A Targetable Fluorescent Probe for Imaging Hydrogen Peroxide in the Mitochondria of Living Cells. *J. Am. Chem. Soc.* **2008**, *130*, 9638-9639.
- (49) Schwarzenbach, G.; Muehlebach, J.; Mueller, K. Peroxo Complexes of Titanium. *Inorg. Chem.* **1970**, *9*, 2381-2390.
- (50) Bonet-Maury, P. Photocolorimetric Method for Determining Small Quantities of Hydrogen Peroxide in Water. *Compt. rend.* **1944**, *218*, 117-119.

- (51) Pattersonb, B. D.; MacRaec, E. A.; Fergusonc, I. B. Estimation of Hydrogen Peroxide in Plant Extracts Using Titanium(IV). *Anal. Biochem.* **1984**, *139*, 487-492.
- (52) Takamura, K.; Matsubara, C. Versatility of the Titanium(D)–Porphyrin Reagent for Determining Hydrogen Peroxide. *Bulletin of the Chemical Society of Japan* **2003**, *76*, 1873-1888.
- (53) Manatt, S. L.; Manatt, M. R. R. On the Analyses of Mixture Vapor Pressure Data: The Hydrogen Peroxide/Water System and Its Excess Thermodynamic Functions. *Chem. Eur. J.* **2004**, *10*, 6540-6557.

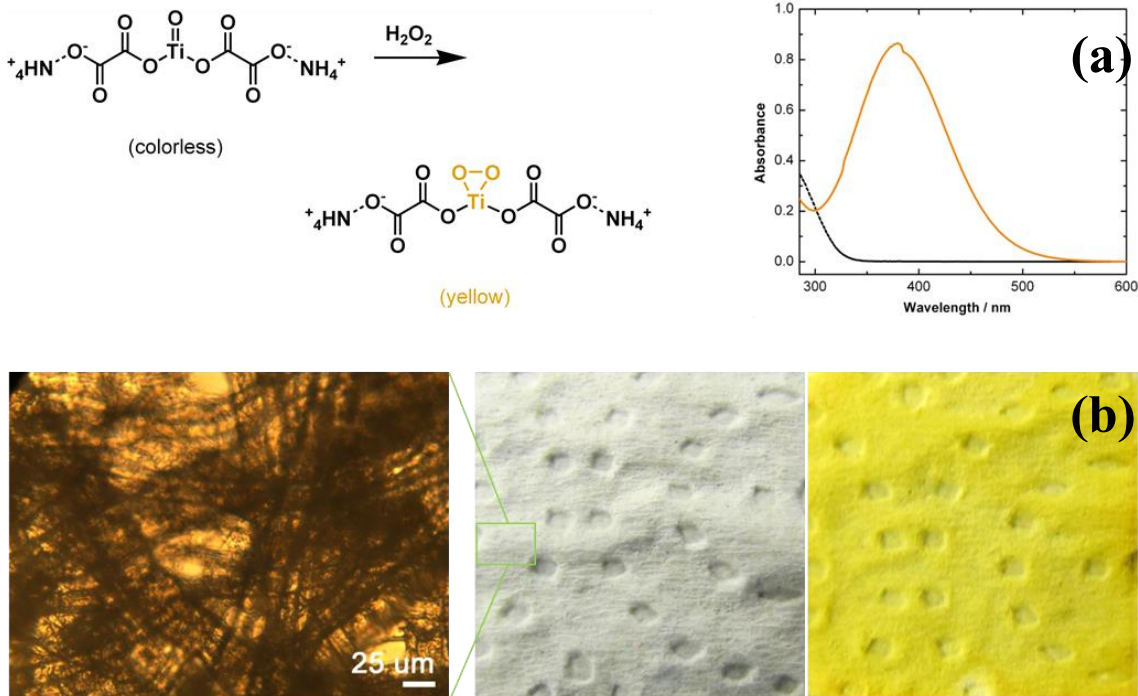


Figure 2.1 The detection mechanism of this paper based sensor is based on colorimetric sensing based on peroxide complexation with Ti(IV) oxo moiety ($>Ti=O$). (a) The UV-vis absorption spectra were obtained for a water solution of titanyl oxalate (1.0×10^{-3} M) before (black) and after (red) addition of 0.04 wt % H_2O_2 . (b) Yellow color formation as envisioned over a piece of paper towel (2×2 cm², loaded with 0.1 mmol titanyl oxalate) upon exposure to the vapor of 35 wt % H_2O_2 solution. Also shown is an optical microscope photograph of the paper towel, revealing the cellulose fibril network.

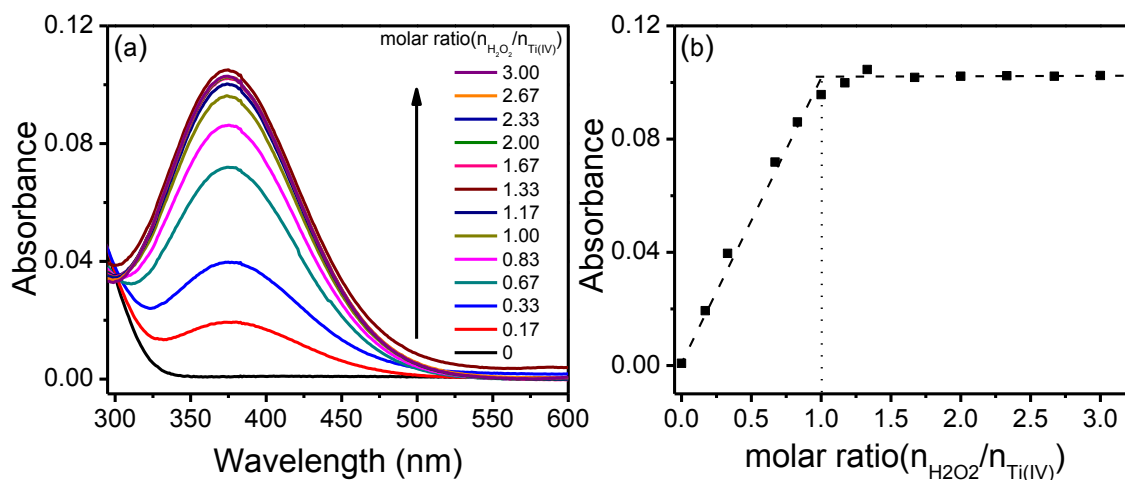


Figure 2.2 The figures show a titration experiment between titanium oxalate salt and H_2O_2 recorded by UV-vis absorption spectra. (a) UV-vis absorption spectra of 1.2×10^{-4} M aqueous solution of titanium oxalate as measured with addition of different molar ratios of hydrogen peroxide solution. (b) Absorbance measured at the maximum wavelength (378 nm) as a function of the molar ratio of $\text{H}_2\text{O}_2/\text{Ti(IV)}$, for which a turning point around molar ratio of 1.0 indicates the 1:1 stoichiometric reaction between H_2O_2 and Ti(IV) salt as illustrated in Figure 2.1.

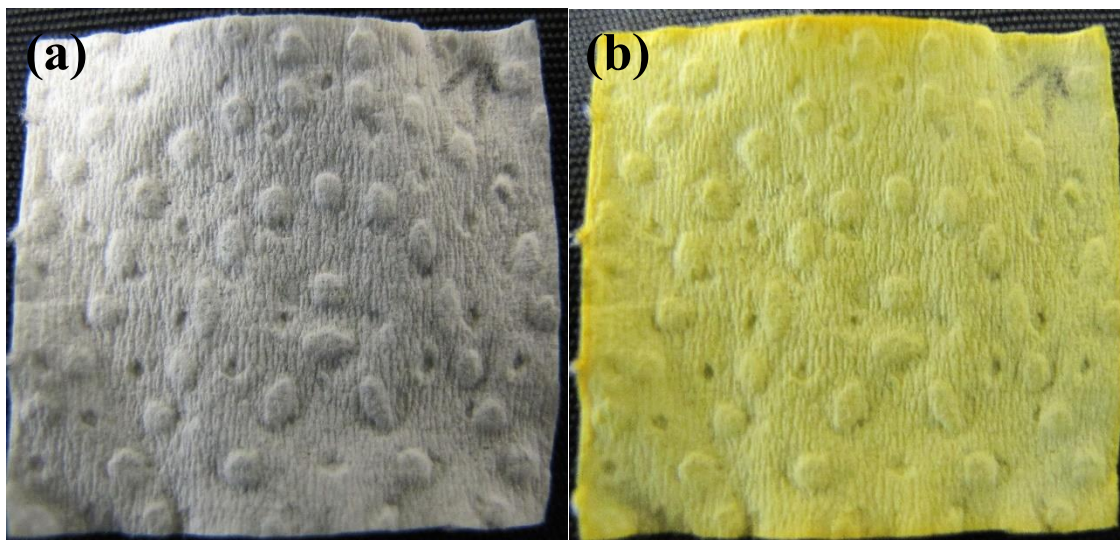


Figure 2.3 Photographs taken over a piece of paper towel (2.5×2.5 cm size) before (a) and after (b) exposure to the saturated vapor of 35 wt % H_2O_2 solution (225.4 ppm) for 5 min. The paper sample was prepared by drop-casting 100 μL of the water solution (0.2 M) of ammonium titanyl oxalate, followed by drying in vacuum at room temperature for 1 h. The uniform color as formed indicates the homogeneous distribution of titanyl salts throughout the paper matrix.

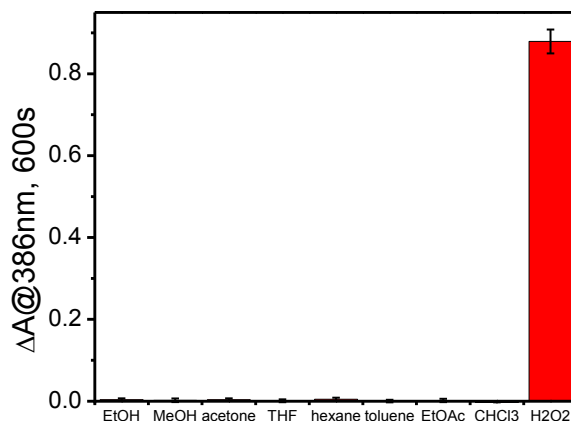


Figure 2.4 The increase of absorbance (ΔA) measured at 386nm over the thin film of titanyl oxalate (the same as fabricated in Figure 2.6) upon exposure to the saturated vapor of 35 wt % H_2O_2 solution (225.4 ppm), compared to the vapors of other common solvents: ethanol (89,000 ppm), methanol (131,000 ppm), acetone (260,000 ppm), THF (173,000 ppm), hexane (130,000 ppm), toluene (26,000 ppm), ethyl acetate (100,000 ppm), chloroform (140,000 ppm). The exposure time was 600 s. The exposure time was fixed at 600 s.

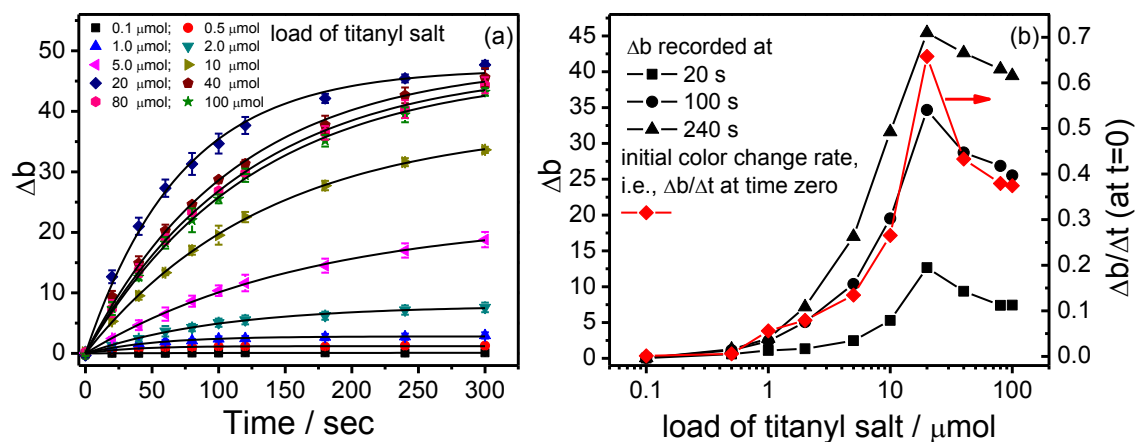


Figure 2.5 The color change versus time plot were recorded upon exposure to a fixed vapor pressure of H_2O_2 . a) Time course of the yellow color formation measured over a piece of paper towel ($2.5 \times 2.5 \text{ cm}^2$ size) loaded with titanyl oxalate salt. The color change was recorded using a CR-10 color reader (from Konica Minolta), and the value Δb refers to the color change between yellow and blue as defined in the CIELAB color space system. Shown in the figure are the series of measurements performed over the paper towels loaded with varying amounts (μmol) of the titanyl salt upon exposure to a saturated vapor of 35 wt % aqueous solution of H_2O_2 . The error bars are standard deviations of the data. (b) Δb recorded at three time intervals (20, 100, 240 s) are plotted as a function of the molar amount of titanyl salt loaded. Plotted in the same figure (right axis) are the initial color change rates $\partial(\Delta b)/\partial t = K'K$ (deduced from the fitting of Figure 2.5a) with the loading amount of titanyl salt.

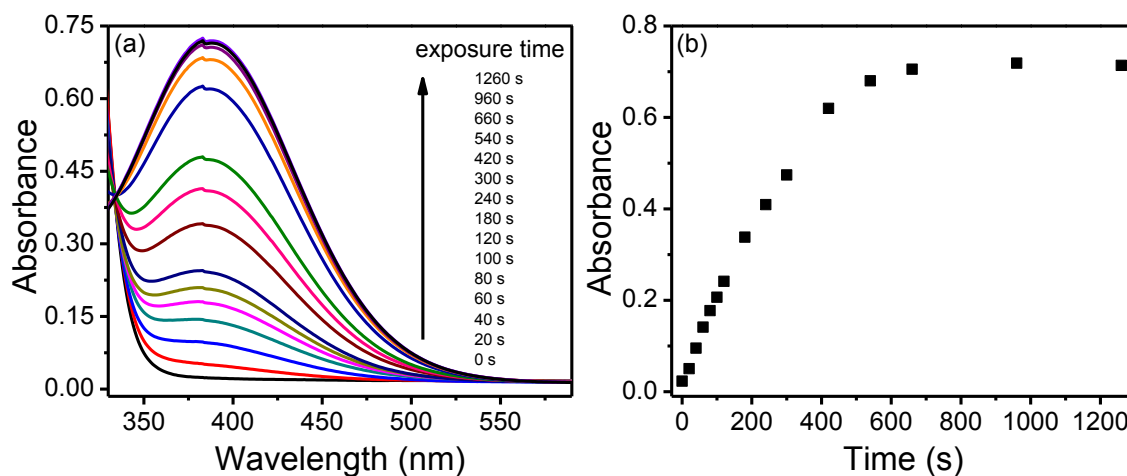


Figure 2.6 The UV-vis absorption spectra of titanyl oxalate salt film were recorded upon exposure to a fixed vapor pressure of H₂O₂. (a) UV-vis absorption spectra of the thin film of titanyl oxalate salt upon exposure to the saturated vapor of 35 wt % H₂O₂ solution (225.4 ppm) at various time intervals: 0, 20, 40, 60, 80, 100, 120, 180, 240, 300, 420, 540, 660, 960, 1260 s. The thin film was made by drop-casting 130 μ L of 0.1 M aqueous solution of ammonium titanyl oxalate onto a quartz slide in an area of ca. 4 cm². (b) Absorbance measured at the maximum wavelength (386 nm) as a function of the exposure time.

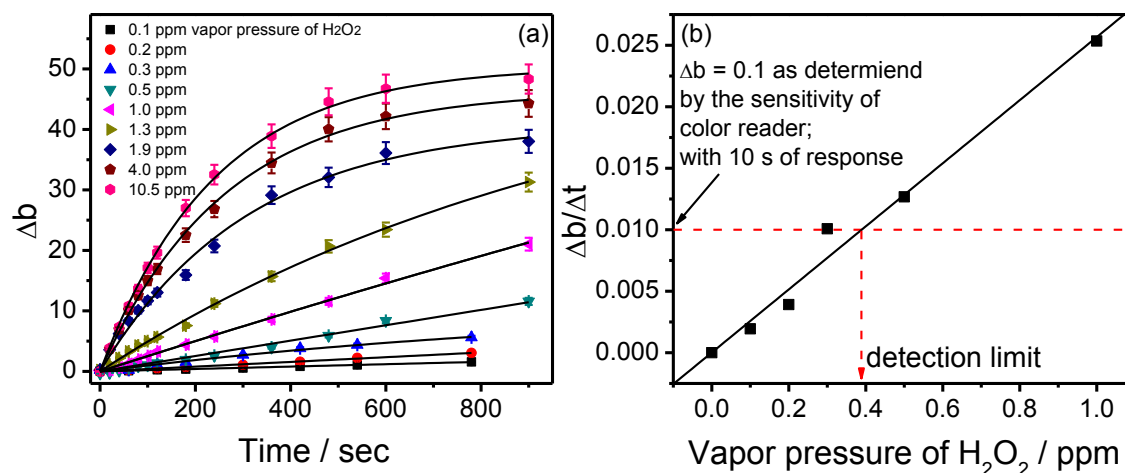


Figure 2.7 The color change verse time plot were recorded upon exposure to different vapor pressure of H_2O_2 . (a) Time course of the yellow color formation measured over the paper towel ($2.5 \times 2.5 \text{ cm}^2$) loaded with a fixed amount of titanyl oxalate salt ($20 \text{ }\mu\text{mol}$) upon exposure to the saturated vapor of aqueous solution of H_2O_2 at various diluted concentrations. The data fitting was based on equation (2.1). For the data obtained under low vapor pressures of H_2O_2 (0.1, 0.2, 0.3, 0.5 and 1.0 ppm), Δb is linearly dependent on time, following the equation $\Delta b = K' K t$. The slope ($\Delta b/\Delta t$) thus extracted can be replotted as a function of the vapor pressure of H_2O_2 , as shown in (b), which yields a linear relationship with a fitting correlation coefficient of 0.99. The error bars are the standard deviations.

CHAPTER 3

A SELECTIVE FLUORESCENCE TURN-ON SENSOR FOR TRACE

VAPOR DETECTION OF HYDROGEN PEROXIDE¹

3.1 Abstract

A fluorescence turn-on sensor molecule (C6NIB) has been synthesized and fabricated into porous matrix to enable trace vapor detection of hydrogen peroxide. The detection limit was projected to be below 5 ppb.

3.2 Introduction

Among the explosive detection methods developed thus far, vapor detection represents a nondestructive way suited for both trace and bulk explosive monitoring. (1-8) For vapor detection, fluorescent sensing represents a simple, rapid, and highly sensitive technology. (1-7) Recently, fluorescence “turn-on” (or enhancement) molecular sensors have drawn increasing attention for explosive detection, (7,9-13) as they improve the detection sensitivity due to the low (ideally zero) fluorescent background of the pristine state of

¹Reproduced by permission of The Royal Society of Chemistry. Xu, M.; Han, J.-M.; Zhang, Y.; Yang, X.; Zang, L., A Selective Fluorescence Turn-on Sensor for Trace Vapor Detection of Hydrogen Peroxide. *Chem. Commun.* **2013**, *49*, 11779-11781 (<http://pubs.rsc.org/EN/content/articlehtml/2013/cc/c3cc47631f>). Copyright (2013) Royal Society of Chemistry.

sensors.

Triacetone triperoxide (TATP), along with other peroxide explosives such as diacetone diperoxide (DADP) and hexamethylene triperoxide diamine (HMTD), represent one class of the most elusive explosives that can be easily made at home from commercially available precursors. These peroxide explosives are difficult to detect by conventional analytical techniques due to their lack of a nitro group, nonfluorescence, low ionizability and minimal UV-vis absorption. (14-15) Hydrogen peroxide (H_2O_2) is usually taken as a signature compound for detecting peroxide explosives, (14,16) from which H_2O_2 can be produced through UV decomposition or simply leaking as an intrinsic impurity. Moreover, liquid mixtures of concentrated hydrogen peroxide and fuels (e.g., alcohols and acetone) can be used as powerful explosives as well. Thereby, expedient trace vapor detection of H_2O_2 becomes critical for these security scenarios. (13)

Although various methods and technologies have been developed to detect H_2O_2 , such as the electrochemical method, (17-20) colorimetric (21-23) and fluorimetric method, (7,10,12,24-27) vapor detection of H_2O_2 (particularly at trace level, e.g., ppb) still remains challenging. This is mainly due to the combined difficulty of molecular design and materials engineering to produce a sensor system that enables not only strong binding with H_2O_2 (for efficient vapor sampling), but also expedient, selective reaction with H_2O_2 to transduce a readable signal. While a few recent papers reported on fluorescence turn-on sensors that can be employed for vapor detection of H_2O_2 , (7,10), the reported sensors either suffer from long response time (> 10 min) or complicated instrument alignments (e.g., involving laser and cooled CCD). There is a great need to develop a simple, expedient fluorescence turn-on sensor system that can detect H_2O_2 vapor, ideally down to a level of ppb.

3.3 Results and Discussion

Inspired by recent works on molecular design of naphthalimide based robust fluorescence turn-on sensors, (28-29) we report herein on a new fluorescence turn-on sensor for H₂O₂, 2-hexyl-6-(4,4,5,5-tetramethyl-1,3,2-dioxaborolan-2-yl)-1H-benzo[de]isoquinoline-1,3(2H)-dione (C6NIB). This molecule is only weakly fluorescent in the UV region (λ_{max} at 392 nm) mainly caused by the π - π^* transition of naphthalimide backbone (Figure 3.1), for which the quantum yield is only 0.6 % under basic conditions as employed for the sensor in this study. However, upon reaction with H₂O₂ the aryl boronate group of C6NIB is transformed to phenol (Figure 3.2a), forming an electron donor-acceptor (push-pull) structure that turns on the charge transfer transition. As shown in Figure 3.3a, the main absorption peak of the oxidation product, 2-hexyl-6-hydroxy-1H-benzo[de]isoquinoline-1,3(2H)-dione (C6NIO) shifts to the red by ca. 90 nm. The new absorption band at the longer wavelength corresponds to the intramolecular charge transfer (ICT) transition between the phenol and naphthalimide groups. (28-30) Before the addition of H₂O₂, the ethanol solution of C6NIB demonstrated no detectable emission in the ICT band, whereas strong emission was observed in the presence of H₂O₂ (Figure 3.3b). Such fluorescence turn-on reaction is intrinsically selective for H₂O₂, with no fluorescence increase observed in the presence of water, oxygen, or common organic reagents such as alcohols, hexane, acetone, etc (Figure 3.2b). The high selectivity is due to the specific chemical reaction between boronate group and H₂O₂, which has been proven by previous studies in solutions, whereas the boronate molecules are based on different backbone structures. (26)

The high chemical selectivity, together with the high fluorescence turn-on sensitivity, makes C6NIB an ideal sensor for vapor detection of H₂O₂, for which fast response and low

detection limit are the two critical goals to approach through materials engineering. The presence of boronate group makes the C6NIB molecule highly hydrophilic, thus suited for blending with hydrophilic porous materials such as silica gel (Figure 3.2d). The composite sensory material thus fabricated possess large surface area, continues porosity and hydrophilic interface, which combined enhance the absorption of H₂O₂ vapor.

Molecular design and synthesis of C6NIB represents an advancement in development of boronate sensors. Direct attachment of boronate group to an electron deficient aromatic system is challenging, even through the efficient Miyaura boration reaction. (31) Indeed, few studies have been reported on the manipulation of the “push-pull” electronic structure of naphthalimide backbone by direct attachment of an electron deficient group. (29,32) Nonetheless, once the molecule is modified with an electron deficient group like boronate, it will become a strong electrophile with increasing reactivity with H₂O₂.

The H₂O₂-mediated oxidation of aryl boronates is kinetically favored under basic conditions, which facilitates the dissociation of H₂O₂ into HO₂⁻ anion (acting as a nucleophile) that can in turn react with the boronate group (a strong electrophile). (26) Moreover, under basic conditions the phenol group of C6NIO undergoes deprotonation, becoming phenolate, which is a stronger electron donor, and thus enhances the ICT fluorescence emission (Figure 3.4). (33) Increased emission produces higher on/off ratio, helping increase detection efficiency. In this study we used an organic base, tetrabutylammonium hydroxide (TBAH) to produce the basic reaction condition (Figure 3.5), under which C6NIB was proven stable, i.e., no detectable change was observed in the fluorescence spectra within the experimental time (Figure 3.6). The fluorescence turn-on reaction of C6NIB was found to be dependent on the concentration of TBAH (Figure 3.7). When dispersed into silica gel, the optimal molar ratio of TBAH to C6NIB was determined

to be 10:1. Under the same molar ratio, the sensor composite of C6NIB/TBAH was comparatively investigated by dispersing it into three different supporting matrices, silica gel thin layer chromatography (TLC) plate, alumina TLC plate and filter paper, and tested under the same vapor condition of H₂O₂. Among the three matrices, silica gel exhibited the fastest sensor response and the highest turn-on efficiency (Figure 3.8). Therefore, the sensor composite of C6NIB/TBAH dispersed in silica gel TLC plate was used as the optimal sensor system in this study for vapor detection of H₂O₂.

TBAH is a highly hygroscopic liquid (similar to glycerol), and miscible with water and alcohols. A mixture of TBAH and C6NIB ethanol solutions is suited for dispersion into the silica gels. Vaporization of ethanol results in a homogeneous dispersion of C6NIB within the silica matrix. Such molecular dispersion is evidenced by the comparative absorption and fluorescence spectral measurements (shown in Figure 3.3, Figure 3.9 and Figure 3.4), which showed no significant difference in either absorption or fluorescence maxima between the ethanol solution and silica gel supported samples. The silica gel based sensor composite thus fabricated is expected to be efficient for vapor sampling of H₂O₂, which is always coexisting with water. The strong hygroscopy of TBAH, in combination with the large interface and porosity of silica gel, is highly conducive to vapor capture of water, as well as H₂O₂.

To examine the response speed of the sensor system, we measured the fluorescence spectral change of C6NIB/TBAH composite dispersed in silica gel TLC plate upon exposure to 1 ppm H₂O₂ vapor for varying time intervals (Figure 3.10a). The fluorescence emission centered at 553 nm increases gradually with exposure time, characteristic of the H₂O₂-mediated conversion of C6NIB to C6NIO. Since C6NIB has no measurable fluorescence emission in the long wavelength region, the sensor reaction kinetics can

simply be monitored by measuring the emission intensity increasing with time (Figure 3.10b). The threshold of detectable emission can be set at an intensity level three times of the standard deviation ($\sigma = 96$) of the emission intensity measurement; this corresponds to a sensor response time of ca. 0.86 sec (as obtained from the fitted data in Figure 3.10b). This rapid sensor response towards H_2O_2 vapor is critical for real-time in-field detection of peroxides. To the best of our knowledge, there has been no fluorescent sensors reported that demonstrate such fast response to H_2O_2 vapor (particularly at a low level of 1 ppm). Indeed, expedient vapor detection of H_2O_2 demands combined materials optimization of sensors to afford efficient vapor sampling, strong interface binding and fast chemical reactions.

Taking advantage of the close to zero fluorescent background of C6NIB in pristine state, the optimal sensor composite of C6NIB/TBAH dispersed in silica gel was expected to reach unprecedented detection limit of H_2O_2 vapor by carefully measuring the turned on fluorescence intensity. To determine the detection limit, the silica gel TLC plate based sensor was exposed for 5 min to the vapor of aqueous solution of H_2O_2 in varying concentrations, (34) and full fluorescence spectrum was recorded each time after the vapor exposure (Figure 3.11). For a given exposure time, the fluorescence intensity increases with the vapor pressure (concentration) of H_2O_2 . Figure 3.11b shows the increase in fluorescence intensity measured at maximal wavelength 553 nm (relative to the value measured under pure water vapor) as a function of the vapor pressure of H_2O_2 . Assuming a quasiequilibrium was reached within 5 min exposure (as implied from the result in Figure 3.10), the results shown Figure 3.11b should follow the Langmuir adsorption model (see Experimental Methods and Materials section). Indeed, the experiment data can be fit nicely into the Langmuir equation, with which we can project the detection limit. If defining an

intensity increase three times the standard deviation as the detectable signal, the detection limit for the current sensor material was projected to be 2.9 ppb, which corresponds to the vapor pressure of a H_2O_2 solution ca. 30,000 times diluted from the commercial 35 wt % solution. Such detection sensitivity is about two orders of magnitude better than the commercial fluorescence detector. It should be noted that the emission measurement employed in this study was based on an open sample holder, which was connected to the photon detector through an optical fiber. Such a simple measurement system usually suffers from high noise level when measuring low intensity of emission, mainly due to influence of scattered light and the significant light transport loss. We believe that upon integration into an enclosed optical detector, where the emission is directly measured by a photodetector aligned at a right angle to the sensor, the same sensor material presented in Figure 3.11 will be able to detect H_2O_2 vapor down to the level of sub ppb, simply by decreasing the signal-to-noise ratio by two to three orders of magnitude as previously practiced by Swager et al. with the Fido detector system. (35)

3.4 Conclusion

In summary, we have developed an expedient fluorescence turn-on sensor system that is suited for trace vapor detection of H_2O_2 . The sensor mechanism is based on H_2O_2 -mediated oxidation of a boronate fluorophore, C6NIB, which is nonfluorescent in ICT band, but turns to be strongly fluorescent upon conversion into the phenol state, C6NIO. This fluorescence turn-on reaction is extremely selective towards to H_2O_2 , with no sensor response to other common reagents. The negligible fluorescence background of C6NIB combined with the high fluorescent emission of C6NIO, makes C6NIB an ideal candidate for efficient sensing. Dispersing C6NIB with TBAH into a silica gel matrix produces a

highly efficient sensor system for vapor detection of H₂O₂, regarding both detection limit (down to 2.9 ppb) and response time (down to 1 sec under 1 ppm H₂O₂).

3.5 Experimental Methods and Materials

3.5.1 Materials and General Instrumentations

4-Bromo-1,8-naphthalic anhydride was purchased from TCI America and used as received. PdCl₂(dppf), 1,1'- Bis (diphenylphosphino) ferrocene (dppf) were purchased from Sigma-Aldrich and used as received. Bis (pinacolato) diboron acid, 9,10-diphenylanthracene (9, 10-DPA) and Rhodamine 6G were purchased from Fisher Scientific and used as received. The silica gel TLC plates used as supporting matrix for incorporating C₆NIB sensor molecules were purchased from EMD Chemicals Inc. (Silicycle Ultrapure Silica Gels SIL-5554-7). For comparison, the filter paper purchased from Whatman (Catalog No. 1001-150) was also used as the supporting matrix, but after boiling in deionized water for 1 h to remove the bleaching reagents contained in the paper. All organic solvents were purchased from commercial manufacturers and used as received.

UV-vis absorption spectra were measured on a PerkinElmer Lambda 25 spectrophotometer or Agilent Cary 100. The fluorescence spectra were measured on a PerkinElmer LS 55 spectrophotometer or Agilent Eclipse spectrophotometer. The fluorescence spectra of the solid sample (e.g., TLC plates) were recorded on an Ocean Optics USB4000 equipped with 395 nm LED light source and optical fiber (Avantes, FCR-UV200/600-2-IND) for light delivery. ¹H and ¹³C NMR spectra were recorded on a Varian Unity 300 MHz Spectrometer at room temperature in appropriate deuterated solvents. All chemical shifts are reported in parts per million (ppm). Matrix-Assisted Laser Desorption/Ionization Time of Flight Mass Spectrometry (MALDI-TOF-MS) was performed on an

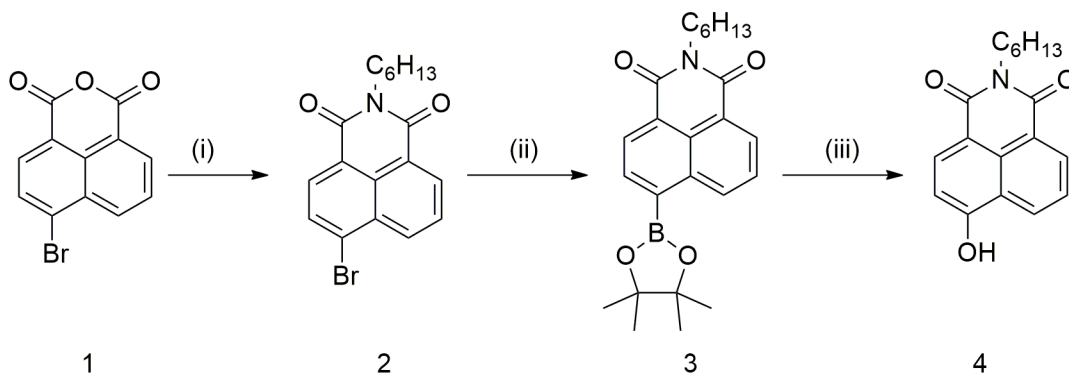
UltrafleXtreme Maldi/ToF/ToF mass spectrometer (Bruker Daltonics), and the solvent used was methanol.

3.5.2 Synthesis

The synthesis route of sensor molecule C6NIB was shown in Scheme 3.1. As shown in Scheme 3.1, the synthesis contains three steps.

6-bromo-2-hexyl-1H-benzo [de] isoquinoline-1, 3(2H)-dione (**2**): 4-Bromo-1,8-naphthalic anhydride (1 g, 3.6 mmol), hexylamine (383 mg, 3.8 mmol), triethylamine (10 mL) were added into 50 mL anhydrous ethanol and refluxed for 4 h. (36) The reaction mixture was evaporated under reduced pressure and then purified through column chromatography on silica gel with hexane/ethyl acetate (5:1, v/v) as eluent. The product was obtained as white crystal (1.10 g, 85 %). ^1H NMR (CDCl_3 , 300 MHz, ppm): δ = 8.52-8.55 (1 H, m, Ar-H), 8.39-8.43 (1 H, m, Ar-H), 8.27-8.29 (1 H, d, J = 7.8 Hz, Ar-H), 7.90-7.93 (1 H, d, J = 7.8 Hz, Ar-H), 7.71-7.76 (1 H, m, Ar-H), 4.07-4.13 (2 H, t, J = 7.2 Hz, CH_2), 1.66-1.71 (2 H, m, CH_2), 1.29-1.40 (6 H, m, CH_2), 0.84-0.8 (3 H, t, CH_3). ^{13}C NMR (CDCl_3 , 75 MHz, ppm): δ 163.32, 163.29, 132.90, 131.76, 130.94, 130.88, 129.95, 128.65, 127.87, 122.90, 122.05, 40.51, 31.45, 27.91, 26.70, 22.49, 14.00.

2-hexyl-6-(4,4,5,5-tetramethyl-1,3,2-dioxaborolan-2-yl)-1H-benzo[de]isoquinoline-1,3(2H)-dione (**3**): **2** (360 mg, 1 mmol), anhydrous potassium acetate (588 mg, 6 mmol), bis(pinacolato)diboron (560 mg, 2.2 mmol), $[\text{PdCl}_2(\text{dppf})]$ (73 mg, 10 mol %), and dppf



Scheme 3.1 The synthesis route of sensor molecule C6NIB (**3**): (i) hexylamine, triethylamine(Et_3N), ethanol, reflux, 4 h; (ii) $\text{PdCl}_2(\text{dppf})$, dppf, potassium acetate (AcOK), bis(pinacolato)diboron, *N,N*-Dimethylformamide (DMF), 120 °C, 3 h; (iii) DMF, 35 % H_2O_2 , room temperature, 3 h.

(55 mg, 10 mol %) and 20 mL DMF were mixed and degassed by three freeze-pump-thaw cycles. The reaction mixture was heated at 120 °C for 3 h. After cooling to room temperature, the reaction mixture was partitioned between water and dichloromethane. The aqueous phase was extracted with 20 mL dichloromethane three times and then combined with the original dichloromethane phase. This dichloromethane solution was washed with brine twice and then washed with water, followed by drying with Na_2SO_4 . After rotary evaporate under reduced pressure to remove excess solvent, the residue was purified through column chromatography on silica gel with hexane/ethyl acetate (5:1, v/v) as eluent. (37) The product was obtained as white powder (180 mg, 44 %). ^1H NMR (CDCl_3 , 300 MHz, ppm, Figure 3.12): δ = 9.05-9.08 (1 H, m, Ar-H), 8.50-8.56 (2 H, m, Ar-H), 8.24-8.26 (2 H, d, J = 7.2 Hz, Ar-H), 7.71-7.76 (1 H, t, J = 7.2 Hz, Ar-H), 4.11-4.16 (2 H, t, J = 7.2 Hz, CH_2), 1.71 (2 H, m, CH_2), 1.30-1.35 (6 H, m, CH_2), 0.85-0.90 (3 H, t, CH_3). ^{13}C NMR (CDCl_3 , 75 MHz, ppm, Figure 3.13): δ 164.16, 164.14, 135.66, 135.11, 134.77,

130.70, 129.59, 127.69, 126.95, 124.62, 122.51, 84.48, 40.43, 31.50, 27.96, 26.74, 24.91, 22.50. MALDI TOF-HRMS m/z : Calcd for $C_{24}H_{30}BNO_4$: 407.2268, Found: 408.2367 $[M+H]^+$.

2-hexyl-6-hydroxy-1H-benzo[de]isoquinoline-1,3(2H)-dione (**4**) : To a solution of **3** (81 mg, 0.20 mmol) in 10 mL DMF, 2 mL H_2O_2 (35 wt %) was added, followed by stirring at room temperature for 3 h. The reaction solution was then diluted with ethyl acetate, extracted with 1 M HCl and brine, and dried over Na_2SO_4 . After removal of solvent, the crude product was purified by flash chromatography (methylene chloride/methanol = 150:1) on silica gel to give 15 mg yellow product **4**, yield 51 %, 1H NMR (CD_3CN , 300 MHz, ppm, Figure 3.14): δ = 8.49-8.54 (2 H, m, Ar-H), 8.36-8.39 (2 H, d, J = 8.1 Hz, Ar-H), 7.69-7.75 (1 H, m, Ar-H), 7.11-7.14 (1 H, d, J = 8.1 Hz, Ar-H), 4.04-4.09 (2 H, m, CH_2), 1.66-1.68 (2 H, m, CH_2), 1.31-1.41 (6 H, m, CH_2), 0.86-0.91 (3 H, t, CH_3). ^{13}C NMR ($DMSO-d_6$, 75 MHz, ppm, Figure 3.15): δ 163.63, 162.97, 160.25, 133.54, 131.11, 129.15, 128.87, 125.59, 122.36, 121.79, 112.58, 109.95, 39.36, 30.97, 27.50, 26.21, 21.98, 13.91. MALDI TOF-HRMS m/z : Calcd for $C_{18}H_{19}NO_3$: 297.1365, Found: 298.1430 $[M+H]^+$.

3.5.3 Other Experimental Details

3.5.3.1 Dispersion of Sensor Molecules in Silica Gel TLC Plate and Filter Paper Matrix

Fifty μL ethanol solution of C6NIB at different concentrations (also containing appropriate concentrations of TBAH as detailed below) was drop-cast uniformly onto a 1.5×1.5 cm² silica gel TLC plate, followed by drying at room temperature in vacuum for 1 h. To adjust the molar amount of C6NIB loading (as indicated in Figure 3.9), various concentrations of C6NIB in ethanol were prepared and used: 0.1, 0.01 and 0.001 M.

Uniform dispersion of C6NIB sensor molecules within the TLC plate is indicated by the uniform emission density shown in the emission photography of the plate after exposure to the H₂O₂ vapor (Figure 3.2d). The same dispersion method was also used for dispersing the sensor molecules into Al₂O₃ TLC plate and filter paper, which were used for comparative sensor investigation as shown in Figure 3.8.

3.5.3.2 Fluorescence Quantum Yield Measurement

As shown in Figure 3.1, molecule C6NIB is only weakly fluorescent in the UV region (λ_{max} at 392 nm) mainly due to the π - π^* transition of naphthalimide backbone, while C6NIO is strongly fluorescent in the longer wavelength region (λ_{max} at 550 nm) due to the charge transfer transition. The quantum yields (Φ) of C6NIB and C6NIO were determined by a single-point measurement with a standard sample of known quantum yield. (38) 9,10-diphenylanthracene(9,10-DPA) ($\Phi = 0.95$ in cyclohexane) (39) and Rhodamine 6G ($\Phi = 0.94$ in ethanol) (40) were chosen as standard samples for C6NIB and C6NIO, respectively. The excitation wavelengths were selected as 340 nm and 480 nm for 9,10-DPA/C6NIB and Rhodamine 6G/C6NIO, respectively. The quantum yields of C6NIB and C6NIO in ethanol (in the presence of 100 fold TBAH) were determined as 0.069 and 0.254, respectively. The quantum yield of C6NIB in ethanol (in the presence of 100 fold TBAH) is only 0.006.

3.5.3.3 Sensor Stability Test on Silica Gel TLC Plate

The C6NIB dispersed TLC plate sample was prepared according to the method described above, and fluorescence spectra were measured at different time intervals after preparation (Figure 3.6), which did not show significant change in fluorescence spectra or

intensity within the experimental investigation period. The same TLC plate was then exposed to 225 ppm H₂O₂ vapor for 5 min, followed by measurement of the fluorescence spectrum.

3.5.3.4 Time Course of Sensor Response in Solid Matrices

To find the optimal concentration of TBAH (or molar ratio TBAH/C6NIB) that would give the fastest sensor reaction, i.e., the H₂O₂ mediated oxidation of C6NIB to C6NIO (as shown in Figure 3.2), we measured the time course of the fluorescence intensity change at 553 nm for the sensor molecules dispersed in silica gel TLC plates. The optimization experiments were performed for the sensor molecules dispersed in silica gel TLC plates as shown in Figure 3.7, where the time course of the fluorescence intensity change was measured at 553 nm for C6NIB dispersed in a 1.5 × 1.5 cm² silica gel TLC plate (containing 0.5 μmol C6NIB) upon exposure to H₂O₂ vapor fixed at 225 ppm. Four series of measurements were performed over the TLC plates containing the same molar amount of C6NIB, but different amounts of TBAH, i.e., at molar ratios of TBAH/C6NIB: 1, 10, 50 and 100. The testing experiment was performed by hanging the loaded TLC plate in the saturated vapor of H₂O₂ (225 ppm) above 10 mL of 35 wt % H₂O₂ solution sealed in a 50 mL jar. The fluorescence emission evolved at different time intervals was measured by Ocean Optics USB4000 spectrophotometer. As shown in Figure 3.7, the fluorescence intensity increased the fastest and reached the highest intensity value at a TBAH/C6NIB ratio of 10, which was determined as the optimal molar ratio for fabricating the sensor composite. The slower sensor response observed at higher TBAH/C6NIB ratio (e.g., 50, 100) is likely due to excessive TBAH blocking the porous structure silica gel, thus weakening the gas intake of H₂O₂ vapor.

For the measurements performed under varying vapor concentrations of H_2O_2 (shown Figure 3.10 and Figure 3.11), the testing experiment was performed by hanging the loaded TLC plate in the saturated vapor of H_2O_2 generated in a 26.5 L container, where approximately 1 L of H_2O_2 solution (diluted down to various concentrations) was put in a vacuum and sealed for 12 h to reach equilibrium vapor pressure. The equilibrium vapor pressure corresponding to a specific diluted concentration of H_2O_2 solution was deduced from the literature. (34) In the container, continuous vapor stream was produced by a mini-fan (Radio Shack, 40mm, 12 VDC, 6500RPM), and the sensor loaded TLC plate was placed against the vapor stream (distanced from the fan by 0.5 cm), and about 20 cm above the solution surface. After exposure to the vapor for different time intervals, the TLC plate was taken out for fluorescence measurement. In this study, various diluted concentrations of H_2O_2 solution were obtained by diluting the commercial 35 wt % solution with pure water 100, 500, 1000, 2000, and 10000 times, which produce saturated (equilibrium) vapor pressures of H_2O_2 of 1000, 200, 100, 50 and 10 ppb, respectively. (34)

3.5.3.5 Comparison of Sensor Response between Different

Supporting Matrices

The sensor testing as shown in Figure 3.7 was also performed over the sensor molecules dispersed in alumina TLC plate and filter paper. Although these two materials also possess large porosity and surface area, the sensor efficiency (regarding both response speed and fluorescence turn-on ratio at saturate stage) was found to be significantly lower than that observed for silica gel TLC plate. This is likely due to the hydrophilic surface of silica gel which is more conducive for the homogeneous dispersion of TBAH/C6NIB as discussed before.

3.5.3.6 Comparison of Sensor Response with Different Bases

The sensor testing as shown in Figure 3.5 was performed over the sensor molecules dispersed in silica TLC plate to compare the different sensing response towards H₂O₂ vapor when using different bases. Compared to NaOH (which is a common base used in deboronation reaction), TBAH produced much higher fluorescence intensity (implying much more efficient sensor conversion) under the same reaction conditions.

3.5.3.7 Selectivity Test

The sensor loaded TLC plate tested in Figure 3.2 was exposed to the saturated vapor of various common solvents such as ethanol (89,000 ppm), methanol (131,000 ppm), acetone (260,000 ppm), THF (173,000 ppm), hexane (130,000 ppm), toluene (26,000 ppm), ethyl acetate (100,000 ppm), chloroform (140,000 ppm), to validate the selectivity of the sensor molecule. The increase in fluorescence intensity was measured at 553 nm over C6NIB loaded silica gel TLC plate (the same component as used in Figure 3.2d) after 5 min exposure to 225 ppm H₂O₂ vapor, in comparison to that upon exposure to the saturated vapor of the common solvents. Although the vapor pressures of the reference solvents are about three orders of magnitude higher than that of H₂O₂, our experiments did not demonstrate any significant fluorescence emission evolution even after extensive exposure to these highly concentrated solvents vapor. This clearly proves the high selectivity of the sensor molecule C6NIB for detection of H₂O₂. The error bars shown in Figure 3.2b are based on the standard deviations of the data.

3.5.3.8 Data Fitting

The data presented in Figure 3.10b can be fitted following the reaction kinetics equation, (41)

$$\Delta I = K'(1 - e^{-Kt}) \quad (3.1)$$

where ΔI is the increase in fluorescence intensity measured at 553 nm, K and K' are constants with K related to the surface reaction rate of C6NIB with H_2O_2 , the given vapor pressure of H_2O_2 and the total load of C6NIB, and K' is referred to as the ratio of the fluorescence intensity to the molar fraction of C6NIO (with respect to the total starting amount of C6NIB). Derivation of this equation is based on the surface reaction kinetics, i.e., the rate of producing C6NIO is proportional to the surface density (or molar fraction) of unreacted C6NIB.

The fitting gives $K' = 28176.33$, $K = 0.01193$, with a $R^2 = 0.9941$, then the reaction time can be projected at a given ΔI

$$t = -\frac{\ln\left(\frac{-\Delta I + K'}{K'}\right)}{K} \quad (3.2)$$

The standard derivation (δ) of the emission intensity measurement shown in Figure 3.11 was about 96 (a.u.). The threshold of detectable emission can be set at an intensity level three times of the standard derivation (3δ), which is 288. Then, the corresponding sensor response time (t) can be determined as ca. 0.86 sec.

Fitting of the data are presented in the inset of Figure 3.11b. Assuming a

quasiequilibrium was reached within 5 min exposure (as implied from the result in Figure 3.10) to H₂O₂ vapor, the results shown Figure 3.11b should follow the Langmuir adsorption model. First, the surface adsorption of H₂O₂ (i.e., the reacted fraction of sensor molecules, X) is related to the vapor pressure of H₂O₂ as described by the Langmuir Equation,

$$X = \frac{b \cdot [\text{H}_2\text{O}_2]}{1 + b \cdot [\text{H}_2\text{O}_2]} \quad (3.3)$$

where b is a constant, $[\text{H}_2\text{O}_2]$ is the vapor pressure (concentration) of H₂O₂.

The fluorescence emission intensity is proportional to the concentration of sensor molecules converted. Then, we have

$$\Delta I = \frac{a \cdot b \cdot [\text{H}_2\text{O}_2]}{1 + b \cdot [\text{H}_2\text{O}_2]} \quad (3.4)$$

where a is a proportional constant. The fitting gives $a = 36986.6$, $b = 0.0027$ with a $R^2 = 0.9813$.

The standard derivation of the emission intensity measurement shown in Figure 3.11 was about 96 (a.u.). The threshold of detectable emission can be set at an intensity level three times of the standard derivation, that is $\Delta I = 288$. Then, the corresponding detection limit can be determined by using the above equation and substituting ΔI with 288. This gives a detection limit of H₂O₂ vapor at 2.9 ppb.

3.5.3.9 Absorption (Extinction) Spectral Measurement

Due to the nontransparency of the TLC plate, the absorption spectra of the sensors dispersed in this medium had to be measured in reflection mode, which can then be converted into extinction spectral data (in analogy to light absorption). The reflection spectra were recorded on a PerkinElmer Lambda 650R spectrophotometer with a built-in universal reflection accessory. The spectra were collected with unpolarized light incident at $\sim 45^\circ$ with respect to the surface and integrated for 0.1 s and at a resolution of 1 nm. The spectra collected were converted and shown as extinction measured as $-\log(R/R_0)$, where R is the reflectance of the loaded sample substrate and R_0 is the reflectance of the unloaded TLC plate substrate. (42)

3.5.3.10 Absorption and Fluorescence Spectra of C6NIO

Solution and Film

To study in detail the spectral property (the ICT transition band) of C6NIO and the dependence on deprotonation of the phenol group, the UV-vis absorption and fluorescent spectra of C6NIO in ethanol solution were measured with addition of TBAH at different molar ratios of TBAH/ C6NIO, ranging from 1 to 100. As shown in Figure 3.4a, the ICT absorption band increased dramatically with the addition of TBAH and reached its maximum at a molar ratio of 10 (TBAH/ C6NIO). This increase in ICT band is due to the deprotonation process, transforming the phenol group of C6NIO to phenolate. The corresponding ICT emission band of C6NIO showed a similar change upon addition of TBAH, also reaching its maximal intensity at a molar ratio of 10 (TBAH/ C6NIO) (Figure 3.4b).

3.6 References

- (1) Yang, J.-S.; Swager, T. M. Fluorescent Porous Polymer Films as TNT Chemosensors: Electronic and Structural Effects. *J. Am. Chem. Soc.* **1998**, *120*, 11864-11873.
- (2) Naddo, T.; Che, Y.; Zhang, W.; Balakrishnan, K.; Yang, X.; Yen, M.; Zhao, J.; Moore, J. S.; Zang, L. Detection of Explosives with a Fluorescent Nanofibril Film. *J. Am. Chem. Soc.* **2007**, *129*, 6978-6979.
- (3) Zyryanov, G. V.; Palacios, M. A.; Anzenbacher, P. Simple Molecule-Based Fluorescent Sensors for Vapor Detection of TNT. *Org. Lett.* **2008**, *10*, 3681-3684.
- (4) Zhang, C.; Che, Y.; Yang, X.; Bunes, B. R.; Zang, L. Organic Nanofibrils Based on Linear Carbazole Trimer for Explosive Sensing. *Chem. Commun.* **2010**, *46*, 5560-5562.
- (5) Kartha, K. K.; Babu, S. S.; Srinivasan, S.; Ajayaghosh, A. Attogram Sensing of Trinitrotoluene with a Self-Assembled Molecular Gelator. *J. Am. Chem. Soc.* **2012**, *134*, 4834-4841.
- (6) Che, Y.; Gross, D. E.; Huang, H.; Yang, D.; Yang, X.; Discekici, E.; Xue, Z.; Zhao, H.; Moore, J. S.; Zang, L. Diffusion-Controlled Detection of Trinitrotoluene: Interior Nanoporous Structure and Low Highest Occupied Molecular Orbital Level of Building Blocks Enhance Selectivity and Sensitivity. *J. Am. Chem. Soc.* **2012**, *134*, 4978-4982.
- (7) Zheng, J. Y.; Yan, Y.; Wang, X.; Shi, W.; Ma, H.; Zhao, Y. S.; Yao, J. Hydrogen Peroxide Vapor Sensing with Organic Core/Sheath Nanowire Optical Waveguides. *Adv. Mater.* **2012**, *24*, OP194-OP199.
- (8) Grate, J. W.; Ewing, R. G.; Atkinson, D. A. Vapor-Generation Methods for Explosives-Detection Research. *TrAC, Trends Anal. Chem.* **2012**, *41*, 1-14.
- (9) Andrew, T. L.; Swager, T. M. A Fluorescence Turn-on Mechanism to Detect High Explosives Rdx and Petn. *J. Am. Chem. Soc.* **2007**, *129*, 7254-7255.
- (10) Sanchez, J. C.; Trogler, W. C. Polymerization of a Boronate-Functionalized Fluorophore by Double Transesterification: Applications to Fluorescence Detection of Hydrogen Peroxide Vapor. *J. Mater. Chem.* **2008**, *18*, 5134-5141.
- (11) Andrew, T. L.; Swager, T. M. Detection of Explosives Via Photolytic Cleavage of Nitroesters and Nitramines. *J. Org. Chem.* **2011**, *76*, 2976-2993.
- (12) Germain, M. E.; Knapp, M. J. Turn-on Fluorescence Detection of H₂O₂ and TATP. *Inorg. Chem.* **2008**, *47*, 9748-9750.
- (13) Sanchez, J. C.; Trogler, W. C. Efficient Blue-Emitting Silafluorene-Fluorene-Conjugated Copolymers: Selective Turn-Off/Turn-on Detection of Explosives. *J. Mater. Chem.* **2008**, *18*, 3143-3156.

- (14) Schulte-Ladbeck, R.; Vogel, M.; Karst, U. Recent Methods for the Determination of Peroxide-Based Explosives. *Anal. Bioanal. Chem.* **2006**, *386*, 559-565.
- (15) Wang, J. Electrochemical Sensing of Explosives. *Electroanalysis* **2007**, *19*, 415-423.
- (16) Burks, R.; Hage, D. Current Trends in the Detection of Peroxide-Based Explosives. *Anal. Bioanal. Chem.* **2009**, *395*, 301-313.
- (17) Bohrer, F. I.; Colesniuc, C. N.; Park, J.; Schuller, I. K.; Kummel, A. C.; Trogler, W. C. Selective Detection of Vapor Phase Hydrogen Peroxide with Phthalocyanine Chemiresistors. *J. Am. Chem. Soc.* **2008**, *130*, 3712-3713.
- (18) Benedet, J.; Lu, D. L.; Cizek, K.; La Belle, J.; Wang, J. Amperometric Sensing of Hydrogen Peroxide Vapor for Security Screening. *Anal. Bioanal. Chem.* **2009**, *395*, 371-376.
- (19) Lu, Y.; Meyyappan, M.; Li, J. Trace Detection of Hydrogen Peroxide Vapor Using a Carbon-Nanotube-Based Chemical Sensor. *Small* **2011**, *7*, 1714-1718.
- (20) Lu, D.; Cagan, A.; Munoz, R. A. A.; Tangkuaram, T.; Wang, J. Highly Sensitive Electrochemical Detection of Trace Liquid Peroxide Explosives at a Prussian-Blue 'Artificial-Peroxidase' Modified Electrode. *Analyst* **2006**, *131*, 1279-1281.
- (21) Lin, H.; Suslick, K. S. A Colorimetric Sensor Array for Detection of Triacetone Triperoxide Vapor. *J. Am. Chem. Soc.* **2010**, *132*, 15519-15521.
- (22) Xu, M.; Bunes, B. R.; Zang, L. Paper-Based Vapor Detection of Hydrogen Peroxide: Colorimetric Sensing with Tunable Interface. *ACS Appl. Mater. Interfaces* **2011**, *3*, 642-647.
- (23) Matsubara, C.; Kawamoto, N.; Takamura, K. Oxo[5, 10, 15, 20-Tetra(4-Pyridyl)Porphyrinato]Titanium(IV): An Ultra-High Sensitivity Spectrophotometric Reagent for Hydrogen Peroxide. *Analyst* **1992**, *117*, 1781-1784.
- (24) Lo, L. C.; Chu, C. Y. Development of Highly Selective and Sensitive Probes for Hydrogen Peroxide. *Chem. Commun.* **2003**, 2728-2729.
- (25) Schuster, G. B. Chemiluminescence of Organic Peroxides. Conversion of Ground-State Reactants to Excited-State Products by the Chemically Initiated Electron-Exchange Luminescence Mechanism. *Acc. Chem. Res.* **1979**, *12*, 366-373.
- (26) Lippert, A. R.; Van de Bittner, G. C.; Chang, C. J. Boronate Oxidation as a Bioorthogonal Reaction Approach for Studying the Chemistry of Hydrogen Peroxide in Living Systems. *Acc. Chem. Res.* **2011**, *44*, 793-804.
- (27) Lee, D.; Khaja, S.; Velasquez-Castano, J. C.; Dasari, M.; Sun, C.; Petros, J.; Taylor, W. R.; Murthy, N. In Vivo Imaging of Hydrogen Peroxide with Chemiluminescent

Nanoparticles. *Nat. Mater.* **2007**, *6*, 765-769.

(28) Marom, H.; Popowski, Y.; Antonov, S.; Gozin, M. Toward the Development of the Direct and Selective Detection of Nitrates by a Bioinspired Mo–Cu System. *Org. Lett.* **2011**, *13*, 5532-5535.

(29) Montoya, L. A.; Pluth, M. D. Selective Turn-on Fluorescent Probes for Imaging Hydrogen Sulfide in Living Cells. *Chem. Commun.* **2012**, *48*, 4767-4769.

(30) Srikun, D.; Miller, E. W.; Domaille, D. W.; Chang, C. J. An Ict-Based Approach to Ratiometric Fluorescence Imaging of Hydrogen Peroxide Produced in Living Cells. *J. Am. Chem. Soc.* **2008**, *130*, 4596-4597.

(31) Liu, Y.; Niu, F.; Lian, J.; Zeng, P.; Niu, H. Synthesis and Properties of Starburst Amorphous Molecules: 1,3,5-Tris(1,8-Naphthalimide-4-Yl)Benzenes. *Synth. Met.* **2010**, *160*, 2055-2060.

(32) Sun, W.; Li, W.; Li, J.; Zhang, J.; Du, L.; Li, M. Naphthalimide-Based Fluorescent Off/on Probes for the Detection of Thiols. *Tetrahedron* **2012**, *68*, 5363-5367.

(33) Lin, M.-J.; Fimmel, B.; Radacki, K.; W ü rthner, F. Halochromic Phenolate Perylene Bisimides with Unprecedented NIR Spectroscopic Properties. *Angew. Chem. Int. Ed.* **2011**, *50*, 10847-10850.

(34) Manatt, S. L.; Manatt, M. R. R. On the Analyses of Mixture Vapor Pressure Data: The Hydrogen Peroxide/Water System and Its Excess Thermodynamic Functions. *Chem. Eur. J.* **2004**, *10*, 6540-6557.

(35) Cumming, C. J.; Aker, C.; Fisher, M.; Fok, M.; La Grone, M. J.; Reust, D.; Rockley, M. G.; Swager, T. M.; Towers, E.; Williams, V. Using Novel Fluorescent Polymers as Sensory Materials for above-Ground Sensing of Chemical Signature Compounds Emanating from Buried Landmines. *IEEE Trans. Geosci. Electron.* **2001**, *39*, 1119-1128.

(36) Wu, J.; Yi, T.; Shu, T.; Yu, M.; Zhou, Z.; Xu, M.; Zhou, Y.; Zhang, H.; Han, J.; Li, F.; Huang, C. Ultrasound Switch and Thermal Self-Repair of Morphology and Surface Wettability in a Cholesterol-Based Self-Assembly System. *Angew. Chem. Int. Ed.* **2008**, *47*, 1063-1067.

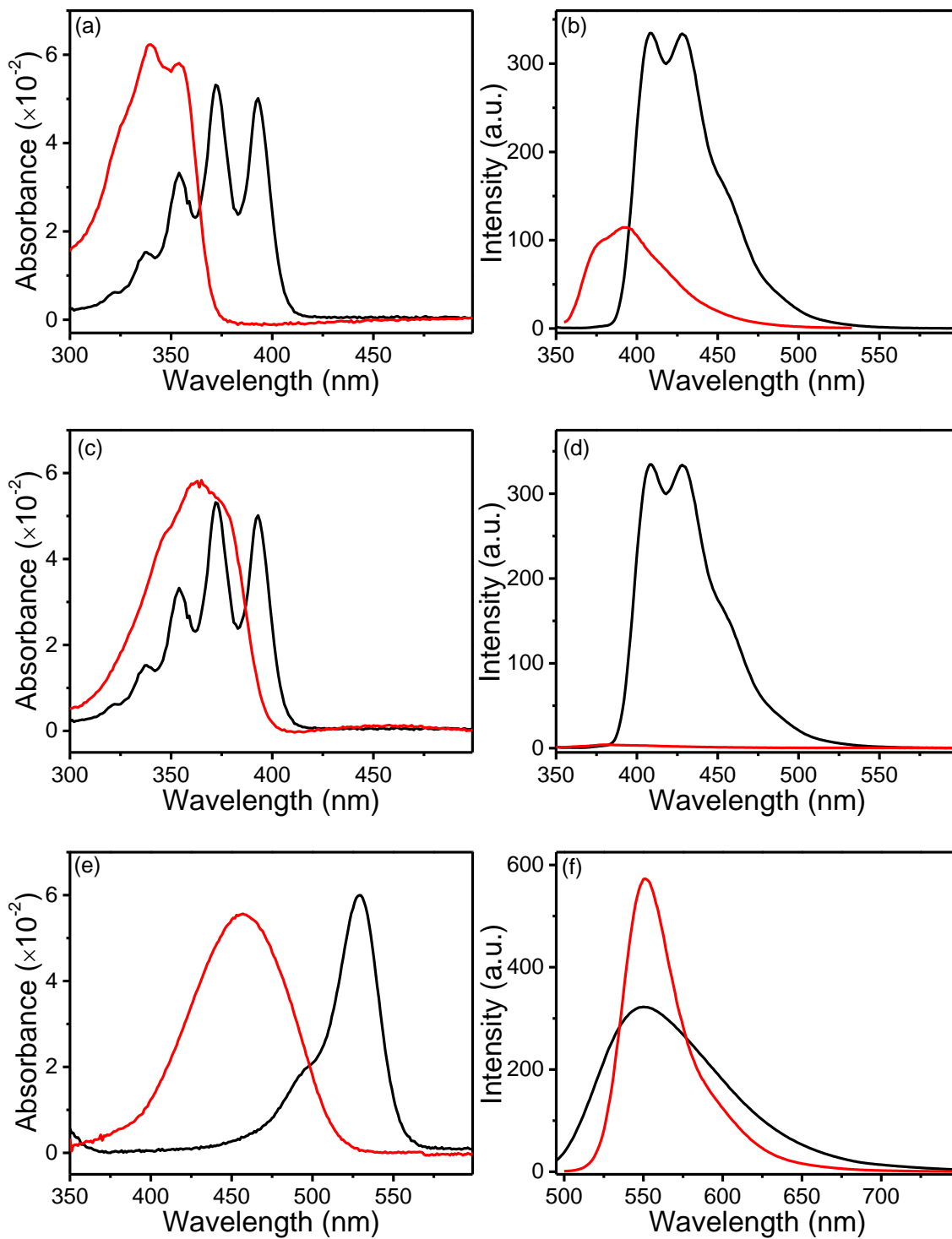
(37) Thiemann, F.; Piehler, T.; Haase, D.; Saak, W.; Lützen, A. Synthesis of Enantiomerically Pure Dissymmetric 2,2'-Disubstituted 9,9'-Spirobifluorenes. *Eur. J. Org. Chem.* **2005**, *2005*, 1991-2001.

(38) Lakowicz, J. R. *Principles of Fluorescence Spectroscopy*; 2nd ed.; Kluwer Academic/Plenum Publishers, New York, 1999.

(39) Mardelli, M.; Olmsted Iii, J. Calorimetric Determination of the 9,10-Diphenyl-Anthracene Fluorescence Quantum Yield. *J. Photochem.* **1977**, *7*, 277-285.

- (40) Fischer, M.; Georges, J. Fluorescence Quantum Yield of Rhodamine 6g in Ethanol as a Function of Concentration Using Thermal Lens Spectrometry. *Chem. Phys. Lett.* **1996**, *260*, 115-118.
- (41) Xu, M.; Bunes, B. R.; Zang, L. Paper-Based Vapor Detection of Hydrogen Peroxide: Colorimetric Sensing with Tunable Interface. *ACS Appl. Mater. Interfaces* **2011**, *3*, 642-647.
- (42) Driskell, J. D.; Lipert, R. J.; Porter, M. D. Labeled Gold Nanoparticles Immobilized at Smooth Metallic Substrates: Systematic Investigation of Surface Plasmon Resonance and Surface-Enhanced Raman Scattering. *J. Phys. Chem. B* **2006**, *110*, 17444-17451.

Figure 3.1 Absorption and fluorescence spectra of C6NIB, C6NIO, and the corresponding standard fluorophores used for measuring the quantum yields: (a,b) C6NIB in ethanol (red) and 9,10-DAP in cyclohexane (black); (c,d) C6NIB with 100 molar fold TBAH in ethanol (red) and 9,10-DAP in cyclohexane (black); (e,f) C6NIO with 100 molar fold TBAH in ethanol (red) and Rhodamine 6G in ethanol (black).



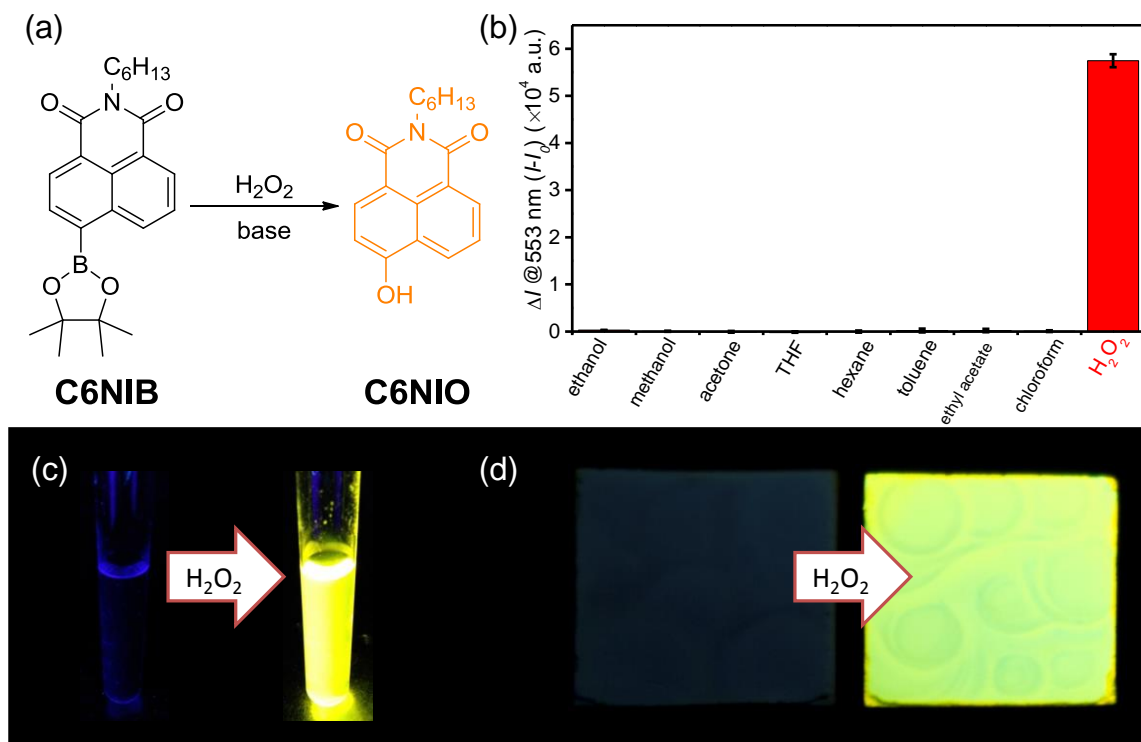


Figure 3.2 Figures show the detection mechanism of this fluorescent sensor: (a) The fluorescence turn-on reaction between the sensor molecule (C6NIB) and H₂O₂. (b) The sensing of C6NIB is extremely selective for H₂O₂ (225 ppm) as tested against the saturated vapor of other common solvents, ethanol (89,000 ppm), methanol (131,000 ppm), acetone (260,000 ppm), THF (173,000 ppm), hexane (130,000 ppm), toluene (26,000 ppm), ethyl acetate (100,000 ppm), chloroform (140,000 ppm). (c, d) Photographs showing the fluorescence turn-on of C6NIB in ethanol solution (1 × 10⁻³ M, containing 1 × 10⁻² M TBAH) and dispersed in a 1.5 × 1.5 cm² silica gel TLC plate (0.5 μmol C6NIB and 5 μmol TBAH) after exposure to H₂O₂.

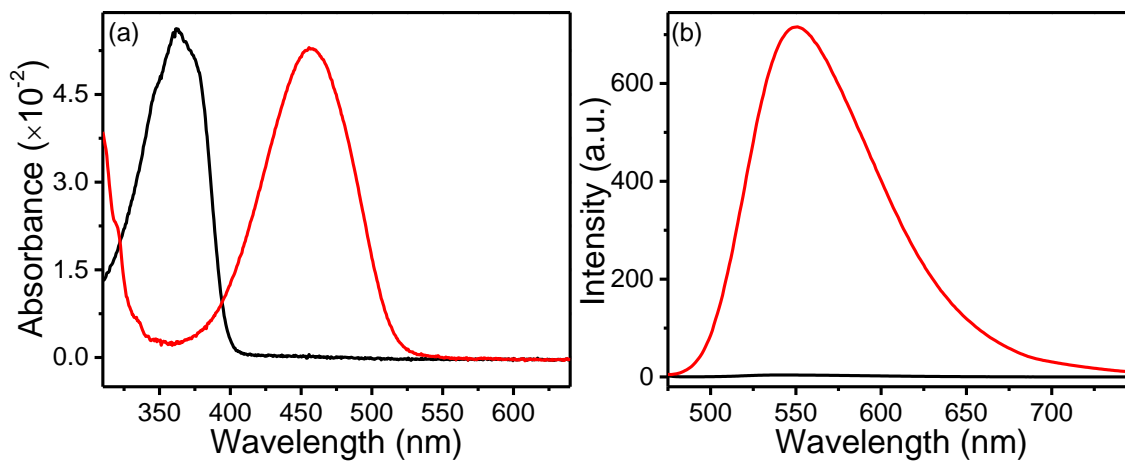


Figure 3.3 The solution spectra of C6NIB solution were recorded before and after the addition of H_2O_2 : (a) Absorption and (b) fluorescence spectra of an ethanol solution of C6NIB (5×10^{-6} M, in the presence of 5×10^{-4} M TBAH) before (black) and after (red) addition of 5×10^{-3} M H_2O_2 .

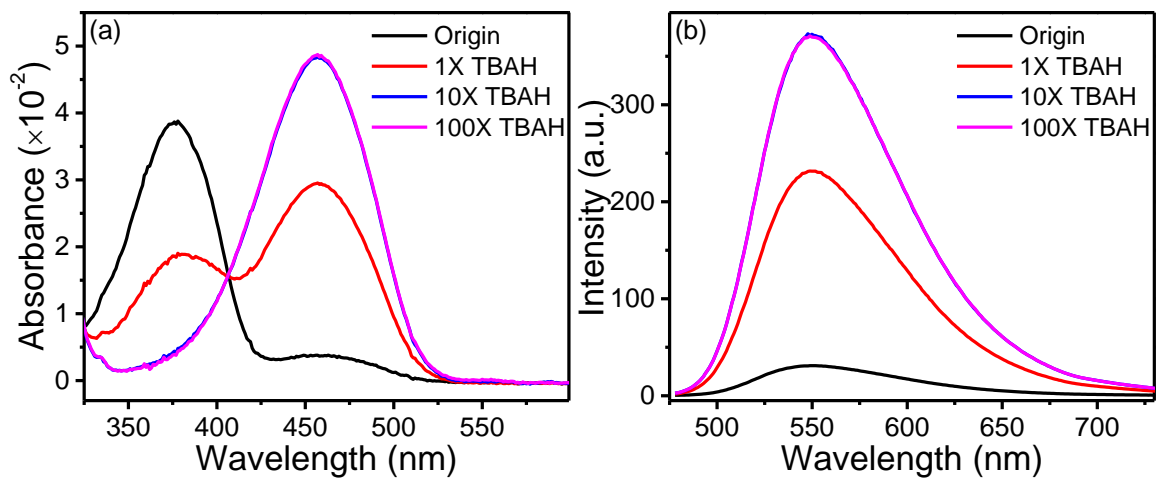


Figure 3.4 The spectra of C6NIO were recorded under the addition of different amounts of TBAH: (a) Absorption and (b) fluorescence spectra of an ethanol solution of C6NIO (black, 5×10^{-6} M) with addition of different amounts of TBAH (red, 5×10^{-6} M; blue, 5×10^{-5} M; purple, 5×10^{-4} M), $\lambda_{\text{ex}} = 458$ nm.

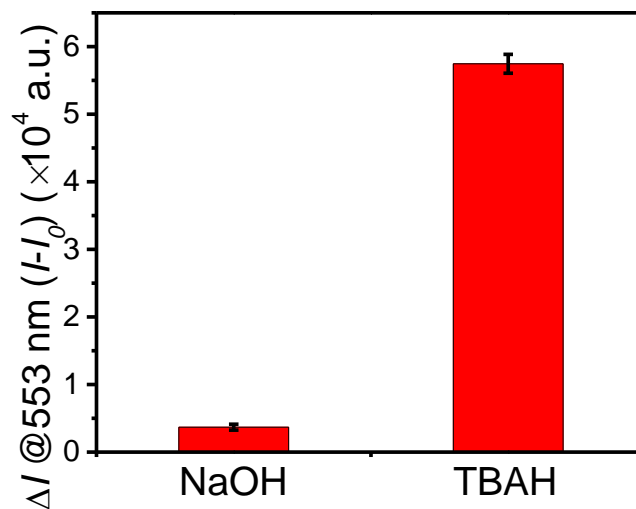


Figure 3.5 The increase in fluorescence intensity observed for the TLC plate samples treated with the same sensor but different bases (NaOH and TBAH); the fluorescence was monitored at 553 nm after exposure to 225 ppm H₂O₂ vapor for 5 min. The TLC plates were in the size of 1.5 × 1.5 cm², and containing 0.5 μmol C6NIB and 5 μmol base. The error bars are based on the standard deviations of the data.

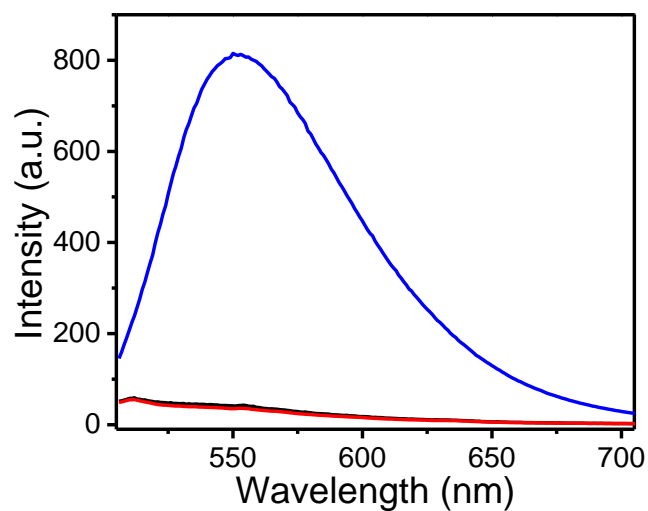


Figure 3.6 The fluorescence spectra of C6NIB dispersed in a $1.5 \times 1.5 \text{ cm}^2$ silica gel TLC plate (containing $0.5 \text{ }\mu\text{mol}$ C6NIB and $5 \text{ }\mu\text{mol}$ TBAH): freshly prepared TLC plate (black), after 7 days (red), and after exposure to 225 ppm H₂O₂ vapor for 5 min (blue).

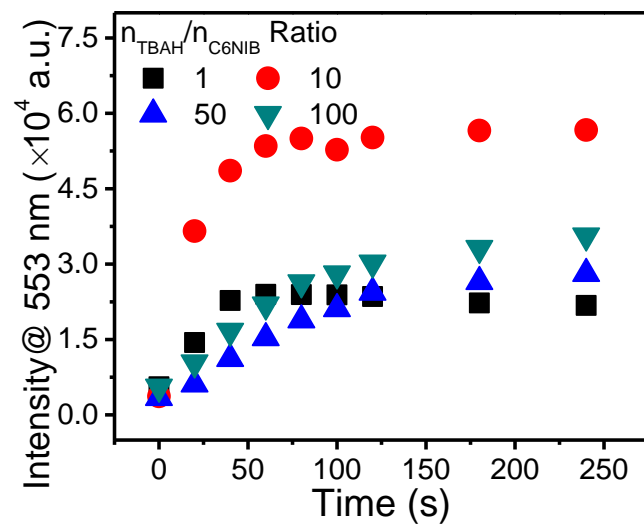


Figure 3.7 Time course of the fluorescence intensity change measured at 553 nm for C6NIB dispersed in a 1.5×1.5 cm² silica gel TLC plate (containing 0.5 μ mol C6NIB) upon exposure to 225 ppm H₂O₂ vapor. Shown in Figure 3.7 are four series of measurements performed over the TLC plates containing the same molar amount of C6NIB, but different amounts of TBAH, i.e., at molar ratios of TBAH/C6NIB: 1, 10, 50 and 100.

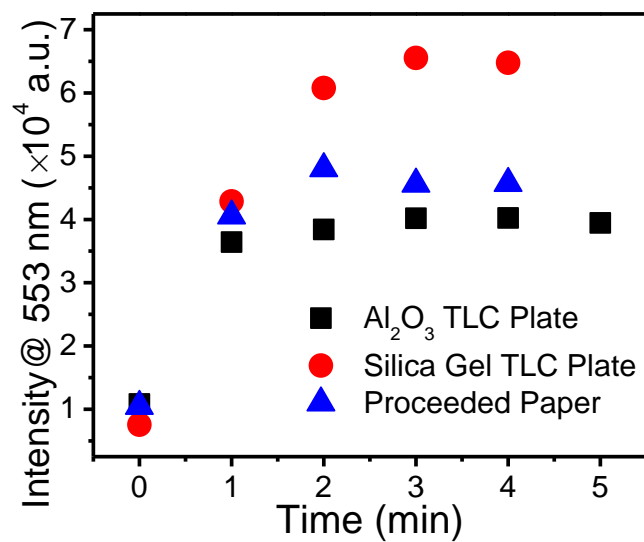


Figure 3.8 Time course of the fluorescence intensity change measured at 553 nm for C6NIB dispersed in different supporting materials (Al₂O₃ TLC plate, silica gel TLC plate, filter paper), all in the area size of 1.5×1.5 cm², and containing 0.5 μ mol C6NIB and 5 μ mol TBAH.

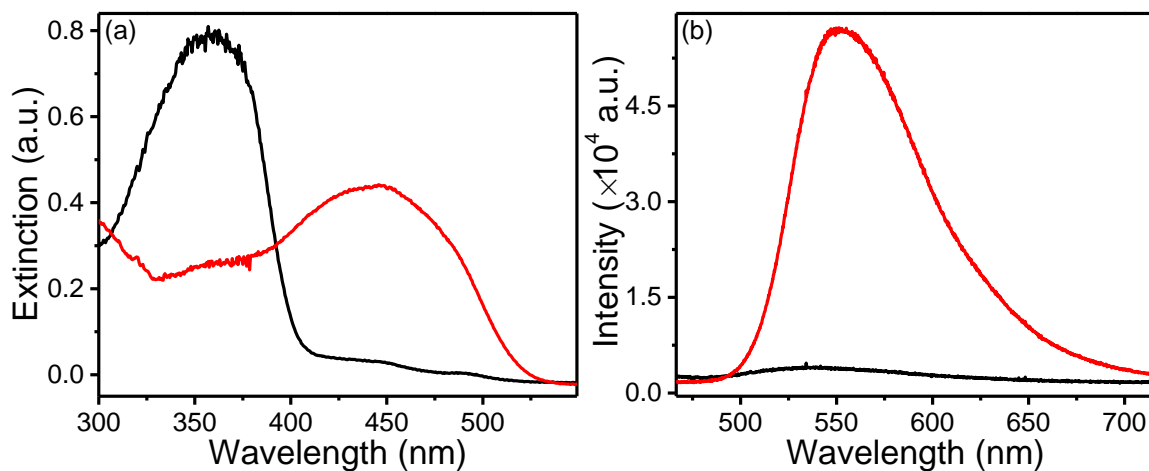


Figure 3.9 The spectra of C6NIB dispersed on TLC plate were recorded: (a) Extinction (converted from reflection spectrum) and (b) fluorescence spectra of C6NIB dispersed in a 1.5×1.5 cm² silica gel TLC plate (containing 0.5 μ mol C6NIB and 5 μ mol TBAH) before (black) and after (red) exposure to 225 ppm H₂O₂ vapor for 5 min.

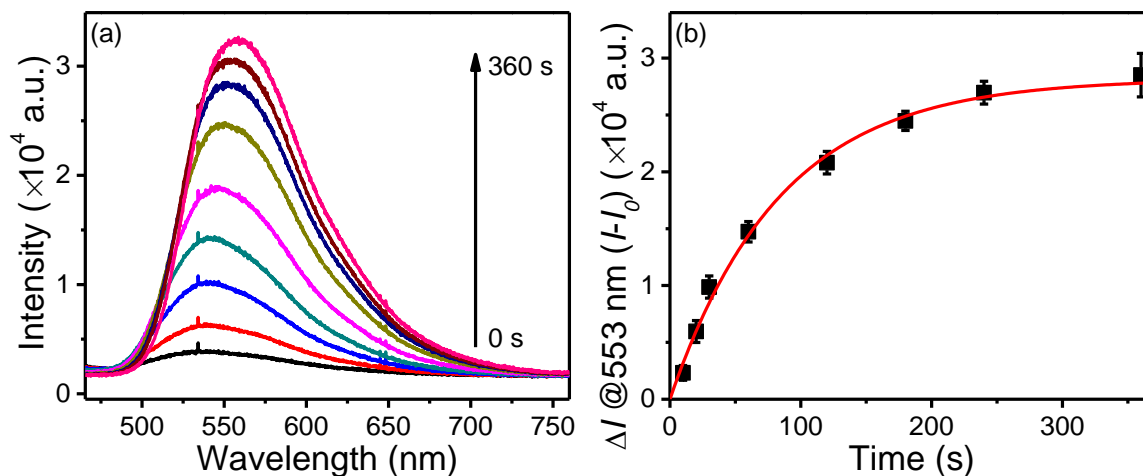


Figure 3.10 The emission spectra of C6NIB dispersed on TLC plate were recorded over H₂O₂ exposure time: (a) The fluorescence spectra of C6NIB dispersed in a 1.5 × 1.5 cm² silica gel TLC plate (containing 0.5 μmol C6NIB and 5 μmol TBAH) recorded at various time intervals after exposure to 1 ppm H₂O₂ vapor. (b) The emission intensity increase ΔI measured at 553 nm as a function of exposure time, for which the data points are fitted following a first order surface reaction between C6NIB and H₂O₂. The error bars are based on the standard derivations of the intensities as measured.

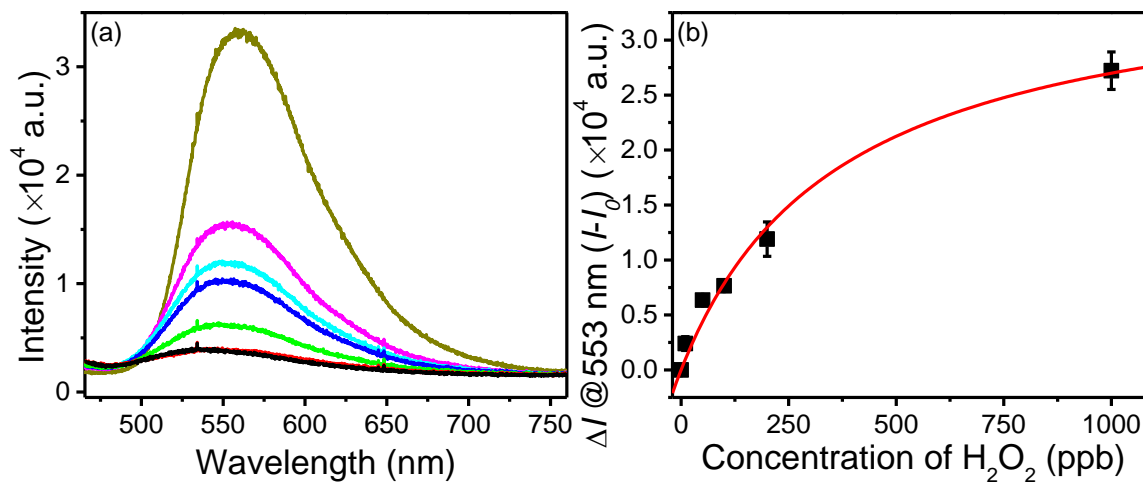
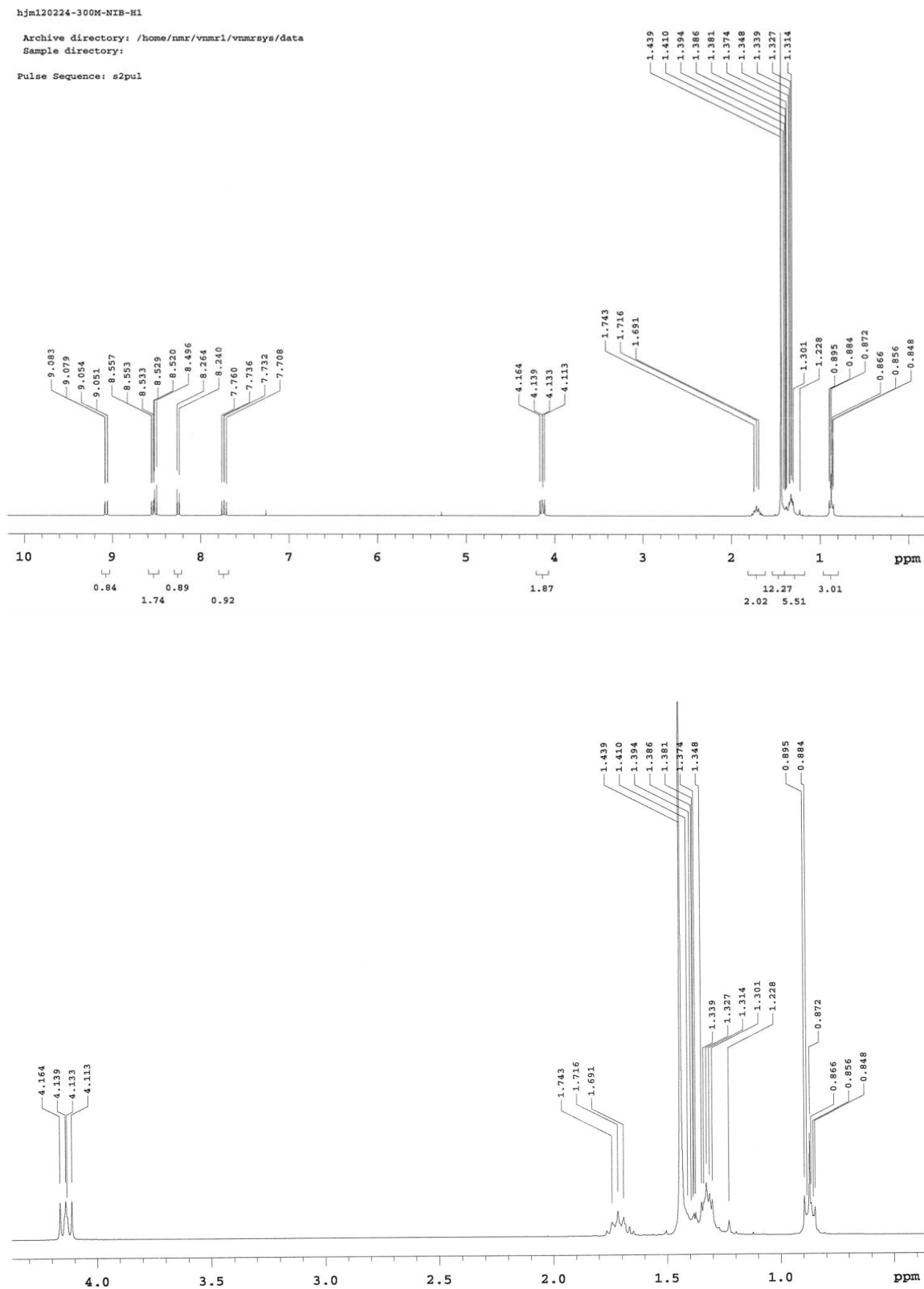


Figure 3.11 The emission spectra of C6NIB dispersed on TLC plate were recorded under different H₂O₂ vapor pressures: (a) The fluorescence spectra of C6NIB dispersed in a silica gel TLC plate (the same as Figure 3.2d) measured before (base line) and after 5 min of exposure to various vapor concentrations of H₂O₂, 0 (pure water vapor, overlapped with the base line), 10, 50, 100, 200, and 1000 ppb. (b) A plot showing the emission intensity increase ΔI as a function of the vapor concentration of H₂O₂, for which the data points are fitted following the Langmuir adsorption model.

Figure 3.12 ^1H NMR spectrum of C6NIB.

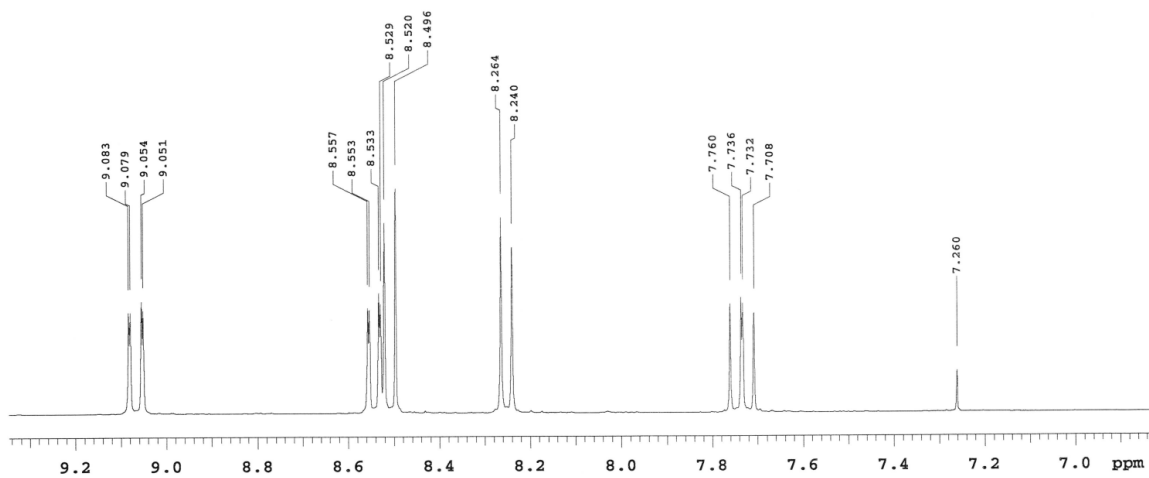


Figure 3.12 (continued).

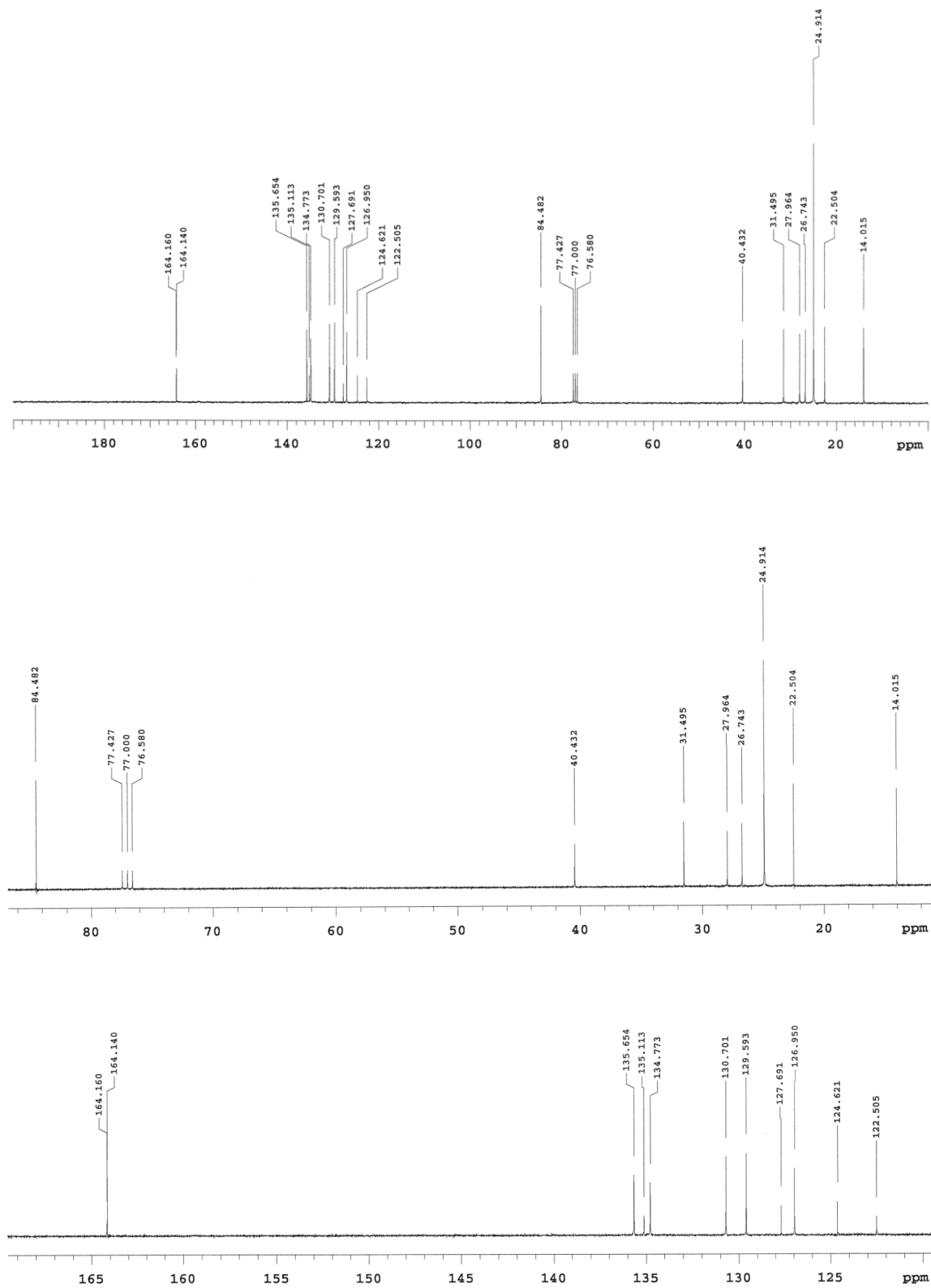
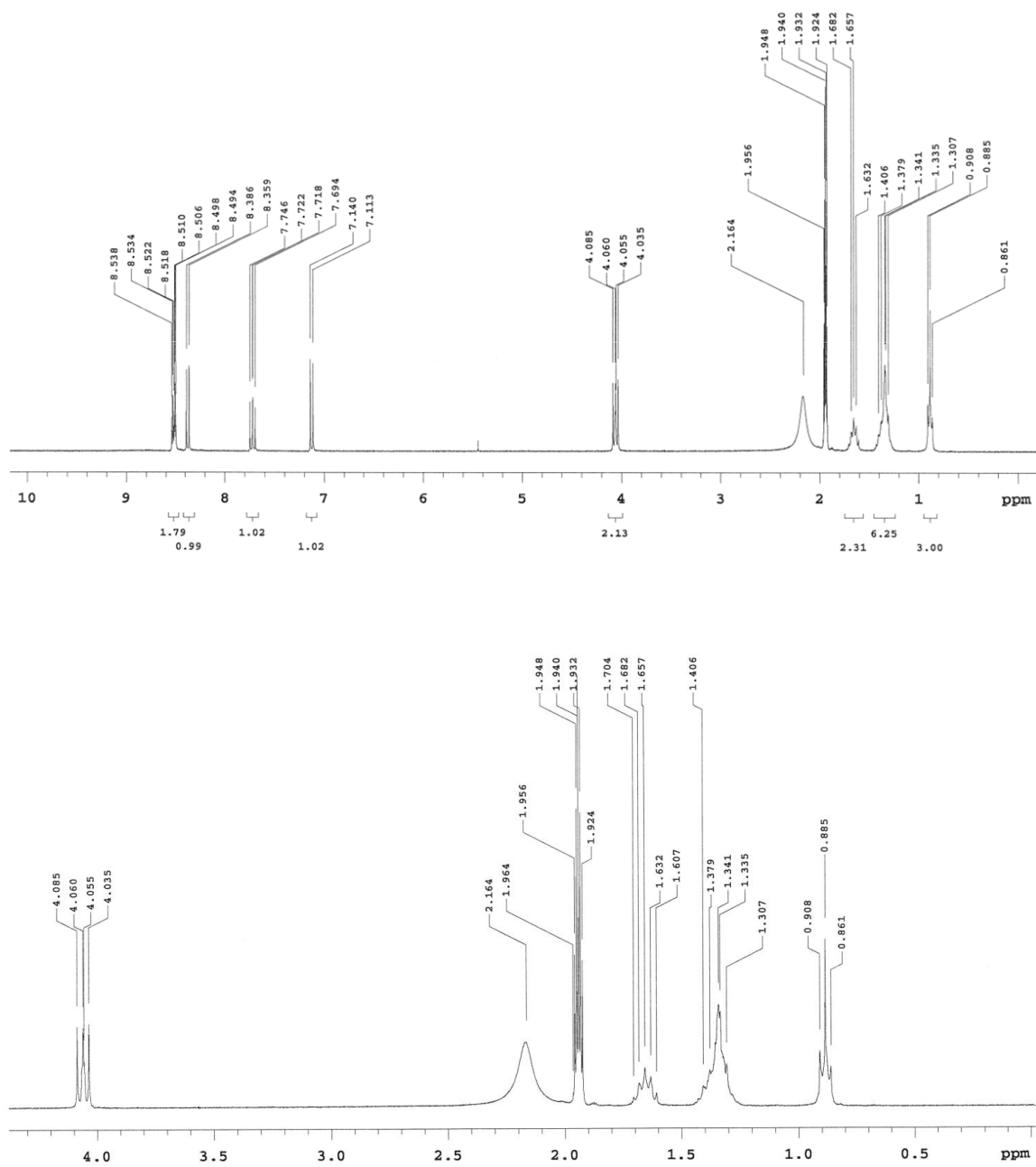


Figure 3.13 ^{13}C NMR spectrum of C6NIB.

C6NIO_CD3CN_091813

Archive directory: /home/nmr/vnmr1/vnmrdata
Sample directory:

Pulse Sequence: s2pul

Figure 3.14 ^1H NMR spectrum of C6NIO.

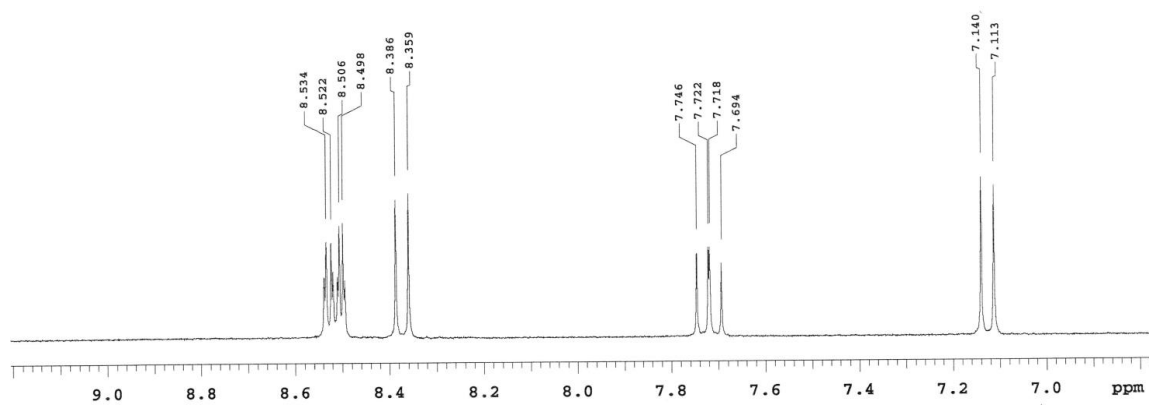


Figure 3.14 (continued).

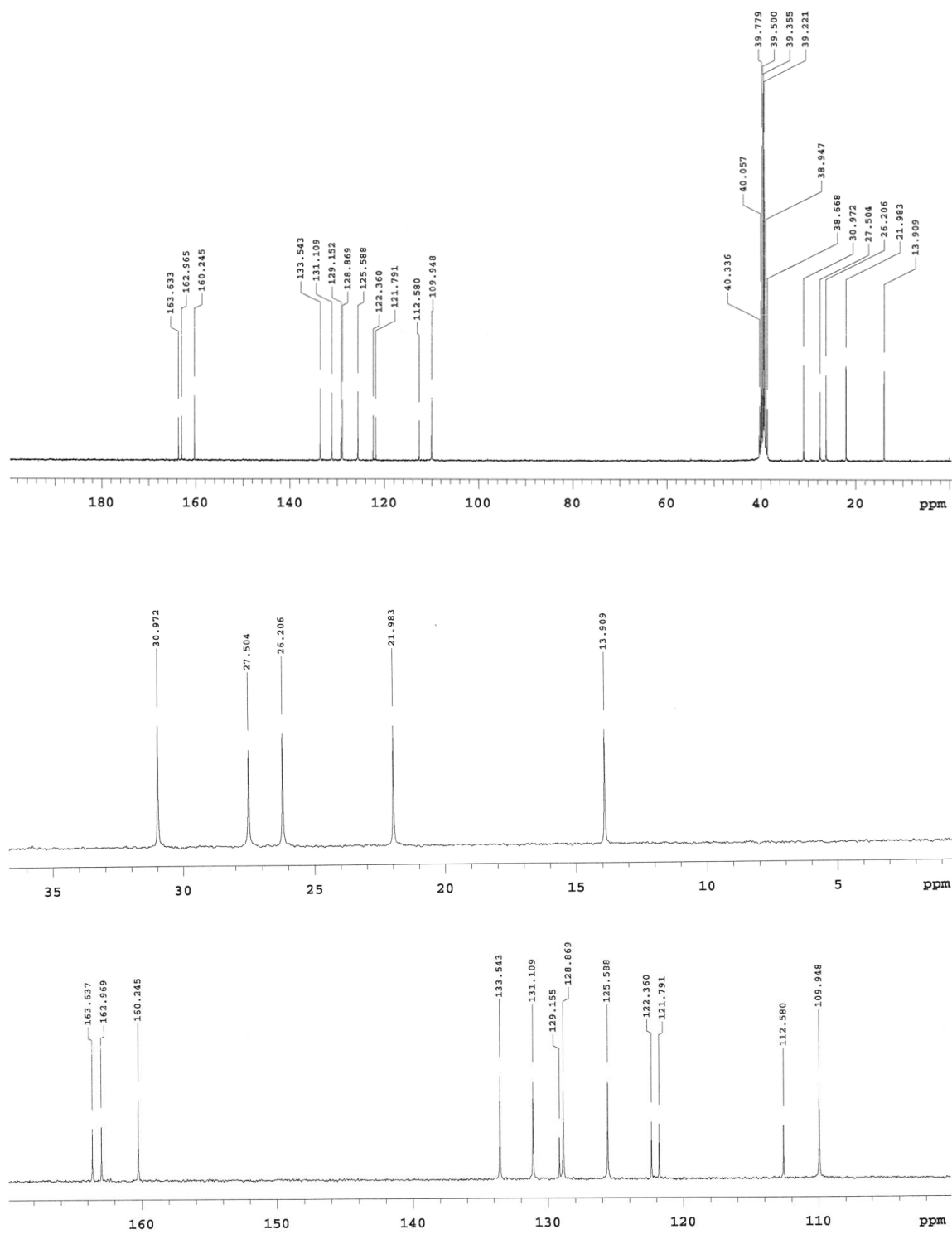


Figure 3.15 ^{13}C NMR spectrum of C_6NIO .

CHAPTER 4

FLUORESCENCE RATIOMETRIC SENSOR FOR TRACE VAPOR

DETECTION OF HYDROGEN PEROXIDE¹

4.1 Abstract

Trace vapor detection of hydrogen peroxide (H₂O₂) represents a practical approach to nondestructive detection of peroxide-based explosives, including liquid mixtures of H₂O₂ and fuels, and energetic peroxide derivatives, such as triacetone triperoxide (TATP), diacetone diperoxide (DADP) and hexamethylene triperoxide diamine (HMTD). Development of a simple chemical sensor system that responds to H₂O₂ vapor with high reliability and sufficient sensitivity (reactivity) remains a challenge. We report a fluorescence ratiometric sensor molecule, diethyl 2, 5-bis((((4-(4,4,5,5-tetramethyl-1,3,2-dioxaborolan-2-yl)benzyl)oxy)carbonyl)amino)terephthalate (DAT-B) for H₂O₂, which can be fabricated into an expedient, reliable and sensitive sensor system suitable for trace vapor detection of H₂O₂. DAT-B is fluorescent in the blue region with emission maximum at 500 nm in solid state. Upon reaction with H₂O₂, DAT-B is converted to an electronic

¹ Reprinted with permission from Xu, M.; Han, J.-M.; Wang, C.; Yang, X.; Pei, J.; Zang, L., Fluorescence Ratiometric Sensor for Trace Vapor Detection of Hydrogen Peroxide. *ACS Appl. Mater. Interfaces* **2014**, *6*, 8708-8714. Copyright (2014) American Chemical Society.

“push-pull” structure, diethyl 2,5-diaminoterephthalate (DAT-N), which has an emission peak at a longer wavelength centered at 574 nm. Such H₂O₂-mediated oxidation of aryl boronates can be accelerated through the addition of an organic base such as tetrabutylammonium hydroxide (TBAH), resulting in a response time less than 0.5 s under 1 ppm H₂O₂ vapor. The strong overlap between the absorption band of DAT-N and the emission band of DAT-B enables efficient Förster resonance energy transfer (FRET), thus allowing further enhancement of the sensing efficiency of H₂O₂ vapor. The detection limit of drop cast DAT-B/TBAH film was projected to be 7.7 ppb. Combining the high sensitivity and selectivity, the reported sensor system may find broad application in vapor detection of peroxide-based explosives and relevant chemical reagents, through fabrication into easy-to-use, cost-effective kits.

4.2 Introduction

Development of simple, cost-effective, and sensitive sensor systems to approach trace explosive detection becomes more critical with increasing concern over homeland security, military operational safety, and environmental and industrial concerns. (1-5) Of the explosive detection methods developed thus far, vapor detection is proven to be one of the practical, nondestructive ways suitable for both trace and bulk explosive monitoring. (6-20) Several methods were applied to developing novel vapor detection systems for explosives, including fluorescence spectroscopy (6,9,19,21-23), colorimetry (14,16,24-25), ion mobility spectrometry (IMS) (26-29) and the electrochemical method (7,10,30-32). Among the current vapor detection technologies, fluorescence spectroscopy is superior in its simple operation system, fast response, and high sensitivity.

Recently, fluorescence “turn-on” molecular sensors have drawn increasing attention

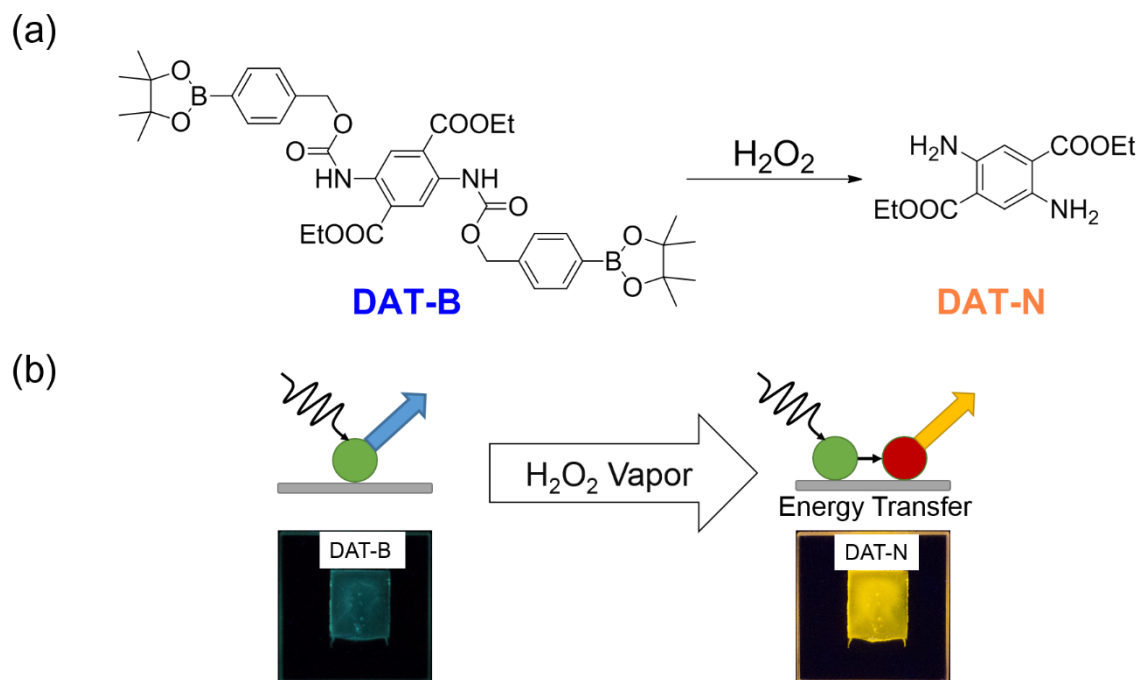
for explosive detection in both liquid and gas phases. (19,21,33-35) However, the influence of sensor concentration, local environment, and excitation intensity on fluorescence enhancement limits the development of these molecular sensors. (36) In general, these challenges can be overcome by the exploitation of ratiometric fluorescence sensors via Förster resonance energy transfer (FRET) between the pristine and reacted sensor molecules. FRET is a fundamental photophysical process and widely used for developing ion sensors (37-39), pH sensors (40-42), as well as explosive sensors (33,43-46) in solution, due to the capability of FRET to enhance the sensitivity and reliability of these sensors (47). The employment of energy transfer can benefit from dual emission wavelength monitoring to improve the reliability and reduce the background noise to improve the sensitivity. However, there are few reports on the FRET based fluorescent sensors for vapor detection.

Peroxide explosives, e.g., triacetone triperoxide (TATP), diacetone diperoxide (DADP) and hexamethylene triperoxide diamine (HMTD), can be easily made from commercially available products, and represent one class of the most elusive explosives. However, development of efficient sensors toward these explosives is hindered due to the lack of nitro group, nonfluorescence and minimal UV-vis absorption of these explosive compounds. (3,48) Hydrogen peroxide (H_2O_2) is typically taken as a signature compound for peroxide-based explosives, (48-49) which comes from either impurity of the explosives (as starting material) or the UV decomposition of peroxides. An appropriate trace vapor detection method for H_2O_2 will facilitate security monitoring. (50) There are various reports on the detection of H_2O_2 vapor, for example, using electrochemical (30,32), colorimetric (14,16), and fluorimetric (19,21-22) methods. However, the vapor detection of H_2O_2 at the trace level (e.g., ppb) remains challenging, mainly due to the combined

difficulty of molecular design and materials engineering to produce a sensor system that not only features strong binding with H_2O_2 (for efficient vapor sampling), but also an expedient, selective reaction with H_2O_2 to transduce a readable signal. Although there are a few recent papers reporting fluorescent vapor sensors for H_2O_2 , the stoichiometric response and single channel output limit the further improvement of sensitivity and reliability. There is a critical need to develop a simple, expedient, reliable fluorescence sensor system that can detect H_2O_2 vapor, ideally down to a few ppb.

4.3 Results and Discussion

Herein, we present a fluorescent ratiometric sensor, diethyl 2,5-bis((((4-(4,4,5,5-tetramethyl-1,3,2-dioxaborolan-2-yl)benzyl)oxy)carbonyl)amino)terephthalate (DAT-B) for H_2O_2 (Scheme 4.1), which enables efficient FRET between the pristine and reacted states in solid films, and serves as a highly sensitive and selective sensor for H_2O_2 vapor. The sensing mechanism lies in the oxidization of a boronate group of DAT-B, resulting in turning on the intramolecular charge transfer (ICT) band at longer wavelength (Figure 4.1). (51) This fluorescent molecule has a blue emission centered at 500 nm in drop cast film (Scheme 4.1b), which is attributed to the central π -conjugation of DAT-B. Upon reaction with H_2O_2 , the aryl boronate group in DAT-B is transformed to a phenol group, followed by a rearrangement of the side benzene group, producing an amino group at the core (Figure 4.2). The product thus formed, diethyl 2,5-diaminoterephthalate (DAT-N), has an electron donor-acceptor (“push-pull”) structure. The formation of a “push-pull” structure turns on the ICT transition, i.e., fluorescent emission in the longer wavelength band (λ_{max} at 574 nm). This new, red shifted emission makes DAT-B a suitable



Scheme 4.1 (a) Chemical reaction between the sensor molecule (DAT-B) and H_2O_2 , leading to formation of DAT-N; (b) illustration showing the intrinsic fluorescence emission of DAT-B and the FRET process between DAT-B and DAT-N; photographs at the bottom panel showing the fluorescence emission change of DAT-B film deposited on a quartz slide ($0.25 \mu\text{mol}$ DAT-B and $1.25 \mu\text{mol}$ TBAH, $1.0 \times 1.0 \text{ cm}^2$) after exposure to 225 ppm H_2O_2 for 5 min.

ratiometric fluorescence sensor for H_2O_2 detection. (52) The two emission bands at 500 and 574 nm can be monitored concurrently to measure the FRET process between DAT-B and DAT-N. Such dual band monitoring will enhance the reliability, while the FRET measurement will further increase the detection efficiency (Figure 4.3).

Recent work has shown that various functionalized DAT-N derivatives containing only one benzene ring as the aromatic component serve as novel fluorophores and emit intense visible light with excellent quantum yields ($> 90 \%$) in the solid state. (53) Taking

advantage of the “push-pull” structure, the emission colors can be tuned in the range from blue to red by simply modifying the side chain substituents. (53-55) Combination of the high solid state quantum yield and facile structure modification is highly conducive to development of solid state sensors that can be tuned to afford efficient FRET to further enhance detection efficiency. The boronate group was chosen to functionalize the DAT-B due to its highly selective reaction with H₂O₂. (51) Moreover, the strong electron withdrawing capability of the amide group weakens the electron donating strength of the amino group, thus blocking the ICT transition with DAT-B.

The H₂O₂ mediated oxidation of boronate (shown in Scheme 4.1a) was investigated in detail through both UV-vis absorption and fluorescence spectral measurements of DAT-B and DAT-N in drop cast films. As shown in Figure 4.4, the main absorption of the reaction product DAT-N shifts to longer wavelength by ca. 103 nm. This red shifted absorption band corresponds to the ICT transition between the amino groups and carbonyl modified π -conjugation core. The conversion from an electron accepting group (amide) to an electron donating group (amino) renders formation of a “push-pull” structure in the molecule, which results in an ICT transition located at the longer wavelength absorption. (22) Before reacting with H₂O₂, the drop cast film of DAT-B mixed with tetrabutylammonium hydroxide (TBAH) emits a blue emission centered at 500 nm, which is attributed to the π - π^* transition of the molecule’s core. The significant spectral overlap between the absorption of DAT-N (acceptor) and the emission of DAT-B (donor) enables FRET between the two molecules. When cast in solid film the short distance between the molecules may produce high efficiency of FRET, which can in turn enhance the sensing sensitivity as discussed below. Due to the intrinsic reaction specificity of the boronate group with H₂O₂, the sensor molecule DAT-B demonstrated no obvious fluorescence shifts

or quenching upon exposure to the vapor of water, or common organic reagents such as alcohols, hexane, acetone, etc. (Figure 4.5).

The reaction speed of H_2O_2 -mediated oxidation of aryl boronates was greatly accelerated by the addition of a base. This assists the formation of HO_2^- anion (acting as a nucleophile) from H_2O_2 , which then reacts with the boronate group (a strong electrophile). (52) We chose TBAH as the base to produce both a basic condition needed for the oxidation reaction and a hydrophilic film surface for efficient condensation of H_2O_2 vapor (Figure 4.6). The DAT-B/TBAH film shows minimal spectral change compared to the pure DAT-B film within at least 7 days, which proves the stability of the composite film (Figure 4.7). The optimal molar ratio of TBAH to DAT-B in the composite film was determined to be 5:1, regarding both the reaction speed and total amount of DAT-B converted (Figure 4.8). Less TBAH gives incomplete oxidization of H_2O_2 and excess TBAH decreases the surface concentration of DAT-B molecules.

To demonstrate the efficient FRET between the sensor molecule DAT-B and its reaction product DAT-N, systematic absorption and emission spectral measurements of DAT-B/TBAH films were performed as shown in Figure 4.3. Figure 4.3a shows the spectra of DAT-B/TBAH film after being exposed to 500 ppb H_2O_2 vapor, in comparison to the spectra recorded over the directly blended DAT-B/DAT-N/TBAH film. Upon exposure to H_2O_2 vapor the major absorption peak of DAT-B at 353 nm decreases about 13 % along with an increase in the region around 420 nm. In contrast, the emission intensity of DAT-B at the main peak (500 nm) decreases over 75 %, along with a new emission band that emerged at the longer wavelength. This large fluorescence quenching of DAT-B cannot be explained by the stoichiometric reaction, which otherwise should be around 13 % as indicated by the absorption measurement. The much enhanced quenching efficiency is

attributed to the FRET between the pristine DAT-B molecule and reaction product DAT-N.

To further confirm the occurrence of FRET in the film, we prepared a film with DAT-B directly blended with DAT-N (molar ratio DAT-B/DAT-N = 9/1) and measured the absorption and emission spectra. Consistent with the 10 % decrease in concentration of DAT-B in the blended film, the absorption at 353 nm peak was decreased about the same percentage (Figure 4.3c). However, the emission intensity of DAT-B measured was decreased over 80 % compared to that of the DAT-B film without DAT-N. This extent of fluorescence quenching is eight times larger than the percentage of concentration decrease of DAT-B, indicating clearly the FRET quenching process between DAT-B and DAT-N. Such FRET based amplification of fluorescence quenching has been utilized in sensing applications, which has been proven to effectively lower the detection limit. (43) However, similar quenching amplification has rarely been applied in vapor detection systems, for which the major technical challenge lies in the molecular design and materials engineering that afford both efficient FRET and suitable interface for effective collection of analyte molecules. It would be interesting to compare the fluorescence quenching data shown in Figure 4.3b and 2d. Considering the comparable extent of emission intensity decrease in the two cases (both about 80 %), we may argue that the concentration of DAT-N produced in Figure 4.3b upon exposure to H₂O₂ vapor should be approximately the same as that blended in the film of Figure 4.3d, i.e., 0.025 μmol. This corresponds to only 10 % of DAT-B (initially 0.25 μmol) converted to DAT-N, though this small fraction of conversion generates as large as 80 % fluorescence quenching. Using a well-calibrated fluorometer, we can measure a 1 % decrease in emission intensity, meaning only 0.1 % conversion of DAT-B within the thin film. This will enable us to significantly shorten the sensor response

time under the same vapor pressure level of H_2O_2 .

The fluorescence spectral change of DAT-B film was also investigated by exposing to 1 ppm H_2O_2 vapor for different time intervals to demonstrate the response speed of this sensor system. The reaction was monitored by measuring the fluorescence emission of DAT-N. As shown in Figure 4.9, the fluorescence emission peak at 574 nm increases gradually with exposure time (corresponding to the generation of DAT-N), and in the same time, the emission peak at 500 nm (corresponding to the consumption of DAT-B) gradually decreases. The reaction kinetics as plotted as the emission intensity increase vs. the exposure time (shown in Figure 4.9b) are fitted to a pseudo-first order reaction kinetics. (56) Three times the standard deviation ($\sigma = 0.9$) of the noise floor is set as the threshold of detectable emission level. The corresponding response time for this sensor system is obtained from the fitted data (Figure 4.9b) as less than 0.5 sec. Such rapid response toward H_2O_2 vapor meets the urgent need of real-time in-field detection of peroxide-based explosives. This expedient sensor response towards low concentration H_2O_2 vapor (as low as 1 ppm) is likely due to the surface property, which is conducive to fast sampling of hydrophilic gas analytes.

To further explore the advantage of this DAT-B sensor system, the optimal sensor composite of DAT-B (blended with TBAH within drop cast film) was expected to afford a competitive detection limit. To determine the detection limit of this system, the DAT-B composite was exposed for 10 min to the vapor of aqueous solution of H_2O_2 in various concentrations (which provide correspondingly different vapor pressures of H_2O_2) (57) and the fluorescence intensity increases at 574 nm (relative to the value measured under pure water vapor) were recorded. The fluorescence intensity increases with the H_2O_2 vapor pressure (shown in Figure 4.10). Assuming a quasiequilibrium was reached within 10 min

exposure (as implied by the result in Figure 4.9b), the results shown Figure 4.10 follow the Langmuir adsorption model (see Supporting Information). After fitting the experimental data into the Langmuir equation, the detection limit of this sensor system is projected to be 7.7 ppb by defining an intensity increase of three times the standard deviation as the detectable signal. It should be noted that such high detection sensitivity (about two orders of magnitude better than the commercial fluorescence detector), was simply obtained through the drop cast film. Further improvement of sensitivity can be achieved by spin casting the sensor material into an optical tube coupled to a photodetector, as previously practiced by Swager et al. with the Fido detector system. (58)

4.4 Conclusion

In summary, we have developed an expedient fluorescence ratiometric sensor system for trace vapor detection of H_2O_2 . The sensing mechanism is based on H_2O_2 -mediated oxidation of a boronate fluorophore, DAT-B, which is then converted to an amino-substituted product, DAT-N. The emission of DAT-B film is blue (centered at 500 nm), whereas the emission of DAT-N within the same film is significantly red-shifted, to 574 nm. The red-shifted emission band is due to the ICT band of DAT-N. The spectral overlap of the DAT-B emission and DAT-N absorption band results in efficient FRET process, which can be exploited to enhance the sensor performance in terms of both sensitivity and response speed. Considering the over 70 nm separation between the emission bands of DAT-B and DAT-N, the sensor system thus developed will also be suited for dual channel (wavelength) monitoring to enhance the detection reliability, particularly compared to conventional fluorescence sensors based on single wavelength monitoring (quenching or turn-on). By blending the DAT-B sensor with a hydrophilic organic base with the

appropriate molar ratio, the sensor composite demonstrated effective vapor sampling (absorption) of H₂O₂, resulting in both high detection sensitivity (down to 7.7 ppb) and fast sensor response (down to 0.5 sec under 1 ppm H₂O₂). The exploitation of FRET in solid films broadens the sensor development for trace vapor detection, providing great potential for improvement of detection limit.

4.5 Experimental Methods and Materials

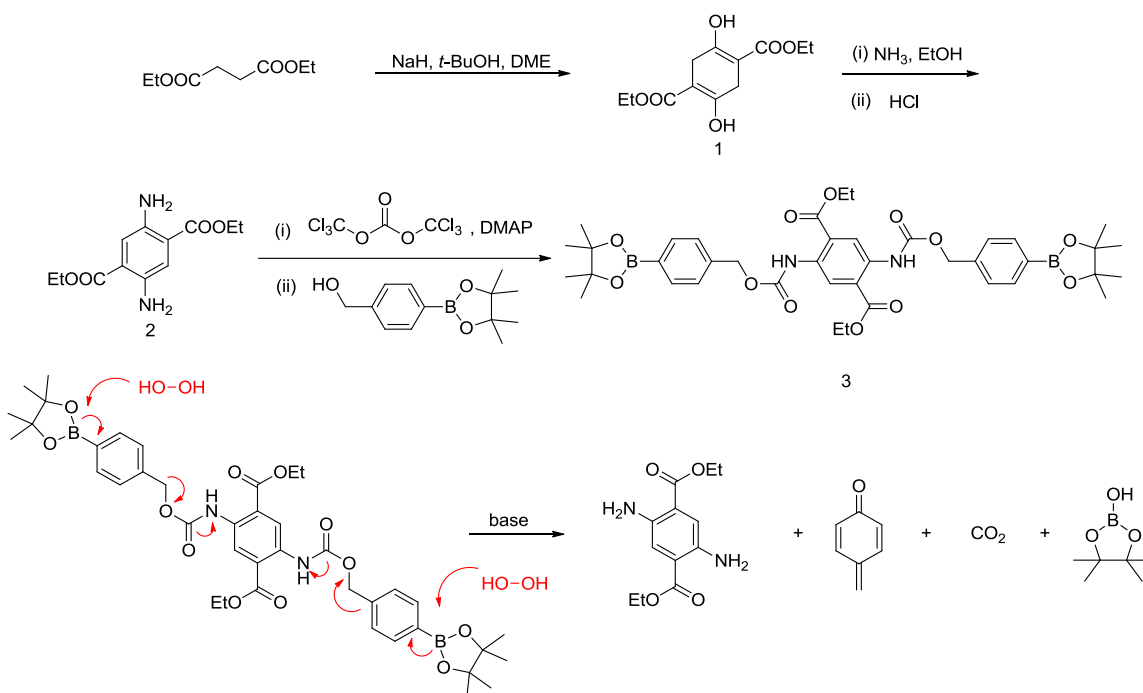
4.5.1 Materials and General Instrumentations

4-(Hydroxymethyl)phenylboronic acid pinacol ester, triphosgene, and 4-dimethylaminopyridine (DMAP) were purchased from Sigma-Aldrich and used as received. All solvents were purchased from the manufacturer and used as received unless otherwise noted.

UV-vis absorption spectra were measured on a PerkinElmer Lambda 25 spectrophotometer or Agilent Cary 100. The fluorescence spectra were measured on a PerkinElmer LS 55 spectrophotometer or Agilent Eclipse spectrophotometer. ¹H and ¹³C NMR spectra were recorded on a Varian Unity 300 MHz Spectrometer at room temperature in appropriate deuterated solvents. All chemical shifts are reported in parts per million (ppm). ESI HRMS spectra were recorded on a Micromass Quattro II Triple Quadrupole Mass Spectrometer, and the solvent used was methanol.

4.5.2 Synthesis

2, DAT-N: DAT-N was synthesized according to literature (see Scheme 4.2). (59) ¹H NMR (CDCl₃, 300 MHz, ppm): $\delta = 7.247$ (2 H, s, Ar-H), 4.376-4.305(4 H, q, CH₂),



Scheme 4.2 The synthetic route of sensor molecule DAT-B (3), and the possible mechanism (51) of the reaction between DAT-B and H₂O₂.

1.416-1.368 (6 H, t, CH₃)

3, DAT-B: DAT-B was synthesized following the method previously reported on the similar compound synthesis. (60) Triphosgene solution (58.8 mg, 0.198 mmol in 5 mL anhydrous toluene) was added dropwise to a mixture solution (4 mL anhydrous toluene) of DAT-N (50 mg, 0.198 mmol) and DMAP (72.6 mg, 0.595 mmol). This mixed solution was heated to reflux for 3 h. After cooling to room temperature, the reaction mixture was diluted with 6 mL anhydrous CH₂Cl₂ and filtered. The filtrate was added the boronated benzyl alcohol (51 mg, 0.218 mmol) and stirred at room temperature for an additional 3 h. The reaction was then concentrated and purified by flash column chromatography (silica gel, CHCl₃/MeOH). The product was obtained as light yellow powder (42 mg, 27.4 %). ¹H NMR (CDCl₃, 300 MHz, ppm, Figure 4.11): δ = 10.352(2 H, s, NH), 9.074 (2 H, s, Ar-H),

7.809-7.835 (4 H, d, Ar-H), 7.406-7.433(4 H, d, Ar-H), 5.238(4 H, s, CH₂), 4.368-4.439(4 H, q, CH₂), 1.396-1.443(6 H, t, CH₃), 1.343(24 H, s, CH₃) ¹³C NMR (CDCl₃, 75 MHz, ppm, Figure 4.12): δ = 167.223, 153.374, 139.024, 135.026, 134.973, 127.171, 121.124, 119.789, 83.794, 77.420, 46.993, 76.573, 66.735, 62.016, 24.807, 14.135. ESI-HRMS *m/z*: Calcd for: 772.3550, Found: [M+H]⁺ 773.3628.

4.5.3 Other Experimental Details

4.5.3.1 Dispersion of Sensor Molecules on Quartz Slide.

Twenty-five μ L ethanol solution of DAT-B at different concentrations (also containing appropriate concentrations of TBAH as detailed below) was drop-cast uniformly onto a 2.5 \times 2.5 cm² quartz slide to form a 1.0 \times 1.0 cm² solid film (guided by Scotch tapes), followed by drying at room temperature in vacuum for 1 h. To adjust the molar amount of DAT-B loading, various concentrations of DAT-B in ethanol were prepared and used: 0.02, 0.01 and 0.004 M. Uniform solid film of DAT-B sensor molecules within the solid film is indicated by the uniform emission density shown in the emission photography of the quartz slide after exposure to the H₂O₂ vapor (Scheme 4.1b). As shown in Figure 4.13, the film with 0.25 μ mol DAT-B gives the largest fluorescence change upon exposure to H₂O₂ vapor, which indicates the optimal sensor molecule amount used in this study.

4.5.3.2 Sensor Stability Test on Quartz Slide

The DAT-B coated quartz slide sample was prepared according to the method described above, and fluorescence spectra were measured at different time intervals after preparation (Figure 4.7), which did not show significant change in fluorescence spectra or intensity within the experimental investigation period. The same quartz slide was then

exposed to 225 ppm H₂O₂ vapor for 5 min, followed by measurement of the fluorescence spectrum.

4.5.3.3 Time Course of Sensor Response in Solid Films

To find the optimal concentration of TBAH (or molar ratio TBAH/DAT-B) that would give the fastest sensor reaction, we measured the time course of the fluorescence intensity change at 574 nm for the sensor films drop cast on quartz slides. The optimization experiments were performed for the sensor films drop cast on quartz slides as shown in Figure 4.8, where the time course of the fluorescence intensity change was measured at 574 nm for DAT-B dispersed on a quartz slide (containing 0.25 μmol DAT-B) upon exposure to H₂O₂ vapor fixed at 225 ppm. Four series of measurements were performed over the quartz slides containing the same molar amount of DAT-B, but different amounts of TBAH, i.e., at molar ratios of TBAH/DAT-B: 1, 3, 5 and 20. The testing experiment was performed by hanging the loaded quartz slide in the saturated vapor of H₂O₂ (225 ppm) above 10 mL of 35 wt % H₂O₂ solution sealed in a 50 mL jar. As shown in Figure 4.8, the fluorescence intensity increased the fastest and reached the highest intensity value at a TBAH/DAT-B ratio of 5, which was determined as the optimal molar ratio for fabricating the sensor composite. The slower sensor response observed at higher TBAH/DAT-B ratio (e.g., 20) is likely due to the excessive TBAH decreasing the concentration of DAT-B molecules on the surface, thus limiting the sensor molecules' interaction with H₂O₂ vapor.

For the measurements performed under varying vapor concentrations of H₂O₂ (shown Figure 4.10), the experiment was performed by hanging the loaded quartz slide in the saturated vapor of H₂O₂ generated in a 26.5 L container, where approximately 1 L of H₂O₂ solution (diluted down to various concentrations) was put in a vacuum and sealed for 12 h

to reach the equilibrium vapor pressure. The equilibrium vapor pressure corresponding to a specific diluted concentration of H₂O₂ solution was deduced from the literature.(57) In the container, a continuous vapor stream was produced by a mini fan (Radio Shack, 40mm, 12 DC, 6500RPM), and the sensor loaded quartz slide was placed against the vapor stream (distance from the fan: 0.5 cm), and about 20 cm above the solution surface. After exposure to the vapor for different time intervals, the quartz slide was taken out for fluorescence measurement. In this study, various diluted concentrations of H₂O₂ solution were obtained by diluting the commercial 35 wt % solution with pure water 100, 200, 1000, 2000, and 10000 times, which produced saturated (equilibrium) vapor pressures of H₂O₂ of 1000, 500, 100, 50 and 10 ppb, respectively.

4.5.3.4 Contact Angle Measurement of DAT-B and DAT-B/TBAH Film

The contact angle measurement of DAT-B (0.25 μmol, 1.0 × 1.0 cm²) and DAT-B/TBAH film (0.25 μmol DAT-B/1.25 μmol TBAH, 1.0 × 1.0 cm²) was performed to determine the surface hydrophilicity of as prepared film. The surface of DAT-B is hydrophobic and the contact angle is 109.9 ° ± 0.6 °. After the addition of TBAH, the surface of the blended film is tuned to hydrophilic and the contact angle is decreased to 80.9 ° ± 2.6 °. This change in contact angle demonstrates another benefit of the addition of TBAH, i.e., the formation of hydrophilic film surface that increases the intake of H₂O₂ vapor in humid air.

4.5.3.5 Absorption and Fluorescence Spectra of DAT-B Before and After Reaction with H₂O₂ in Solution

In situ UV-vis absorption and fluorescence spectral measurements were performed in a DAT-B solution in ethanol (1×10^{-5} mol/L, in the presence of 1×10^{-3} mol/L TBAH) before and after addition of H₂O₂ (1×10^{-2} mol/L). As shown in Figure 4.1, the absorption peak of DAT-B moved from 371 nm to 433 nm upon reaction with H₂O₂, which indicates the characteristic ICT band of DAT-N. Meanwhile, the emission peak of DAT-B was shifted from 452 nm to 570 nm upon reaction with H₂O₂, also characteristic of the ICT band of DAT-N. Both the absorption and fluorescence spectra of the reacted state of DAT-B match well the spectra of pure DAT-N solution, clearly indicating the H₂O₂ mediated conversion of DAT-B to DAT-N as presented in Scheme 4.2.

4.5.3.6 Selectivity Test

The sensor DAT-B coated quartz slides (containing 0.25 μ mol DAT-B and 1.25 μ mol TBAH, 1.0×1.0 cm²) were exposed to the saturated vapor of various common solvents such as methanol (131,000 ppm), water (31,000 ppm), ethanol (89,000 ppm), acetone (260,000 ppm), chloroform (140,000 ppm), THF (173,000 ppm), toluene (26,000 ppm), hexane (130,000 ppm), ethyl acetate (100,000 ppm), to validate the selectivity of the sensor molecule. The increase in fluorescence intensity was measured at 574 nm over DAT-B coated quartz slide (the same component as used in Scheme 4.1) after 10 min exposure to 225 ppm H₂O₂ vapor, in comparison to that upon exposure to the saturated vapor of the common solvents. The minimum change of the fluorescent peak at 574 nm after extensive exposure to these highly concentrated solvents vapors (three orders of magnitude higher than H₂O₂ vapor used in this experiment) demonstrates that sensor molecule DAT-B is

highly selective towards H₂O₂.

4.5.3.7 IR spectra of DAT-B and DAT-N

The IR spectra of DAT-B before and after reaction with H₂O₂ (converting to DAT-N) were measured to demonstrate the function group changing. As shown in Figure 4.2, the CO-NH vibration of DAT-B (3300, 1733 cm⁻¹) shifted to 3463 and 1579 cm⁻¹, which are characteristic of the -NH₂ vibration. Concurrently, the C-B vibration in DAT-B(61) (1056 cm⁻¹) disappears when converted into DAT-N. These IR spectral changes explicitly demonstrate the function group change from boronate group to amino group, as illustrated in Scheme 4.2.

The IR spectra were measured by mixing DAT-B or DAT-N within KBr pellet. DAT-N used for IR measurement was made from the reaction of DAT-B with H₂O₂ in a solution. Briefly, a solution of DAT-B (100 mg, 0.13 mmol, in 20 mL ethanol) was added in 4 mL H₂O₂ (35 wt %), followed by stirring at room temperature for 4 h. The reaction solution was then diluted with ethyl acetate, extracted with brine and water, and dried over Na₂SO₄. After removal of solvent, the crude product was purified by flash chromatography (methylene chloride/ethyl acetate = 10:1) on silica gel to give 18 mg orange product, yield 54 %. ¹H NMR (CDCl₃, 300 MHz, ppm): δ = 7.29 (2 H, s, Ar-H), 4.30-4.38 (4 H, q, CH₂), 1.37-1.42 (6 H, t, CH₃). The NMR data match well the data obtained from the pure DAT-N synthesized separately through the route in Scheme 4.2.

4.5.3.8 Data Fitting

The data presented in Figure 4.9b can be fitted following the reaction kinetics equation,

(56)

$$\Delta I = K'(1 - e^{-Kt}) \quad (4.1)$$

where ΔI is the increase in fluorescence intensity measured at 574 nm, K and K' are constants with K related to the surface reaction rate of DAT-B with H_2O_2 , the given vapor pressure of H_2O_2 and the total amount of DAT-B, and K' is referred to as the ratio of the fluorescence intensity to the molar fraction of DAT-B (with respect to the total starting amount of DAT-B). Derivation of this equation is based on surface reaction kinetics, i.e., the rate of producing DAT-N is proportional to the surface density (or molar fraction) of unreacted DAT-B (22). The fitting gives $K' = 378.93$, $K = 0.0588$, with a $R^2 = 0.9698$.

Fitting of the data are presented in Figure 4.10. Assuming a quasiequilibrium was reached within 10 min exposure (as implied from the result in Figure 4.9b) to H_2O_2 vapor, the results shown Figure 4.10 should follow the Langmuir adsorption model (the film on quartz slide used here is the same with Figure 4.9, containing 0.25 μmol DAT-B and 1.25 μmol TBAH, $1.0 \times 1.0 \text{ cm}^2$). First, the surface adsorption of H_2O_2 (i.e., the reacted fraction of sensor molecules, X) is related to the vapor pressure of H_2O_2 as described by the Langmuir Equation,

$$X = \frac{b \cdot [H_2O_2]}{1 + b \cdot [H_2O_2]} \quad (4.2)$$

where b is a constant, $[H_2O_2]$ is the vapor pressure (concentration) of H_2O_2 .

The fluorescence emission intensity is proportional to the concentration of sensor molecules converted. Then, we have

$$\Delta I = \frac{a \cdot b \cdot [\text{H}_2\text{O}_2]}{1 + b \cdot [\text{H}_2\text{O}_2]} \quad (4.3)$$

where a is a proportional constant.

The fitting gives $a = 3.65 \times 10^6$, $b = 9.67 \times 10^{-8}$ with a $R^2 = 0.9732$.

The standard deviation of the emission intensity measurement shown in Figure 4.10 was about 0.9 (a.u.). The threshold of detectable emission can be set at an intensity level three times of the standard deviation of the noise floor, that is $\Delta I = 2.7$. Then, the corresponding detection limit can be determined by using the above equation and substituting ΔI with 2.7. This gives a detection limit of H_2O_2 vapor at 7.7 ppb.

4.5.3.9 Sensor Performance Comparison

There have been a few papers that reported on vapor detection of H_2O_2 . In comparison, our result is overall better regarding both sensitivity and response time, as shown in Table 4.1 and Table 4.2.

4.6 References

- (1) Toal, S. J.; Trogler, W. C. Polymer Sensors for Nitroaromatic Explosives Detection. *J. Mater. Chem.* **2006**, *16*, 2871-2883.
- (2) Thomas, S. W.; Joly, G. D.; Swager, T. M. Chemical Sensors Based on Amplifying Fluorescent Conjugated Polymers. *Chem. Rev.* **2007**, *107*, 1339-1386.
- (3) Wang, J. Electrochemical Sensing of Explosives. *Electroanalysis* **2007**, *19*, 415-423.
- (4) Moore, D. Recent Advances in Trace Explosives Detection Instrumentation. *Sens. Imaging* **2007**, *8*, 9-38.
- (5) Germain, M. E.; Knapp, M. J. Optical Explosives Detection: From Color Changes to Fluorescence Turn-On. *Chem. Soc. Rev.* **2009**, *38*, 2543-2555.

- (6) Yang, J.-S.; Swager, T. M. Fluorescent Porous Polymer Films as TNT Chemosensors: Electronic and Structural Effects. *J. Am. Chem. Soc.* **1998**, *120*, 11864-11873.
- (7) Staii, C.; Johnson, A. T.; Chen, M.; Gelperin, A. DNA-Decorated Carbon Nanotubes for Chemical Sensing. *Nano Lett.* **2005**, *5*, 1774-1778.
- (8) Johnson, A. T. C.; Staii, C.; Chen, M.; Khamis, S.; Johnson, R.; Klein, M. L.; Gelperin, A. DNA-Decorated Carbon Nanotubes for Chemical Sensing. *Phys. Stat. Sol. (b)* **2006**, *243*, 3252-3256.
- (9) Naddo, T.; Che, Y.; Zhang, W.; Balakrishnan, K.; Yang, X.; Yen, M.; Zhao, J.; Moore, J. S.; Zang, L. Detection of Explosives with a Fluorescent Nanofibril Film. *J. Am. Chem. Soc.* **2007**, *129*, 6978-6979.
- (10) Bohrer, F. I.; Colesniuc, C. N.; Park, J.; Schuller, I. K.; Kummel, A. C.; Trogler, W. C. Selective Detection of Vapor Phase Hydrogen Peroxide with Phthalocyanine Chemiresistors. *J. Am. Chem. Soc.* **2008**, *130*, 3712-3713.
- (11) Zyryanov, G. V.; Palacios, M. A.; Anzenbacher, P. Simple Molecule-Based Fluorescent Sensors for Vapor Detection of TNT. *Org. Lett.* **2008**, *10*, 3681-3684.
- (12) Díaz Aguilar, A.; Forzani, E. S.; Leright, M.; Tsow, F.; Cagan, A.; Iglesias, R. A.; Nagahara, L. A.; Amlani, I.; Tsui, R.; Tao, N. J. A Hybrid Nanosensor for TNT Vapor Detection. *Nano Lett.* **2009**, *10*, 380-384.
- (13) Tenhaeff, W. E.; McIntosh, L. D.; Gleason, K. K. Synthesis of Poly(4-Vinylpyridine) Thin Films by Initiated Chemical Vapor Deposition (Icvd) for Selective Nanotrench-Based Sensing of Nitroaromatics. *Adv. Funct. Mater.* **2010**, *20*, 1144-1151.
- (14) Lin, H.; Suslick, K. S. A Colorimetric Sensor Array for Detection of Triacetone Triperoxide Vapor. *J. Am. Chem. Soc.* **2010**, *132*, 15519-15521.
- (15) Zhang, C.; Che, Y.; Yang, X.; Bunes, B. R.; Zang, L. Organic Nanofibrils Based on Linear Carbazole Trimer for Explosive Sensing. *Chem. Commun.* **2010**, *46*, 5560-5562.
- (16) Xu, M.; Bunes, B. R.; Zang, L. Paper-Based Vapor Detection of Hydrogen Peroxide: Colorimetric Sensing with Tunable Interface. *ACS Appl. Mater. Interfaces* **2011**, *3*, 642-647.
- (17) Kartha, K. K.; Babu, S. S.; Srinivasan, S.; Ajayaghosh, A. Attogram Sensing of Trinitrotoluene with a Self-Assembled Molecular Gelator. *J. Am. Chem. Soc.* **2012**, *134*, 4834-4841.
- (18) Che, Y.; Gross, D. E.; Huang, H.; Yang, D.; Yang, X.; Discekici, E.; Xue, Z.; Zhao, H.; Moore, J. S.; Zang, L. Diffusion-Controlled Detection of Trinitrotoluene: Interior Nanoporous Structure and Low Highest Occupied Molecular Orbital Level of Building Blocks Enhance Selectivity and Sensitivity. *J. Am. Chem. Soc.* **2012**, *134*, 4978-4982.

- (19) Zheng, J. Y.; Yan, Y.; Wang, X.; Shi, W.; Ma, H.; Zhao, Y. S.; Yao, J. Hydrogen Peroxide Vapor Sensing with Organic Core/Sheath Nanowire Optical Waveguides. *Adv. Mater.* **2012**, *24*, OP194-OP199.
- (20) Grate, J. W.; Ewing, R. G.; Atkinson, D. A. Vapor-Generation Methods for Explosives-Detection Research. *TrAC, Trends Anal. Chem.* **2012**, *41*, 1-14.
- (21) Sanchez, J. C.; Trogler, W. C. Polymerization of a Boronate-Functionalized Fluorophore by Double Transesterification: Applications to Fluorescence Detection of Hydrogen Peroxide Vapor. *J. Mater. Chem.* **2008**, *18*, 5134-5141.
- (22) Xu, M.; Han, J.-M.; Zhang, Y.; Yang, X.; Zang, L. A Selective Fluorescence Turn-on Sensor for Trace Vapor Detection of Hydrogen Peroxide. *Chem. Commun.* **2013**, *49*, 11779-11781.
- (23) Gopalakrishnan, D.; Dichtel, W. R. Direct Detection of Rdx Vapor Using a Conjugated Polymer Network. *J. Am. Chem. Soc.* **2013**, *135*, 8357-8362.
- (24) Bernasconi, C. F. Kinetic and Spectral Study of Some Reactions of 2,4,6-Trinitrotoluene in Basic Solution. I. Deprotonation and Janovsky Complex Formation. *J. Org. Chem.* **1971**, *36*, 1671-1679.
- (25) Forzani, E. S.; Lu, D.; Leright, M. J.; Aguilar, A. D.; Tsow, F.; Iglesias, R. A.; Zhang, Q.; Lu, J.; Li, J.; Tao, N. A Hybrid Electrochemical-Colorimetric Sensing Platform for Detection of Explosives. *J. Am. Chem. Soc.* **2009**, *131*, 1390-1391.
- (26) McGann, W.; Haigh, P.; Neves, J. L. Expanding the Capability of Ims Explosive Trace Detection. *Int. J. Ion Mobility Spectrom.* **2002**, *5*, 119-122.
- (27) Tam, M.; Hill, H. H. Secondary Electrospray Ionization-Ion Mobility Spectrometry for Explosive Vapor Detection. *Anal. Chem.* **2004**, *76*, 2741-2747.
- (28) Oxley, J. C.; Smith, J. L.; Kirschenbaum, L. J.; Marimganti, S.; Vadlamannati, S. Detection of Explosives in Hair Using Ion Mobility Spectrometry. *J. Forensic Sci.* **2008**, *53*, 690-693.
- (29) Najarro, M.; Davila Morris, M. E.; Staymates, M. E.; Fletcher, R.; Gillen, G. Optimized Thermal Desorption for Improved Sensitivity in Trace Explosives Detection by Ion Mobility Spectrometry. *Analyst* **2012**, *137*, 2614-2622.
- (30) Benedet, J.; Lu, D. L.; Cizek, K.; La Belle, J.; Wang, J. Amperometric Sensing of Hydrogen Peroxide Vapor for Security Screening. *Anal. Bioanal. Chem.* **2009**, *395*, 371-376.
- (31) Schnorr, J. M.; van der Zwaag, D.; Walish, J. J.; Weizmann, Y.; Swager, T. M. Sensory Arrays of Covalently Functionalized Single-Walled Carbon Nanotubes for Explosive Detection. *Advanced Functional Materials* **2013**.

- (32) Komkova, M. A.; Karyakina, E. E.; Marken, F.; Karyakin, A. A. Hydrogen Peroxide Detection in Wet Air with a Prussian Blue Based Solid Salt Bridged Three Electrode System. *Anal. Chem.* **2013**, *85*, 2574-2577.
- (33) Freeman, R.; Finder, T.; Bahshi, L.; Gill, R.; Willner, I. Functionalized Cdse/Zns Qds for the Detection of Nitroaromatic or Rdx Explosives. *Adv. Mater.* **2012**, *24*, 6416-6421.
- (34) Andrew, T. L.; Swager, T. M. Detection of Explosives Via Photolytic Cleavage of Nitroesters and Nitramines. *J. Org. Chem.* **2011**, *76*, 2976-2993.
- (35) Ma, H.; Gao, R.; Yan, D.; Zhao, J.; Wei, M. Organic-Inorganic Hybrid Fluorescent Ultrathin Films and Their Sensor Application for Nitroaromatic Explosives. *J. Mater. Chem. C* **2013**, *1*, 4128-4137.
- (36) Yuan, L.; Lin, W.; Zheng, K.; Zhu, S. Fret-Based Small-Molecule Fluorescent Probes: Rational Design and Bioimaging Applications. *Acc. Chem. Res.* **2013**, *46*, 1462-1473.
- (37) Zhou, Z.; Yu, M.; Yang, H.; Huang, K.; Li, F.; Yi, T.; Huang, C. Fret-Based Sensor for Imaging Chromium(III) in Living Cells. *Chem. Commun.* **2008**, 3387-3389.
- (38) Yu, H.; Fu, M.; Xiao, Y. Switching Off Fret by Analyte-Induced Decomposition of Squaraine Energy Acceptor: A Concept to Transform 'Turn Off' Chemodosimeter into Ratiometric Sensors. *Phys. Chem. Chem. Phys.* **2010**, *12*, 7386-7391.
- (39) Yu, H.; Xiao, Y.; Guo, H.; Qian, X. Convenient and Efficient Fret Platform Featuring a Rigid Biphenyl Spacer between Rhodamine and Bodipy: Transformation of 'Turn-on' Sensors into Ratiometric Ones with Dual Emission. *Chem. Eur. J.* **2011**, *17*, 3179-3191.
- (40) Snee, P. T.; Somers, R. C.; Nair, G.; Zimmer, J. P.; Bawendi, M. G.; Nocera, D. G. A Ratiometric Cdse/Zns Nanocrystal Ph Sensor. *J. Am. Chem. Soc.* **2006**, *128*, 13320-13321.
- (41) Jin, T.; Sasaki, A.; Kinjo, M.; Miyazaki, J. A Quantum Dot-Based Ratiometric Ph Sensor. *Chem. Commun.* **2010**, *46*, 2408-2410.
- (42) Peng, H.-s.; Stolwijk, J. A.; Sun, L.-N.; Wegener, J.; Wolfbeis, O. S. A Nanogel for Ratiometric Fluorescent Sensing of Intracellular Ph Values. *Angew. Chem.* **2010**, *122*, 4342-4345.
- (43) Freeman, R.; Willner, I. Nad⁺/Nadh-Sensitive Quantum Dots: Applications to Probe Nad⁺-Dependent Enzymes and to Sense the Rdx Explosive. *Nano Lett.* **2008**, *9*, 322-326.
- (44) Freeman, R.; Gill, R.; Shweky, I.; Kotler, M.; Banin, U.; Willner, I. Biosensing and Probing of Intracellular Metabolic Pathways by Nadh-Sensitive Quantum Dots. *Angew.*

Chem. Int. Ed. **2009**, *48*, 309-313.

(45) Zhang, K.; Zhou, H.; Mei, Q.; Wang, S.; Guan, G.; Liu, R.; Zhang, J.; Zhang, Z. Instant Visual Detection of Trinitrotoluene Particulates on Various Surfaces by Ratiometric Fluorescence of Dual-Emission Quantum Dots Hybrid. *J. Am. Chem. Soc.* **2011**, *133*, 8424-8427.

(46) Wang, Y.; La, A.; Bruckner, C.; Lei, Y. Fret- and Pet-Based Sensing in a Single Material: Expanding the Dynamic Range of an Ultra-Sensitive Nitroaromatic Explosives Assay. *Chem. Commun.* **2012**, *48*, 9903-9905.

(47) Lakowicz, J. R. *Principles of Fluorescence Spectroscopy*; 3rd ed.; Kluwer Academic/Plenum Publishers, New York, 2006; Vol. 1.

(48) Schulte-Ladbeck, R.; Vogel, M.; Karst, U. Recent Methods for the Determination of Peroxide-Based Explosives. *Anal. Bioanal. Chem.* **2006**, *386*, 559-565.

(49) Burks, R.; Hage, D. Current Trends in the Detection of Peroxide-Based Explosives. *Anal. Bioanal. Chem.* **2009**, *395*, 301-313.

(50) Sanchez, J. C.; Trogler, W. C. Efficient Blue-Emitting Silafluorene-Fluorene-Conjugated Copolymers: Selective Turn-Off/Turn-on Detection of Explosives. *J. Mater. Chem.* **2008**, *18*, 3143-3156.

(51) Lo, L. C.; Chu, C. Y. Development of Highly Selective and Sensitive Probes for Hydrogen Peroxide. *Chem. Commun.* **2003**, 2728-2729.

(52) Lippert, A. R.; Van de Bittner, G. C.; Chang, C. J. Boronate Oxidation as a Bioorthogonal Reaction Approach for Studying the Chemistry of Hydrogen Peroxide in Living Systems. *Acc. Chem. Res.* **2011**, *44*, 793-804.

(53) Zhao, Y.; Gao, H.; Fan, Y.; Zhou, T.; Su, Z.; Liu, Y.; Wang, Y. Thermally Induced Reversible Phase Transformations Accompanied by Emission Switching between Different Colors of Two Aromatic-Amine Compounds. *Adv. Mater.* **2009**, *21*, 3165-3169.

(54) Zhang, Y.; Starynowicz, P.; Christoffers, J. Fluorescent Bis(Oligophenylamino)Terephthalates. *Eur. J. Org. Chem.* **2008**, *2008*, 3488-3495.

(55) Shimizu, M.; Takeda, Y.; Higashi, M.; Hiyama, T. 1,4-Bis(Alkenyl)-2,5-Dipiperidinobenzenes: Minimal Fluorophores Exhibiting Highly Efficient Emission in the Solid State. *Angew. Chem. Int. Ed.* **2009**, *48*, 3653-3656.

(56) Yuan, L.; Lin, W.; Yang, Y. A Ratiometric Fluorescent Probe for Specific Detection of Cysteine over Homocysteine and Glutathione Based on the Drastic Distinction in the Kinetic Profiles. *Chem. Commun.* **2011**, *47*, 6275-6277.

(57) Manatt, S. L.; Manatt, M. R. R. On the Analyses of Mixture Vapor Pressure Data: The Hydrogen Peroxide/Water System and Its Excess Thermodynamic Functions. *Chem.*

Eur. J. **2004**, *10*, 6540-6557.

(58) Cumming, C. J.; Aker, C.; Fisher, M.; Fok, M.; La Grone, M. J.; Reust, D.; Rockley, M. G.; Swager, T. M.; Towers, E.; Williams, V. Using Novel Fluorescent Polymers as Sensory Materials for above-Ground Sensing of Chemical Signature Compounds Emanating from Buried Landmines. *IEEE Trans. Geosci. Electron.* **2001**, *39*, 1119-1128.

(59) Sinnreich, J. Chemistry of Succinylsuccinic Acid Derivatives; VI. A Specific Synthesis of P-Phenylenediamine. *Synthesis* **1980**, *1980*, 578-580.

(60) Srikun, D.; Miller, E. W.; Domaille, D. W.; Chang, C. J. An Ict-Based Approach to Ratiometric Fluorescence Imaging of Hydrogen Peroxide Produced in Living Cells. *J. Am. Chem. Soc.* **2008**, *130*, 4596-4597.

(61) Romanos, J.; Beckner, M.; Stalla, D.; Tekeei, A.; Suppes, G.; Jalisatgi, S.; Lee, M.; Hawthorne, F.; Robertson, J. D.; Firlej, L.; Kuchta, B.; Wexler, C.; Yu, P.; Pfeifer, P. Infrared Study of Boron–Carbon Chemical Bonds in Boron-Doped Activated Carbon. *Carbon* **2013**, *54*, 208-214.

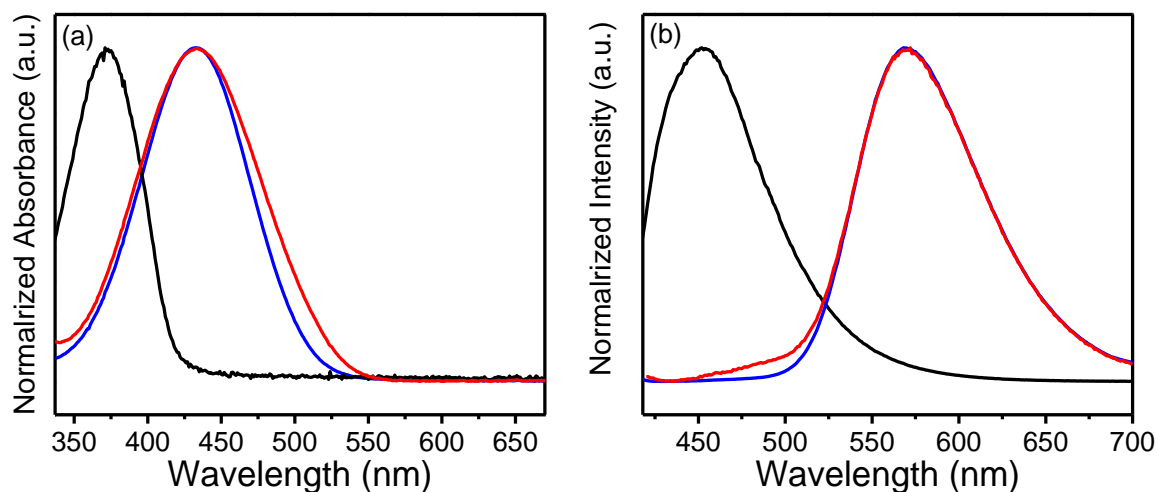


Figure 4.1 Absorbance (a) and fluorescence (b) spectra of DAT-B solution in ethanol (1×10^{-5} mol/L, in the presence of 1×10^{-3} mol/L TBAH) before (black) and after (red) addition of H_2O_2 (1×10^{-2} mol/L). For comparison, pure DAT-N solution in ethanol (blue, 1×10^{-5} mol/L, in the presence of 1×10^{-3} mol/L TBAH) is also presented.

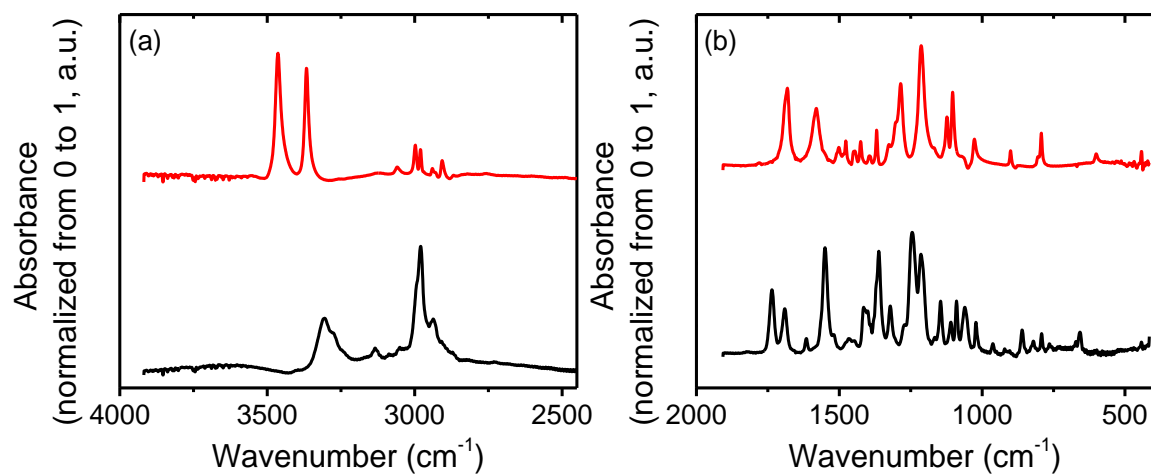


Figure 4.2 IR spectra of DAT-B (black) and DAT-N (red) in (a) 3900-2400 and (b) 1900-400 cm⁻¹ range.

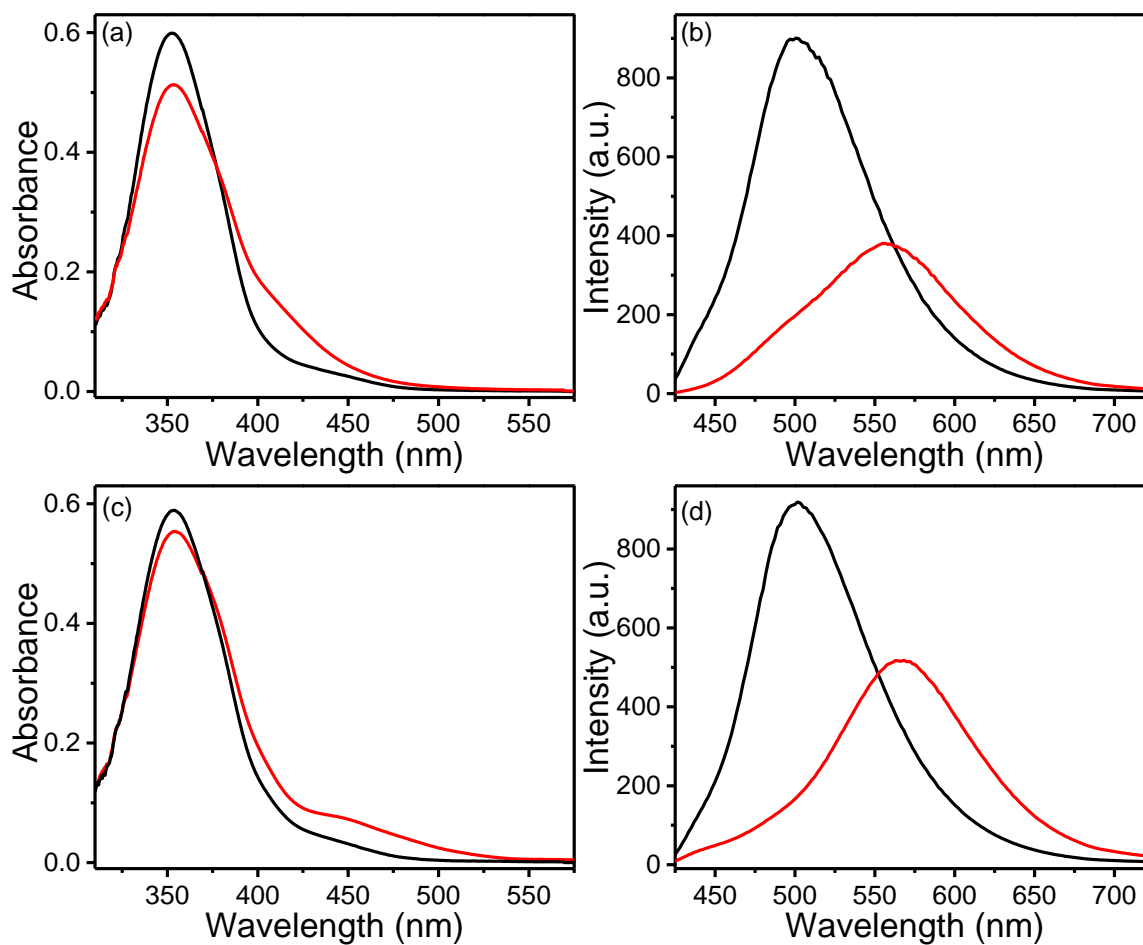


Figure 4.3 The absorption (a) and fluorescence (b) spectra of pristine DAT-B film (black) and the same film after expose to 500 ppb H₂O₂ vapor for 360 s (red) (0.25 μmol DAT-B and 1.25 μmol TBAH). The absorption (c) and fluorescence (d) spectra of DAT-B (black, 0.25 μmol DAT-B and 1.25 μmol TBAH) and DAT-B/DAT-N blended film (red, 0.225 μmol DAT-B, 0.025 μmol DAT-N and 1.25 μmol TBAH). All films were deposited to form a 1.0 × 1.0 cm² square on quartz slides, excited at 353 nm.

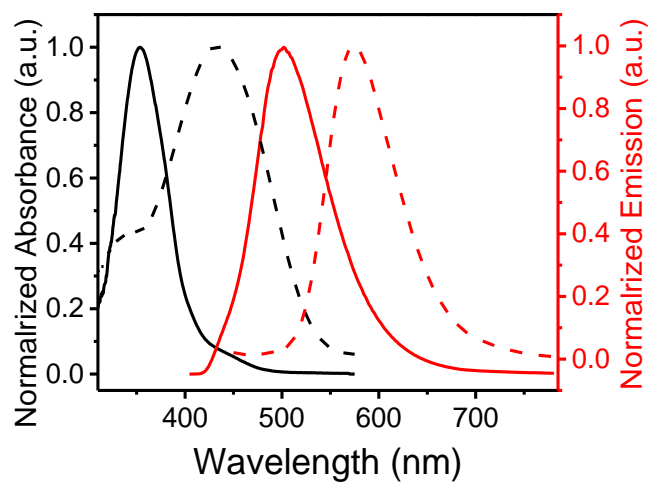


Figure 4.4 The absorption (black) and fluorescence (red) spectra of DAT-B film (0.25 μmol DAT-B, both blended with 1.25 μmol TBAH, $1.0 \times 1.0 \text{ cm}^2$) deposited on quartz slides before (solid) and after (dash) exposure to H_2O_2 vapor (225 ppm, 15 min).

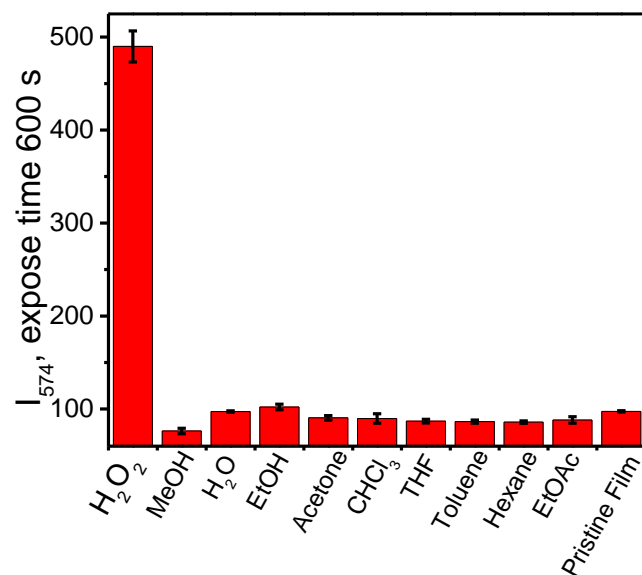


Figure 4.5 The selectivity plot of DAT-B (quartz slide containing 0.25 μmol DAT-B and 1.25 μmol TBAH, $1.0 \times 1.0 \text{ cm}^2$) over saturated vapor of common solvents and 225 ppm H_2O_2 vapor. The exposure time was fixed at 10 min; the error bars are based on the standard deviations of the data.

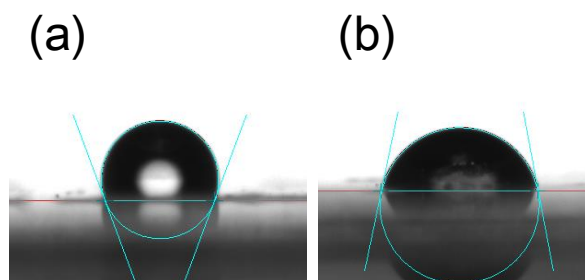


Figure 4.6 Contact angle measurement of DAT-B film ($0.25 \mu\text{mol}$, $1.0 \times 1.0 \text{ cm}^2$) and DAT-B/TBAH film ($0.25 \mu\text{mol}$ DAT-B/ $1.25 \mu\text{mol}$ TBAH, $1.0 \times 1.0 \text{ cm}^2$).

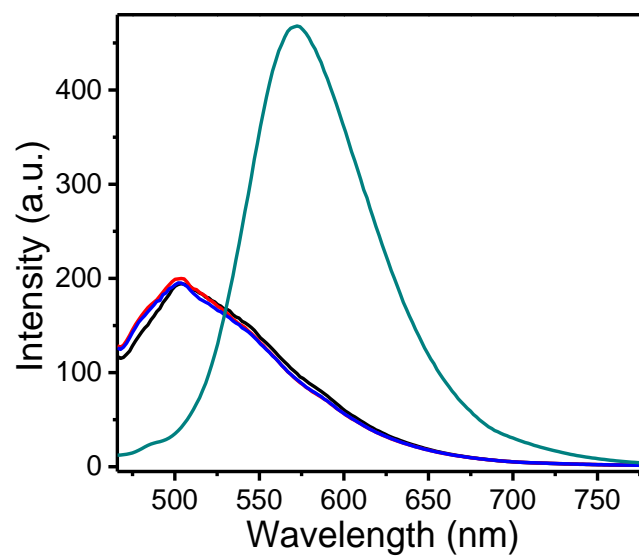


Figure 4.7 The fluorescence spectra of the DAT-B coated quartz slide (containing 0.25 μmol DAT-B and 1.25 μmol TBAH, $1.0 \times 1.0 \text{ cm}^2$): freshly prepared film (black), after 24 h (red), after 7 days (blue), and after exposure to 225 ppm H_2O_2 vapor for 5 min (green), $\lambda_{\text{ex}} = 427 \text{ nm}$.

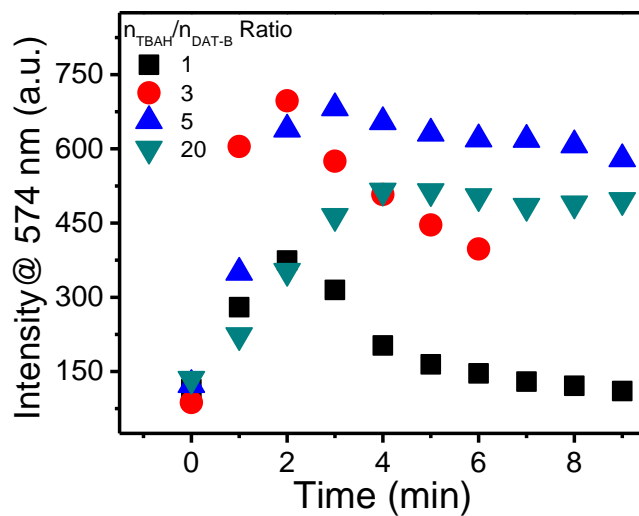


Figure 4.8 Time course of the fluorescence intensity change measured at 574 nm for DAT-B coated quartz slides (containing 0.25 μmol DAT-B mixed with different amounts of TBAH, $1.0 \times 1.0 \text{ cm}^2$) upon exposure to 225 ppm H_2O_2 vapor ($\lambda_{\text{ex}} = 427 \text{ nm}$). Shown in this plot are results of four slides containing the same molar amount of DAT-B, but different amounts of TBAH, i.e., at molar ratios of TBAH/DAT-B: 1 (black), 3 (red), 5 (blue) and 20 (purple).

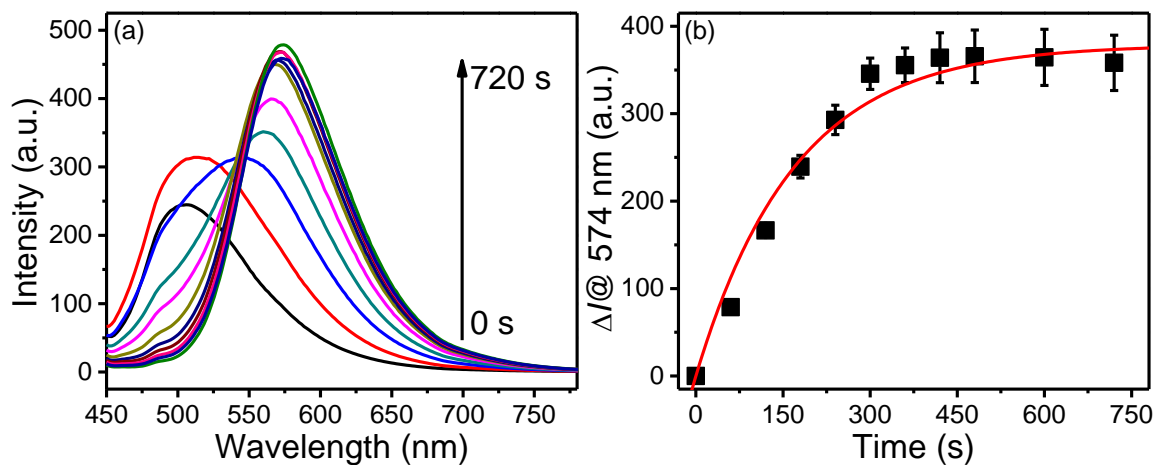


Figure 4.9 The fluorescence spectra of DAT-B coated on a $1.0 \times 1.0 \text{ cm}^2$ quartz slides (containing $0.25 \text{ }\mu\text{mol}$ DAT-B and $1.25 \text{ }\mu\text{mol}$ TBAH) and recorded at various time intervals after exposure to 1 ppm H₂O₂ vapor. ($\lambda_{\text{ex}} = 427 \text{ nm}$). (b) The emission intensity increase ΔI measured at 574 nm ($\lambda_{\text{ex}} = 427 \text{ nm}$) as a function of exposure time, for which the data points are fitted following a first order surface reaction between DAT-B and H₂O₂. The error bars are based on the standard derivations of the intensities as measured.

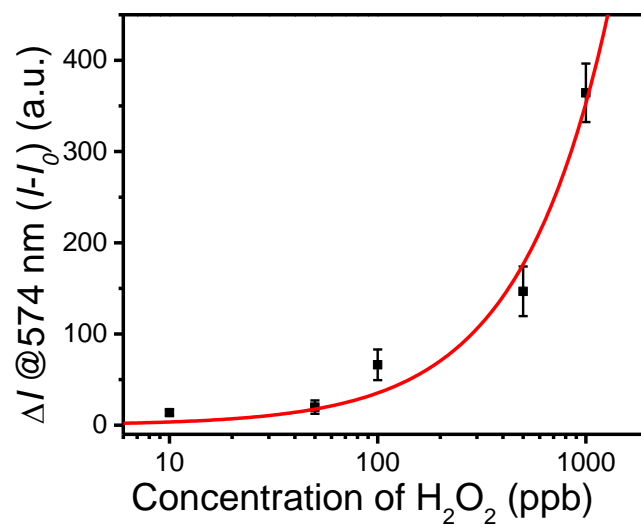


Figure 4.10 A plot showing the fluorescence intensity increase (ΔI) measured at 574 nm ($\lambda_{\text{ex}} = 427$ nm) as a function of the vapor pressure of H₂O₂, for which the data points are fitted following the Langmuir adsorption model. The error bars are based on the standard deviations of the emission intensities as measured.

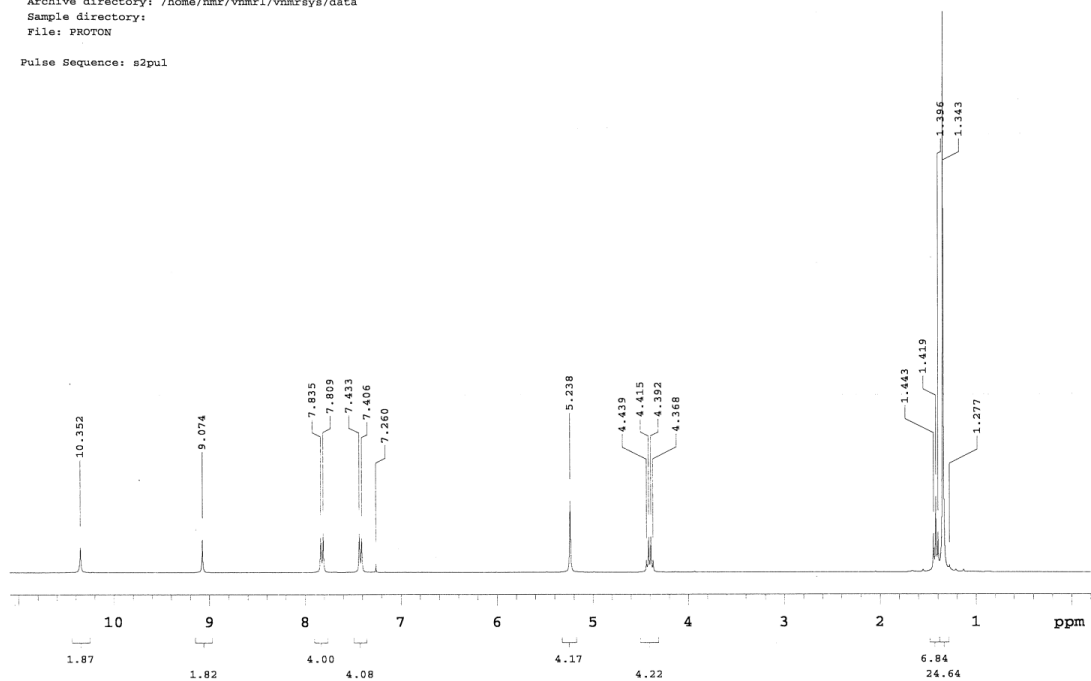
hjm120223-300M-H1

Archive directory: /home/nmr/vnmr1/vnmrSYS/data

Sample directory:

File: PROTON

Pulse Sequence: s2pul

Figure 4.11 ^1H NMR spectrum of DAT-B.

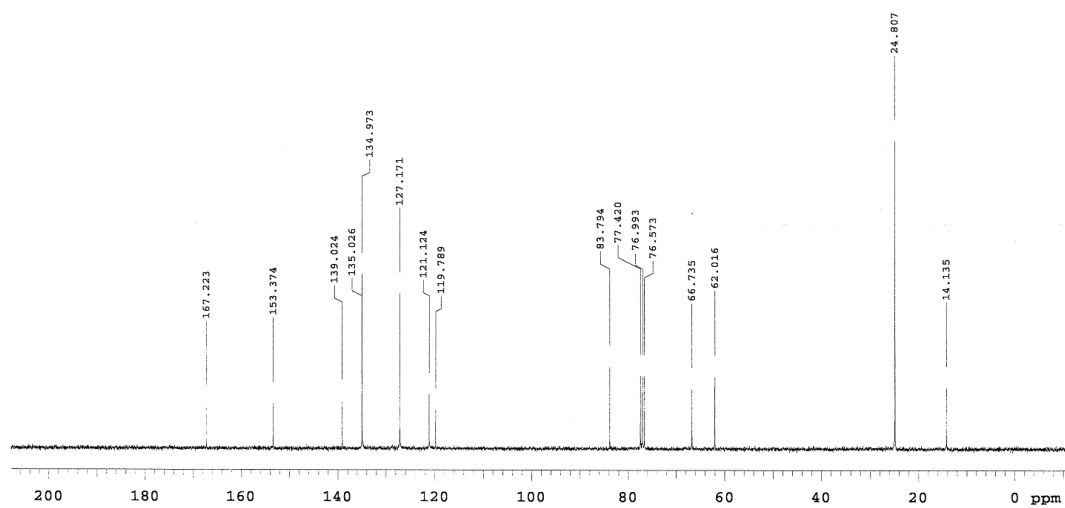


Figure 4.12 ^{13}C NMR spectrum of DAT-B.

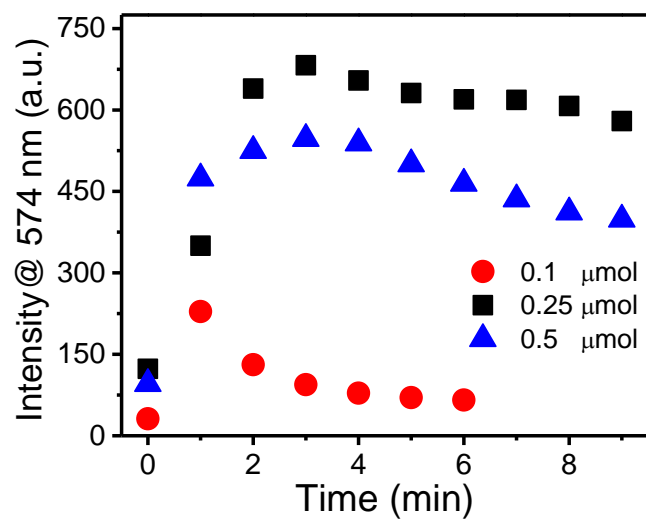


Figure 4.13 Time course of the fluorescence intensity change measured at 574 nm for DAT-B coated quartz slide at different molar amounts (0.1 μmol , red; 0.1 μmol , black; 0.5 μmol , blue, $1.0 \times 1.0 \text{ cm}^2$) with the same TBAH/DAT-B ratio (5:1) upon exposure to 225 ppm H_2O_2 vapor.

Table 4.1 Sensor performance comparison between our sensor and other fluorescence sensors for H₂O₂ vapor.

Reference	Limit of detection /exposure time	Response time at 1 ppm H ₂ O ₂ exposure
<i>J. Mater. Chem.</i> 2008 , <i>18</i> , 5134-5141. (21)	3 ppb / 8 h	800 s (1.2 ppm)
<i>Chem. Commun.</i> 2013 , <i>49</i> , 11779-11781. (22)	2.9 ppb / 5 min	0.86 s
This work	7.7 ppb / 10 min	< 0.5 s

Table 4.2 Sensor performance comparison between our sensor and other types of sensors for H₂O₂ vapor.

Sensor technique	Limits of detection / exposure time	Response time at 1 ppm H ₂ O ₂ exposure
Colorimetric [16]	400 ppb / 10 s	n/a
Chemiresistor [10]	50 ppb / minutes	n/a
Electrochemistry [30]	6 ppb / 2 min	n/a
This work	7.7 ppb / 10 min	< 0.5 s

CHAPTER 5

DISSERTATION CONCLUSIONS AND PROPOSED FUTURE WORK

Vapor detection has been widely exploited as one practical, noninvasive explosive detection method for its high sensitivity and reliability among current explosive detection technologies. The cost efficiency, simple instrumentation combined with the high sensitivity and selectivity of optical detection methods (especially colorimetric and fluorescence spectral methods) make for its application in security monitoring and screening. Peroxide-based explosives have been broadly employed by terrorists for their synthetic ease and lack of efficient detection method. Hydrogen peroxide (H_2O_2) is recognized as the signature compound for peroxide-based explosives, which is a synthetic precursor and decomposition product of such peroxide explosives. Trace vapor detection of H_2O_2 offers an ideal approach to noninvasive detection of peroxide-based explosives. However, the development of such a vapor sensor system with high accuracy, sufficient sensitivity (reactivity) and fast response still remains challenging. Three vapor detection methods for H_2O_2 were designed and developed in this study. They all take advantage of the specific chemical reaction towards H_2O_2 to secure the detection selectivity, and the materials surface and structural engineering to afford high vapor sampling efficiency.

5.1 Dissertation Conclusions

First, an efficient colorimetric sensing system for the vapor detection of H_2O_2 was developed. The sensory materials were based on the cellulose fibril network of paper towels, which provide a tunable interface for modification with Ti(IV) oxo complexes for binding and reaction with H_2O_2 . This one time use paper-based sensor material provides a simple and economical method for noninvasive detection of peroxides. Prospectively, the reported vapor sensor system proves the technical feasibility of developing enhanced colorimetric sensing using nanofibril materials that will be fabricated from building-block molecules functionalized with a Ti(IV) oxo moiety. Such a “bottom-up” approach provides plenty of opportunities to enlarge the surface area (by shrinking the fiber size), enhancing the surface interaction with the gas phase. It should be noted that sensitivity and response speed of this colorimetric method at low concentration range is not ideal for field application.

An expedient fluorescence turn-on sensor system that is suitable for trace vapor detection of H_2O_2 was then developed, which provides high sensitivity and rapid response compared to the colorimetric method. The sensor mechanism is based on H_2O_2 -mediated oxidation of a boronate fluorophore (C6NIB), which is nonfluorescent in the ICT band, but turns strongly fluorescent upon conversion into the phenol state (C6NIO). This fluorescence turn-on reaction is extremely selective towards H_2O_2 , with no sensor response to other common reagents. The negligible fluorescence background of C6NIB combined with the high fluorescent emission of C6NIO, makes C6NIB an ideal candidate for efficient sensing. Dispersing C6NIB with an organic base like TBAH into a silica gel matrix produces a highly efficient sensor system for vapor detection of H_2O_2 , regarding both detection limit (down to 2.9 ppb) and response time (down to 1 s under 1 ppm H_2O_2).

However, some technical factors such as sensor concentration, local chemical environment and excitation light intensity were found difficult to control in the system to make the sensor sufficiently reproducible, thus limiting the further development for practical field use.

In the last chapter, a novel fluorescence ratiometric sensor system was proposed and developed for trace vapor detection of H_2O_2 , which took advantages of high sensitivity from the fluorescence method and reliability from the dual emission wavelength monitoring (ratiometric sensing). The sensing mechanism is based on H_2O_2 -mediated oxidation of a boronate fluorophore, DAT-B, which is then converted to an amino-substituted product, DAT-N. The emission of DAT-B film is due to the π - π transition and located in the blue region (centered at 500 nm), whereas the emission of DAT-N within the same film is significantly red-shifted, to 574 nm. The red-shifted emission band is due to the ICT band of DAT-N. The spectral overlap of the DAT-B emission and DAT-N absorption band results in efficient FRET process, which can be exploited to enhance the sensor performance in terms of both sensitivity and response speed. Considering the over 70 nm separation between the emission bands of DAT-B and DAT-N, the sensor system thus developed will also be suited for dual channel (wavelength) monitoring to enhance detection reliability, particularly compared to conventional fluorescence sensors based on single wavelength monitoring (quenching or turn-on). By blending the DAT-B sensor with a hydrophilic organic base with the appropriate molar ratio, the sensor composite demonstrated effective vapor sampling (absorption) of H_2O_2 , resulting in both high detection sensitivity (down to 7.7 ppb) and fast sensor response (down to 0.5 s under 1 ppm H_2O_2). The exploitation of FRET in solid films broadens the sensor development for trace vapor detection, and can significantly enhance the fluorescence sensing efficiency in

comparison to the normal single-band sensor system, for which the sensing efficiency is solely determined by the stoichiometric conversion of sensor molecules.

5.2 Suggestions for Future Work

The following suggestions are recommended for continuing research on the trace vapor detection of peroxide based explosives:

1. Future work on the colorimetric detection method can focus on the exploration of new sensor molecules with novel chemical structure and reaction, which have high absorption coefficient to further enhance the sensitivity and/or fast reaction kinetics for improved response speed. An alternative route to address the response speed issue will be the optimization of the reaction medium, which facilitates the reaction speed.
2. Future work on the fluorescence detection method can be centered on the faster, one-step detection of peroxide compounds (e.g., TATP, HMTD), while still maintaining the advantages of current sensors (e.g., rapid response, high selectivity and sensitivity). Since peroxide compounds can be decomposed by UV irradiation or acidic treatment, a pretreatment of peroxide vapor stream combined with parallel validation test of current detection setting can be used to approach one-step detection of peroxide explosives. Besides, the employment of Förster Resonance Energy Transfer (FRET) is proven to improve the response speed and sensitivity for trace vapor detection of H_2O_2 . A combination of quantum dots with the appropriate peroxide reactive functional group will take advantage of not only the high fluorescence quantum yield of the quantum dots but also the signal amplification effect from the FRET process. Combined, this will result in a ultra-low detection limit as well as fast response.
3. Chemiresistive sensors will also be a good candidate for peroxide based explosives,

for their simple instrumentation and highly accurate measurement. The selectivity towards peroxide is an issue, but can be addressed by the employment of either specific surface binding of the sensor material or differential sensing enabled by sensor assay. Graphene and carbon nanotubes modified with specific peroxide binding or reactive moieties decoration will be among the potential candidate materials for this application due to the high electrical conductivity, air stability and large surface area of these materials.